Defense Against the Dark Arts
Notes on dark matter and particle physics

Flip Tanedo

Institute for High Energy Phenomenology,
Physical Sciences Building / Clark Hall,
Cornell University, Ithaca, NY 14853, USA

E-mail: pt267@cornell.edu

This version: August 4, 2011

Abstract

This is a set of ongoing LaTeX'ed notes on dark matter. They're not associated with any one particular project and are not meant for publication.

Contents

The Dark Arts are many, varied, ever-changing, and eternal. Fighting them is like fighting a many-headed monster, which, each time a neck is severed, sprouts a head even fiercer and cleverer than before. You are fighting that which is unfixed, mutating, indestructible. – Severus Snape, *Harry Potter and the Half-Blood Prince*

1 Introduction

This is a set of notes on dark matter that I started writing to keep track of well-known results. They are not meant for publication and are a work-in-progress. Some common references for basic WIMP dark matter and cosmology include the textbooks by Dodelson [1], Kolb & Turner [2], and Bertone (collection of reviews) [3]. Introductory pedagogical sources include the lectures at SSI 2007 [4]. Additional websites which aggregate review literature and are regularly updated can be found in [5]. Other reviews of interest include: [6], [7]...

2 A historical introduction to dark matter

This section is from the author's A-exam and is purely for cultural context. Readers interested in physics should skip this.

We begin with a selective history of dark matter highlighting some motivation and leading up to a subjective description of recent experimental and theoretical developments in the field. A more encyclopedic history can be found in [8]. We attempt to provide relevant references to assist those—such as the author—who intend to continue in this field.

2.1 'Dark Matter' Pre-History

The big question for dark matter experimentalists is how should we detect 'stuff' that isn't observable in the conventional sense. It is well known that dark matter was originally discovered through its gravitational effects, but the idea that non-luminous astronomical objects could be detected in this way is actually much older. Two of the earliest examples (from [9]) include (i) the discovery of white dwarfs due to the position of the stars Sirius and Procyon, and (ii) the discovery of Neptune from an anomalous orbit perturbation in Uranus.

2.2 The Dark Matter Dark Ages

An early history of dark matter with original references is presented in [10]. We will only briefly and selectively mention parts of this story. Dark matter was first proposed in 1933 by Fritz Zwicky to account for the radial velocity dispersion of galaxies in the Coma cluster [11] (English reprint [12]) which were suggestive of the presence of non-luminous matter. Zwicky's phrase '*dunkle (kalte) Materie*' is regarded as the origin of the term (cold, i.e. non-relativistic) dark matter. Zwicky's observations were later seen in the Virgo cluster [13] and later in the local group [14]. There is a rather famous photograph of Zwicky making a silly face (originally taken as part of a

series of deliberately exaggerated expressions [15]) that now seems to be a *de facto* requirement for any public talk on dark matter.

At around the same time another set of astrophysical observations would lead to the 'classic' evidence for dark matter which undergrads will recite in some Pavlovian manner: the rotational velocity curves of spiral galaxies. Astronomers found that the outer regions of galaxies were rotating with unexpectedly high velocities given what was expected of their matter distribution based on luminous matter. The first such observations came in 1939 from the Andromeda galaxy [16] and were later extended in the to larger radii in the 1970s; see [17] for a history and references.

It is worth noting that papers on the 'missing mass' in galaxy clusters and that in the outer regions of spiral galaxies did not make connections between the two. These were also the dark ages of scientific publication, well before the arXiv. At this point these astrophysical results were, "at best, received with skepticism in many colloquia and meeting presentations" [10]. It is not necessarily comforting to remark that our scientific society has advanced so much that some of us are no longer burdened by such skepticism against experimental results [18].

A turning point came in 1973 with the work of Ostriker and Peebles that showed that instabilities in models of galaxy disks could be solved by a massive spherical component, a so-called **halo** [19]. (Such a halo is a generic prediction of collision-less dark matter [20].) Further, with Yahil they noted that galaxy masses appear to increase linearly with radius [21]. These results, combined with the latest velocity curves at the time, provided a strong case for the existence of 'missing mass' in galaxies.

2.3 The Dark Matter Renaissance

Following this there were a Renaissance of astrophysical results which confirmed (in the scientific sense) and refined the missing mass hypothesis while ruling out known reasonable alternatives. These are reviewed nicely in Blitz's lectures in [4] and Gaitskell's lectures in [22]. An undergraduate-level discussion with calculations can be found in [23]. In addition to refined astrophysical searches of the general type discussed above[1] that rely on the virial theorem and hydrostatic equilibrium (reviwed in [25]), the 1990s brought about new astrophysical and cosmological methods to probe the nature of this 'missing mass' (see reviews in [26]).

The detection of X-rays from hot gas in elliptical galaxies provided a new confirmation of the dark matter hypothesis. This provides a handle to determine the luminous matter content of the galaxy which one can compare to the matter required to maintain hydrostatic equilibrium. Fabricant et al. found that the total mass of the M87 galaxy is indeed ten times larger than the luminous mass [27]. While this was effectively the same type of analysis as the aforementioned 'dark age' experiments, this was convincing evidence that the 'missing mass' phenomenon was not exclusive to spiral galaxies.

Another clear observation of dark matter comes from the prediction of gravitational lensing in general relativity, reviewed in [28]. Here one observes the dark matter's presence by the way it gravitationally warps space and changes the path of light as it comes between luminous astrophysical objects and our telescopes. The effect can be seen at different magnitudes depending on

[1]We will not discuss these further. One of the important lessons in the emerging field of particle astrophysics is that particle physicists should take astrophysical anomalies with a grain of salt, e.g. [24]. We will return to a modern manifestation of this in Section 2.5.

the gravitational potential of the lensing object. Strong lensing refers to easily visible distortions of an individual light source. Weak lensing, on the other hand, requires a statistical analysis of a large number of sources to search for coherent distortions. Finally, microlensing comes from relatively light lensing objects whose distortions of the luminous object cannot be resolved so that one instead searches for a change in that objects overall luminosity. The most advanced lensing analyses have not only detected dark matter, but have even allowed astrophysicists to construct three dimensional maps of its distribution [28].

The previous two methods (X-ray spectroscopy and gravitational lensing) converged with the relatively recent observation of the Bullet cluster which was formed by the collision of two large galaxy clusters [29]. By using X-ray spectroscopy to image the hot (luminous) matter and weak gravitational lensing to image mass density, it was seen that the luminous matter lags behind the total mass as one would expect from weakly-interacting dark matter. This observation effectively put the nail in the coffin of dark matter alternative theories, such as modified Newtonian gravity.

The cosmic microwave background (CMB) has lifted cosmology out of its status as a largely-theoretical discipline[2]. A combination of theoretical and experimental cosmological constraints have cemented the so-called 'concordance' or ΛCDM (dark energy with cold dark matter) paradigm as an accurate description of our universe [23, 31]. The general strategy here is to measure the matter density of the universe $\Omega_m \approx 0.04$ and compare to the baryonic energy density $\Omega_b \approx 0.26$ of the universe and conclude that most of the matter in the universe must be composed of non-baryonic dark matter. Indirect measurements of Ω_b include analyses of primordial nucleosynthesis of ^{4}He, ^{2}H and ^{7}Li [32]; the Sunyaev Zel'dovich effect in which the spectrum of X-ray emission from hot gasses is shifted from inverse scattering off the CMB [33], and the Lyman-α forest whose absorption lines indicate the make up of the intergalactic medium [34]. The highlight of observational cosmology, however, was the direct measurement of the CMB spectrum from the COBE [35] and WMAP [36] satellites. The measurement of the acoustic peaks in this spectrum provide the most stringent constraints on dark matter (and dark energy) [37].

Further evidence comes from the requirement of dark matter in cosmology to generate the density perturbations that led to large scale structure [38] and to account for big bang nucleosynthesis [39].

2.4 Romanticist Dark Matter

While we have been necessarily brief and incomplete, it should be clear that the ΛCDM model with weakly-interacting cold dark matter has been well-established by a variety of astrophysical observations using orthogonal techniques and taken at a range of scales (galactic, galaxy cluster, and cosmological). What is remarkable is that at roughly the same time that the need for dark matter was becoming accepted dogma in astrophysics and cosmology, realistic theories of particle physics beyond the standard model also generically began to predict the existence of new stable massive states that were natural dark matter candidates. Thus the forefront of cosmology and astrophysics converged with particle physics and gave rise to particle-astrophysics (or astro-particle physics).

[2]As Shamit Kachru once remarked, "Until very recently, string cosmology was the marriage of a field with no data with a field with no predictions" [30].

The theory community's favorite candidate for new fundamental physics is supersymmetry[3] (SUSY). Constraints on $B-L$ violation (proton decay) tend to set very restrictive bounds on new physics—often pushing them into an unnatural regime—unless some sort of parity is imposed to prevent dangerous higher-dimensional operators. In SUSY the standard solution is to impose R-parity, which makes the lightest supersymmetric partner (LSP) stable and a benchmark candidate for weakly-interacting massive particle (WIMP) dark matter.

The theory-side highlight of the dark matter Renaissance is the **Boltzmann equation**, whose integral determines the relic abundance of a thermally-produced WIMP particle species of known interaction cross section after the universe cools and the particle 'freezes out' of thermal equilibrium. This is the key to connect particle physics data (interaction cross section) with astrophysical data (relic density). This is the first tool for any honest theorist interested in dark matter and is discussed in classic (particle-)cosmology texts [2, 40]; also see [41] for a slightly more advanced analysis. Honestly integrating the Boltzmann equation is a notorious pain in the ass for generic models due to threshold effects and potential numerical instabilities. Fortunately, numerical tools now exist [42, 43]. Non-thermal models (e.g. non-thermal axions) are significantly more complicated but—due to kinetic equilibrium—tend to also contribute to thermal dark matter [44]; for constraints see, e.g. [45].

As reviewed in [46], there are a number of viable dark matter candidates that go beyond the standard WIMP paradigm. These include sterile neutrinos, axions, and more recently explored exotica that we will mention in Section 2.7. (Other non-particle candidates, such as massive compact halo objects—MACHOs, have been shown to be unable to account for most of the dark matter mass.) However, there is a compelling coincidence called the **WIMP miracle** that has made WIMP models a favorite dark matter candidate among theorists [47]. If one assumes only that the dark matter couplings are on the order of those for the weak interaction ($g \approx 0.65$), then cranking through the Boltzmann equation gives a model-independent statement that the dark matter mass should be on the order of 100 GeV to 1 TeV. This happens to be "*precisely*" where particle physicists already expect to find new physics to solve the hierarchy problem and illuminate the mechanism of electroweak symmetry breaking. (Though, see Section 3.7.)

Since this brings us to the current era, let us review what is 'known' about dark matter [48]:

1. It explains observations over a wide range of scales and experimental methodologies. In particular, it allows $\Omega_M h^2 \approx 0.1$ as required by cosmological observations.
2. It is neutral. This is strongly constrained by, for example, searches for heavy hydrogen [49]. (Millicharged DM is constrained by cosmology [50].)
3. It is not made up of Standard Model particles but is stable on Hubble time scales.
4. It is *cold*, i.e. non-relativistic at freeze-out ($T \sim$ keV), or else structure formation would fail.
5. It is effectively non-(self-)interacting due to the stability of the halo. (A more conservative statement is that DM must have negligible annihilation and dissipation, see e.g. [51].)
6. If DM interacts with a massless vector[4], then the coupling $\alpha \lesssim 10^{-3}$ for $m_\chi \sim$ TeV [52].
7. It violates the equivalence principle [53].

[3] Given the overabundance of excellent references for SUSY, we will not mention any in particular.

[4] This restriction is not as random as it seems. Our favorite DM benchmark is the neutralino which is a Majorana fermion so that any interaction with gauge vectors would violate gauge invariance. The restriction that *generic* DM should have very small gauge vector couplings means that the neutralino is still a valid benchmark [48].

A similar 'ten point test' with further discussion can be found in [54].

2.5 Baroque Dark Matter

> *Particle physicists* also saw the dramatic style of Baroque *laboratory experiments* as a means of impressing visitors and expressing triumphant power and control [55] (modified by the author, who is aware that the Baroque period predated Romanticism).

The current era has particle physicists attempting to pull dark matter out of the sky and into the lab, where one might hope to directly measure dark matter scattering events against detector material. This so-called **direct detection** benefits from being largely independent of astrophysical uncertainties and unknowns (astrophysical assumptions will be explained in Section 5.2). These experiments are placed deep underground to shield against cosmic ray backgrounds and make use of state-of-the art techniques to determine the dark matter cross section and mass. The heuristic picture of direct detection is as follows:

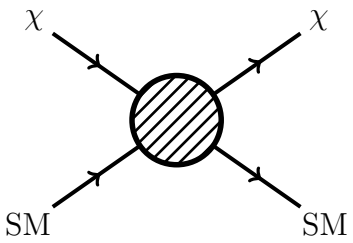

A WIMP from the local dark matter halo interacts with a target nucleus (composed of Standard Model quarks) in a detector and recoils. By counting the number of nuclear recoils, one can hope to determine information about the dark matter mass and cross section. The review of direct detection via liquid noble gas detectors is the main focus of this report so we shall leave further discussion of this topic to the rest of this document.

It is important to note that while exclusions plots continue to chip away at the allowed region (under standard assumptions), to date there has been no universally-accepted 'smoking gun signal' for dark matter via these techniques. A single experiment, the DAMA collaboration [56], has a many-standard deviation result. While the DAMA signal observes an annual modulation with the correct phase that one would expect from the motion of the Earth relative to the galactic dark matter halo, it has been effectively ruled out within the standard WIMP paradigm by, for example, the CDMS collaboration [57, 58, 59]. Additionally, DAMA's rudimentary background rejection and its exclusive contract with the company producing its NaI detector material have added to particle physics community's skepticism of their result; for an informal review see [60], or see [61] (lecture three) for a discussion of potential background sources. In fact, until recently these results were largely ignored by dark matter model-builders.

2.6 Impressionist Dark Matter

While a generation of particle physicists turned to direct detection to "pull dark matter from the sky and into the lab," astrophysicists had turned to **indirect detection** techniques to go back to

the sky to search for dark matter annihilation, which is very nicely reviewed in [62]. The heuristic picture is

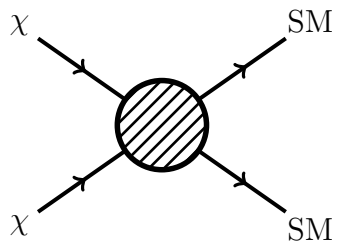

Here one hopes to detect the Standard Model products (or the products thereof) of dark matter annihilation in the halo. Smoking gun signatures include antimatter (positrons and anti-protons), gamma rays (mono-energetic), and neutrinos. These signals are affected by astrophysics, including hitherto unknown but otherwise boring astrophysics such as the possible existence of nearby pulsars that could mimic the above signals.

Several such intriguing astrophysical signals have existed for some time, but interest peaked rapidly in 2008 with the release of the positron and anti-proton flux data from the PAMELA satellite[5] [64]. PAMELA is particularly interesting because it is a 'toy' particle detector in space with its own magnetic field to determine particle charge (and hence discriminate between particles and anti-particles). The satellite found an unexpected increase in the charged lepton flux and a corresponding increase in the positron fraction[6] [66] with no similar feature in anti-protons [67]. More recently the Fermi Large Area Telescope [68] does not rule out PAMELA.

Astrophysicists were cautious to herald the PAMELA signal as an avatar of dark matter; see, e.g., [69] for two early alternate astrophysical explanations. On the other hand, having been starved of any data vaguely resembling new physics for some time, the particle theory community was quick to build new models [70] selectively invoking astrophysical hints. Other signals include HESS [71], INTEGRAL [72], EGRET [73], and the Fermi/WMAP "haze" (see [74] for a recent critical discussion) [75]. ATIC, a balloon experiment commonly cited in dark matter literature between 2008 and 2009, seems to have been ruled out by Fermi [68]. A general feature of these anomalies is that they seem to suggest dark matter with unusual spectra and/or couplings—though these are not necessarily consistent with one another.

2.7 Postmodern Dark Matter: looking forward

> Like all tyrannies, there is a single yoke of control: the one thing we know about WIMPs is their relic abundance. We've lived with this tyranny for a long time. It's provided all of us with jobs... and some of us with tenure.
> – Neal Weiner, on the 'tyranny' of the WIMP Miracle paradigm [76].

[5] Actually, interest in dark matter interpretations began well before data was officially released. One particularly bold collaboration published a paper based on a photograph preliminary results presented at a conference and even had the audacity to reproduce the preliminary results well before the official results were released [63].

[6] HEAT found a similar anomaly in the positron flux before PAMELA but could not rule our secondary sources [65]; we thank Bibhushan Shakya for this comment.

The prospect that astronomers had already indirectly detected dark matter beyond the standard neutralino-like paradigm spurred much interest in more exotic 'phenomenological' dark matter models that were motivated primarily from astrophysical anomalies rather than models of electroweak symmetry breaking. Key ideas include light dark matter [72, 77], inelastic dark matter [78, 79], annihilating dark matter [80], exothermic dark matter [81], superWIMPs [82] and WIMP-less dark matter [83]. (Additionally, some older top-down ideas have stuck around, e.g. axions [84].)

A watershed paper by Arkani-Hamed and Weiner [85] (using many ideas earlier proposed by the latter) established new rules for dark matter model building: pick your favorite anomalies (direct or indirect) and construct a model that explains them and makes some unique dark matter signature at colliders. The particle physics community, sitting on its thumbs while delays to the Large Hadron Collider (LHC) dampened their expectations of when to expect signals of new physics, was eager to pick up the trend. Thus came a renewed emphasis on direct production (collider signatures) of dark matter:

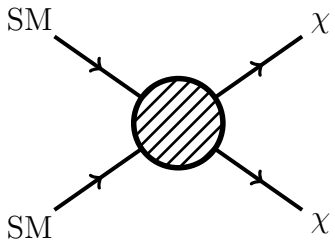

Note that this is just related by crossing symmetry to our picture of indirect detection. Thus even for 'phenomenological' models with arbitrary couplings and sectors, one would necessarily expect there to be some collider given sufficient luminosity and energy.

One effect of this resurgence was the cautious re-admittance of DAMA into the group of viable dark matter hints. While other direct detection experiments had seemed to rule out DAMA assuming a neutralino-like WIMP, these new models had various ways to be simultaneously consistent with the DAMA annual modulation and the other direct detection constraints [86]. As will be discussed below, one easy way to do this is to have dark matter with predominantly spin-dependent coupling [87] since DAMA's NaI detector material is notably more sensitive to such couplings compared to the Si and Ge targets used for the other existing direct detection bounds. An additional handle comes from including channelling and blocking effects [88] in DAMA [89] (these effects seem to only be particularly relevant for DAMA's NaI crystals and do not affect other existing direct detection experiments).

Finally, the most recent hints for dark matter come from the CDMS and CoGeNT collaborations. In December of 2009, CDMS announced two events that they could not rule out as dark matter hits [58]; see also [57] for recorded seminars announcing this result. While this is nowhere near a 'discovery,' optimists hope that this is a harbinger of actual events in the next generation of direct detection experiments (some of which are the subject of the rest of this exam). Finally, just a two months before the preparation of this document, the CoGeNT collaboration released a similar 'hint' that could be interpreted as a dark matter event [90]. It is perhaps interesting to note that while the CoGeNT and DAMA signal regions appear mutually exclusive, invoking the

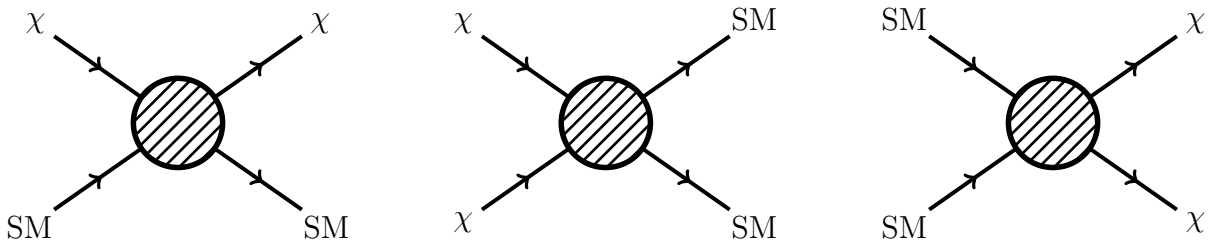

(a) Direct detection (b) Indirect detection (c) Collider production

Figure 1: Unknowns in dark matter experiments. (1a) What are the quark couplings? (1b) What are the final states? (1c) What are the parent species? This should be compared to the three wise monkeys: See no evil, hear no evil, speak no evil.

channeling effects of the previous paragraph appears to give enough of a handle to allow the two regions to overlap outside of the region that is otherwise excluded by direct detection.

To close, we remark that a proper experimental understanding of dark matter can only come from combined results from all three methods of detection (direct, indirect, and collider); each method is complementary in that each depends on a different source of unknown input. These are summarized in Fig. 1a.

3 WIMP Relic Density

Here we will assume that dark matter is a thermal WIMP, i.e. a species that was in thermal equilibrium before freezing out and leaving a relic density. This means that freeze-out occurs when the WIMP species are nearly at rest; for an 'improved analysis' of the abundance of a stable particle that does not depend on the low relative velocities, see the article by Gelmini and Gondolo [91]. Recently others have begun to explore the possibilities for non-thermal relics through the 'freeze-in' of hidden sector species [92].

The primary references we will follow are Dodelson [1] and Kolb & Turner [2]. (Dodelson is more readable, while Kolb & Turner are more thorough. Both are rather old.) For a summary of more 'recent' developments as of 1991, see Griest and Seckel and the references therein [93]. For the current draft, this derivation very closely follows Dodelson. Note that Kolb & Turner have a slightly different treatment in which they use the entropy density of the universe as a fiducial quantity. For a nice (and one of the first) treatment, see [94].

3.1 The Boltzmann Equation

For a general derivation, see Appendix D. The main idea is that particles were in thermal equilibrium with the early universe. This means that the production rate of particles from the thermal bath is equivalent to the annihilation rate, Γ. If we adiabatically lowered the temperature of a static universe below the DM mass, then the DM abundance would freeze out to a value that is thermally suppressed by $\exp(-m/T)$. However, we know that the universe is expanding at a rate

given by the Hubble parameter H. Because of this, freeze-out occurs when the expansion rate overtakes the annihilation rate, $H \gg \Gamma$.

The Boltzmann equation quantifies this picture and can be written as

$$a^{-3}\frac{d(na^3)}{dt} = \langle\sigma v\rangle\left[(n_{\rm EQ})^2 - n^2\right], \tag{3.1}$$

where a is the scale factor, n is the dark matter number density, $n_{\rm EQ}$ is the equilibrium number density,

$$n_{{\rm EQ},i} \equiv g_i \int \frac{d^3p}{(2\pi)^3} e^{-E_i/T} \begin{cases} g_i \left(\frac{m_i T}{2\pi}\right)^{3/2} e^{-m_i/T} \\ g_i \frac{T^3}{\pi^2} \end{cases}, \tag{3.2}$$

where g_i is the number of degrees of freedom for the field. The general Boltzmann equation is derived in Appenxix D; see also statistical physics textbooks, Kolb & Turner [2], and Dodelson [1]. To simplify this, use the fact that (aT) is independent of t so that one can write $na^3 = na^3T^3/T^3$ and pull a factor of $(aT)^3$ out of the time derivative. It is convenient to write these quantities in terms of dimensionless quantities

$$Y \equiv \frac{n}{T^3} \sim \frac{n}{s} \qquad\qquad x = \frac{m}{T}. \tag{3.3}$$

These quantities are useful not only because they're dimensionless, but because of their scaling properties. For example, the cubed temperature scales like R^{-3} so that $\dot{s} + 3Hs = 0$. Compare this to the Boltzmann equation, which can be written as $\dot{n} + 3Hn = \langle\sigma v\rangle\left[(n_{\rm EQ})^2 - n^2\right]$. Using the variable Y cancels the $3H$ term.

Let's now rewrite the Boltzmann equation in a few steps,

$$\frac{dY}{dt} = T^3\langle\sigma v\rangle\left(Y_{\rm EQ}^2 - Y^2\right), \tag{3.4}$$

where $Y_{\rm EQ} = n_{\rm EQ}/T^3$. See (C.28) for the non-relativistic expression of $n_{\rm EQ}$.

Alternate formulations. We can write the Boltzmann equation in different ways depending on how we define Y [94]. For example, for $Y = n/s$, n/s_γ, or n/n_γ, we have

$$\dot{Y} = \langle\sigma v\rangle \begin{pmatrix} s \\ s_\gamma \\ n_\gamma \end{pmatrix} \left(Y^2 - Y_{\rm EQ}^2\right). \tag{3.5}$$

Note that there are some prefactors that come along with whether one chooses $Y = n/T^3$ or $Y = n/s$, the two most common conventions. The relevant conversion is

$$s = \frac{2\pi^2}{45} g_{*s} T^3. \tag{3.6}$$

For a rough derivation see the discussion before (C.46). If you ever compare to other literature, e.g. Kolb & Turner, *remember this conversion factor.*

We now change variables from t to x, for which we need $dx/dt = Hx$. In particular, since dark matter production typically occurs in the radiation era where energy density scales like T^4, the Hubble parameter is $H = H(m)/x^2$ so that

$$\frac{dY}{dx} = -\frac{\lambda}{x^2}\left(Y^2 - Y_{\rm EQ}^2\right), \tag{3.7}$$

where the parameter λ relates the annihilation rate to the expansion rate of the universe,

$$\lambda = \frac{m^3\langle\sigma v\rangle}{H(m)}. \tag{3.8}$$

For s-wave processes λ is constant, but in principle one can have some temperature dependence in $\langle\sigma v\rangle$. In general, we should write $\langle\sigma v\rangle(x)$ and $\lambda(x)$.

For reference, you might want to recall the cosmological formulae

$$H(T)^2 = \frac{8\pi}{3}G\rho(T) \tag{3.9}$$

$$\rho_R(T) = \frac{\pi^2}{30}g_* T^4, \qquad \text{(radiation dominated)} \tag{3.10}$$

where $H = (\dot{a}/a)$ and ρ_R is the energy density of relativistic species; see (C.9) and (C.35). Note that $8\pi G = 1/M_{\rm Pl}^2$.

Before proceeding, let us discuss the qualitative solution to (3.7). While the annihilation rate $\Gamma \sim \langle\sigma v\rangle T^3$ is much greater than the expansion rate H, the 'number density' Y remains in thermal equilibrium and tracks $Y_{\rm EQ}$. This is because λ is large and Y wants to change to match $Y_{\rm EQ}$. However, λ is decreasing. Eventually $\Gamma \approx H$ at some 'time' x_f. From that point on, dY/dx becomes small and Y doesn't want to change. We're left with $Y(x) \approx Y(x_f)$ so that the number of particles per comoving volume has frozen out. For neutrinos this occurs while the species are still relativistic, see Appendix C.7. For WIMPs, this occurs when the particles are already non-relativistic.

3.2 Solving the Boltzmann equation: s-wave

Unfortunately, (3.7) is a type of Riccati equation with no analytic solution. Despite not being exactly solvable, we can still see this through by invoking some physics intuition. We know that most of the action happens at $x \sim 1$. In this region, we can see that the left-hand side of (3.7) is $\mathcal{O}(Y)$ while the right-hand side is $\mathcal{O}(\lambda Y^2)$. We will see shortly that $\lambda \gg 1$, so the right-hand side must have a cancellation in the $Y^2 - Y_{\rm EQ^2}$ term.

After freeze out, $Y_{\rm EQ}$ will continue to decrease according to the thermal suppression $\exp(-m/T)$ so that $Y \gg Y_{\rm EQ}$. This happens at late times $x \gg 1$ where the Boltzmann equation reduces to

$$\frac{dY}{dx} \approx -\frac{\lambda(x)}{x^2}Y^2. \tag{3.11}$$

This is not yet solvable due to the x-dependence of λ coming from the temperature dependence of $\langle\sigma v\rangle$.

Since we assume freeze-out occurs when WIMPs are non-relativistic, we may expand $\langle \sigma v \rangle = a + bv^2 + \cdots$, where a corresponds to an s-wave piece, b corresponds to a p-wave (and some s-wave) piece, and so forth. For now, let us assume that the process is s-wave so that we may drop all powers of v^2 from the thermally-averaged cross section. In this case $\lambda(x) = \lambda$.

This is now a tractable differential equation which we *can* solve. The trick will be to match the solution in the asymptotic future to a good approximation at $x \sim 1$; i.e. we go from an intractable ODE (3.7) to a solvable ODE (3.11) at the cost of determining a boundary condition. The solution of (3.11) is

$$\frac{1}{Y_\infty} - \frac{1}{Y_f} = \frac{\lambda}{x_f}, \tag{3.12}$$

where Y_∞ is the asymptotic dimensionless number density and Y_f is the value at the freeze out boundary condition x_f. Typically $Y_f \gg Y_\infty$ so that we may approximate this solution as

$$Y_\infty \approx \frac{x_f}{\lambda}. \tag{3.13}$$

A simple order of magnitude estimate for this solution is $x_f \sim 10$; more precise values are on the order of $x_f \approx 20$ or 25. At this level plugging in this value is a kludge. A more honest approximation comes from solving

$$n_{\mathrm{EQ}}(x_f)\langle \sigma v \rangle = H(x_f). \tag{3.14}$$

We give an even more explicit expression below. The plot for the dark matter relic density is well-known[7]. The qualitative features are as follows:

- Y tracks its equilibrium value Y_{EQ} until $x \sim 10$, and then levels off to a frozen-out constant.
- As one increases the annihilation cross section, the freeze out time is later.
- The distinction between Bose and Fermi statistics is negligible by the time the dark matter species freezes out. (The use of Boltzmann statistics was assumed in when we wrote the Boltzmann equation.)

3.3 Solving the Boltzmann equation: general

Before moving on, let's turn to a more general solution to the Boltzmann equation that extends our s-wave analysis above. The general conclusions are the same, so we'll focus on some technical details. We will follow Scherrer and Turner [94]. Useful note: that paper uses $Y = n/s$, which differs from our definition of Y by the overall conversion factor in (3.6).

Suppose that in a velocity expansion, the leading order term in the thermally averaged cross section goes like the p-th power of v,

$$\langle \sigma v \rangle \propto v^p. \tag{3.15}$$

[7]It is notoriously difficult to plot in *Mathematica*; see homework 5 from Hitoshi Murayama's Physics 229C course for suggestions: `http://hitoshi.berkeley.edu/229C/index.html`.

For s-wave $p = 0$, while for p-wave $p = 2$, and so forth. From the Boltzmann velocity distribution, we know that $\langle v \rangle \sim \sqrt{T}$ so that we may write

$$\langle \sigma v \rangle \propto x^{-n}, \tag{3.16}$$

where $n = p/2$. If we write $\langle \sigma v \rangle = \langle \sigma v \rangle_0 x^{-n}$, then we may define

$$\lambda_0 = \frac{m^3 \langle \sigma v \rangle_0}{H(m)} = \lambda x^n. \tag{3.17}$$

In this way λ_0 is independent of x. In this way we may pull out the x-dependence from λ in (3.7),

$$\frac{dY}{dx} = -\frac{\lambda_0}{x^{2+n}} \left(Y^2 - Y_{\rm EQ}^2 \right). \tag{3.18}$$

We will rewrite this in terms of $\Delta \equiv Y - Y_{\rm EQ}$:

$$\frac{d\Delta}{dx} = -\frac{dY_{\rm EQ}}{dx} - \frac{\lambda_0}{x^{2+n}} \Delta (2Y_{\rm EQ} + \Delta). \tag{3.19}$$

Here we've just used $Y^2 - Y_{\rm EQ}^2 = (Y + Y_{\rm EQ})(Y - Y_{\rm EQ})$.

First consider the case where x is small; say $1 < x \ll x_f$. We'll give a more precise definition of x_f below. In this limit, we know that Y is very close to $Y_{\rm EQ}$ so that $\Delta \ll Y_{\rm EQ}$ and $|\Delta'| \ll -Y'_{\rm EQ}$, where we've written a prime to mean d/dx. In this regime we can algebraically solve (3.19):

$$\Delta = -\frac{dY_{\rm EQ}}{dx} \frac{x^{2+n}}{\lambda_0 (2Y_{\rm EQ} + \Delta)} \tag{3.20}$$

$$= \left(1 - \frac{3}{2x} \right) \frac{x^{2+n}}{\lambda_0 (2 + \Delta/Y_{\rm EQ})} \tag{3.21}$$

$$\approx \frac{x^{2+n}}{2\lambda_0}. \tag{3.22}$$

Here we have used $Y_{\rm EQ} = n_{\rm EQ}/T^3$ and (C.28), i.e.

$$Y_{\rm EQ} = \frac{g}{(2\pi)^{3/2}} x^{3/2} e^{-x} \equiv a x^{3/2} e^{-x}. \tag{3.23}$$

Now consider what happens when $x \gg x_f$. In this regime we know that $Y_{\rm EQ}$ is exponentially small compared to $\Delta \approx Y \gg Y_{\rm EQ}$. We can thus drop $Y_{\rm EQ}$ and $Y'_{\rm EQ}$ in (3.19) to obtain

$$\frac{d\Delta}{dx} = -\frac{\lambda}{x^{2+n}} \Delta^2. \tag{3.24}$$

Physically, particle creation has practically halted while annihilations are still somewhat important, leading to a slight reduction to Y compared to the value of $Y_{\rm EQ}$ at $\Gamma = H$ (the natural back-of-the-envelope rough estimate the for the relic abundance). Integrating this approximation from x_f—which we nebulously take to be the lower-limit of the valid range for this approximation—to $x = \infty$ gives

$$Y_\infty = \frac{(n+1)}{\lambda_0} x_f^{n+1}. \tag{3.25}$$

The importance of this quantity is that $Y(\text{today}) \approx Y_\infty$, i.e. *this* is what we plug into ρ_χ and Ω_χ to check if we've obtained the correct (observed) dark matter relic density. As mentioned in the simplified s-wave case, we've obtained this by resorting to an approximation in the $x \gg x_f$ case. The cost is that we've introduced a boundary condition at x_f, the freeze out 'time,' where we must match our approximation.

Now let's precisely define x_f. We are interested in the regime where $\Delta \approx Y_{\rm EQ}$. We define freeze-out precisely by the condition

$$\Delta(x_f) = cY_{\rm EQ}(x_f), \tag{3.26}$$

where $c = \mathcal{O}(1)$ and is determined empirically. We will plug into (3.19). We shall take two limits: first we will assume that $d\Delta/dx \ll 1$ and further that the particle is non-relativistic at freeze-out, in particular $x \gg 3/2$. The $3/2$ comes from $dY_{\rm EQ}/dx = a(3/2 - x)x^{1/2}e^{-x}$. Plugging in and solving gives,

$$e^{x_f} \approx \frac{a\lambda_0 c(2+c)}{x_f^{n+1/2}} \tag{3.27}$$

$$x_f \approx \ln\left[a\lambda_0 c(2+c)\right] - (n+1/2)\ln\ln\left[(2+c)\lambda_0 ac\right]. \tag{3.28}$$

Here we've further used the limit $x_f \gg 3/2$, as appropriate for a particle which is non-relativistic at freeze out. In (3.28) we now have a detailed expression for x_f which we may take as a definition.

One must still pick a value for c. It turns out that the best fit to numerical results sets

$$c(c+2) = n+1 \tag{3.29}$$

which is better than 5% for any $x_f \gtrsim 3$. Plugging in (3.17), (3.10), (3.9), and $M_{\rm Pl}^2 = 8\pi G$, we obtain:

$$a\lambda_0 = \frac{g}{(2\pi)^{3/2}} \cdot \frac{m^3}{H(m)}\langle\sigma v\rangle_0 \tag{3.30}$$

$$= \frac{g}{(2\pi)^{3/2}} \cdot m^3 \frac{1}{m^2}\frac{1}{\sqrt{8\pi G}}\sqrt{\frac{90}{\pi^2 g_*}}\langle\sigma v\rangle_0 \tag{3.31}$$

$$= \underbrace{\sqrt{\frac{45}{4\pi^5}}}_{\approx 0.19}\frac{g}{\sqrt{g_*}}\frac{m}{\sqrt{8\pi G}}\langle\sigma v\rangle_0. \tag{3.32}$$

Putting it all together,

$$x_f \approx \ln\left[\sqrt{\frac{45}{4\pi^5}}\frac{g}{\sqrt{g_*}}\frac{m}{\sqrt{8\pi G}}\langle\sigma v\rangle_0\right] - \left(n+\frac{1}{2}\right)\ln^2\left[\cdots\right], \tag{3.33}$$

where the second bracket contains the same junk as the first bracket. Note that the corrections to $x_f \approx 20$ (for s-wave) are only logarithmic. Note that we can write $m/\sqrt{8\pi G} = mM_{\rm Pl}$ where $M_{\rm Pl}$ is the *reduced* Planck mass, $M_{\rm Pl} = 2.44 \times 10^{18}$ GeV.

3.4 Solving Boltzmann Equation Again

For instructive purposes ("*just for shits and giggles*"), we'll re-do our derivation of the Boltzmann equation following Murayama-san's example in Homework #5 of his P229C (Fall 2007) course at Berkeley[8]. We will do this for two reasons: first it will be a quick way to go over the analogous formulae using the definition $Y = n/s$ rather than the Dodelson definition $Y = n/T^3$. More importantly, it will also illustrate the solution of the Boltzmann equation in *Mathematica*, including some of the numerical difficulties. Note, Hitoshi uses the *relativistic* formulae for some of his quantities, but at some point these appear to cancel out to give the same result as when one (correctly) uses the *nonrelativistic* versions.

In terms of $Y = n/s$ and $x = m/T$, the Boltzmann equation is

$$\frac{dY}{dx} = -\frac{1}{x^2}\frac{s(m)}{H(m)}\langle\sigma v\rangle\left(Y^2 - Y_{\rm EQ}\right) \tag{3.34}$$

We can then plug in (3.6), (3.10), and (3.9),

$$\frac{s(m)}{H(m)} = \frac{2\pi^2}{45}g_{*s}m^3\left(\frac{8\pi G}{3}\frac{\pi^2}{30}g_* m^4\right)^{-1/2} \tag{3.35}$$

$$= \underbrace{\left(\frac{2\pi\sqrt{90}}{45}\right)}_{\approx 1.32}\frac{g_{*s}}{\sqrt{g_*}}\frac{m}{\sqrt{8\pi G}}. \tag{3.36}$$

Note that $1/\sqrt{8\pi G} \sim M_{\rm Pl,red} \approx 0.2\, M_{\rm Pl,true}$. In most of this document we'll use $M_{\rm Pl} = M_{\rm Pl,red}$, the reduced Planck ass. Kolb and Turner use the 'true' Planck mass. To avoid confusion, in this section we'll keep factors of $\sqrt{8\pi G}$ explicit as long as we can.

The equilibrium number density is $Y_{\rm EQ} = n_{\rm EQ}/s$,

$$Y_{\rm EQ} = g\left(\frac{mT}{2\pi}\right)^{3/2} e^{-m/T}\cdot\left(\frac{2\pi^2}{45}g_{*s}T^3\right)^{-1} \tag{3.37}$$

$$= \underbrace{\left(\frac{45}{2\pi^4}\sqrt{\frac{\pi}{8}}\right)}_{\approx 0.145}\left(\frac{g}{g_{*s}}\right)x^{3/2}e^{-x} \equiv a x^{3/2}e^{-x}, \tag{3.38}$$

where we're using the non-relativistic expression for $n_{\rm EQ}$ with zero chemical potential. Note that g is the number of internal degrees of freedom for the dark matter, e.g. $g = 2$ for a Majorana fermion.

Let us also expand $\langle\sigma v\rangle = \langle\sigma v\rangle_0 x^{-n}$, dropping higher angular momentum contributions. We then have

$$\frac{dY}{dx} = \frac{-\lambda}{x^{2+n}}\left(Y^2 - Y_{\rm EQ}^2\right) \qquad\qquad \lambda = \frac{s(m)}{H(m)}\langle\sigma v\rangle_0. \tag{3.39}$$

[8] `http://hitoshi.berkeley.edu/229C/index.html`

This is now precisely the same form as (3.18), though since we are using $Y = n/s$ instead of $Y = n/T^3$, the definition of λ is different by a factor of $s(m)$. Note that this factor exactly cancels an additional factor of $1/s(m)$ in the 'a' coefficient of (3.38). The combination λa is indeed independent of how we defined Y. In particular, (3.33) and (3.25) still hold with the new definition of λ in (3.39).

Now let's go in a different direction and see how we can numerically solve the Boltzmann equation in *Mathematica*. This is a notoriously difficult thing to do because in the interesting region, the Boltzmann equation depends on the small difference between two big numbers. (Specifically, the difference between two big numbers times a small number in the regime where the product becomes small.) Rushing naïvely into solving the equation can lead to numerical instabilities and grumpy code. One trick is to try to and rescale to use variables where large factors (like $M_{\rm Pl} \sim 1/\sqrt{G}$) naturally are cancelled against small factors (like $\langle\sigma v\rangle_0$). Let's start again with the Boltzmann equation, expanded slightly:

$$\frac{dY}{dx} = -\frac{s(m)}{H(m)}\frac{\langle\sigma v\rangle_0}{x^{2+n}}\left(Y^2 - Y_{\rm EQ}^2\right). \tag{3.40}$$

We can shift by the x-independent prefactor by defining a variable

$$y \equiv \frac{s(m)}{H(m)}\langle\sigma v\rangle_0 Y = \lambda Y. \tag{3.41}$$

Multiplying both sides of the Boltzmann equation by λ we obtain

$$\frac{dy}{dx} = \frac{-1}{x^{2+n}}\left(y^2 - y_{\rm EQ}^2\right) \tag{3.42}$$

$$y_{\rm EQ} = a\frac{s(m)}{H(m)}\langle\sigma v\rangle_0 x^{3/2}e^{-x} \tag{3.43}$$

$$= \underbrace{\left(\frac{45}{2\pi^4}\sqrt{\frac{\pi}{8}}\right)}_{\approx 0.145}\underbrace{\left(\frac{2\pi\sqrt{90}}{45}\right)}_{\approx 1.32}\frac{g}{\sqrt{g_*}}\frac{m}{\sqrt{8\pi G}}\langle\sigma v\rangle_0 x^{3/2}e^{-x} \tag{3.44}$$

$$= 0.192\frac{g}{\sqrt{g_*}}\frac{m}{\sqrt{8\pi G}}\langle\sigma v\rangle_0 x^{3/2}e^{-x} \tag{3.45}$$

We see that all of the *physics* has been crammed into the prefactor of $y_{\rm EQ}$. Let's throw some typical numbers in: we assume two degrees of freedom (e.g. a Majorana fermion) $g = 2$, normalize about $g_* = 100$, $m = 1000$ GeV. The reduced Planck mass is $M_{\rm Pl} = (8\pi G)^{-1/2} = 2.44 \times 10^{18}$ GeV. We'll throw in a typical 'weak-ish scale' cross section with $\langle\sigma v\rangle_0 = 10^{-10}$ GeV-2. This leaves us with

$$y_{\rm EQ} = \left(9.34 \times 10^9\right)\frac{g}{2}\sqrt{\frac{100}{g_*}}\left(\frac{m}{1000\text{ GeV}}\right)\left(\frac{\langle\sigma v\rangle_0}{10^{-10}\text{ GeV}^{-2}}\right)x^{3/2}e^{-x}. \tag{3.46}$$

Let's go ahead and use these 'default' values in a plot. We'd like to set boundary conditions $Y = Y_{\rm EQ}$ at $x = 0$, but this is of course outside of the range of validity of the non-relativistic

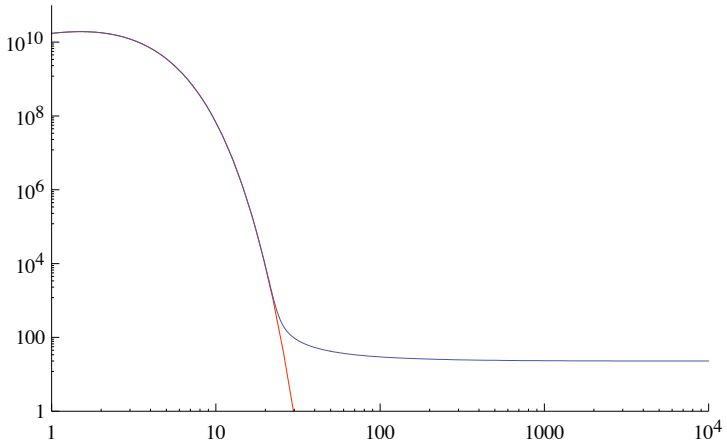

Figure 2: Output of our toy freeze out calculation in *Mathematica*. The blue line is the plot of Y by x, while the red line plots $Y_{\rm EQ}$.

expressions we used. Instead, we'll settle on $Y = Y_{\rm EQ}$ at $x = 1$ and verify *a posteriori* that there is no strong dependence on x.

Let's start with the case of s-wave annihilation, $n = 0$. To avoid numerical issues, start by integrating y from $1 < x < 50$.

```
MyAssumptions = {m -> 1000, g -> 100, \[Sigma] -> 10^-10,
   Subscript[M, Pl] -> 2.44 10^18};
solution1 =
  NDSolve[{y'[
       x] == -(1/
        x^2) (y[x]^2 - (0.192 Subscript[M, Pl] m \[Sigma] x^(3/2)
           E^-x)^2),
     y[1] == 0.192 Subscript[M, Pl] m \[Sigma] 1^(3/2) E^-1} /.
    MyAssumptions, y, {x, 1, 50}];
bc = Evaluate[y[50] /. solution1];
```

Evaluating y at $x = 50$ gives 42.14. We'll use this as a boundary condition for the remainder of the range, say up to $x = 10,000$:

```
solution2 =
  NDSolve[{y'[
       x] == -(1/
        x^2) (y[x]^2 - (0.192 Subscript[M, Pl] m \[Sigma] x^(3/2)
           E^-x)^2), y[50] == bc} /. MyAssumptions,
   y, {x, 50, 10000}];
```

We can now patch together the solutions in a nice plot

```
LogLogPlot[Evaluate[y[x] /. solution1], {x, 1, 50},
  PlotRange -> {{1, 10000}, {1, 10^11}}];
LogLogPlot[Evaluate[y[x] /. solution2], {x, 50, 10000},
  PlotRange -> {{1, 10000}, {1, 10^11}}];
```

```
Show[%, %%]
```

This yields the blue line in Fig. 2. Next we can also plot the equilibrium solution,

```
LogLogPlot[
  0.192 Subscript[M, Pl] m \[Sigma] x^(3/2) E^-x /. MyAssumptions, {x,
    1, 1000}, PlotRange -> {{1, 10000}, {1, 10^11}},
  PlotStyle -> RGBColor[1, 0, 0]];
Show[%, %%]
```

This produces the red line in Fig. 2.

What we notice is that Y closely tracks $Y_{\rm EQ}$ until $x = x_f \approx 20$. In Fig. 3 you can see that this is a fairly robust value. The value of Y then freezes out after x_f and becomes constant. We thus verify that it does not really matter where we pick our boundary condition when solving the differential equation; as long as we're in a regime where $x \lesssim 10$, $Y = Y_{\rm EQ}$ is a reliable boundary condition. To verify this point, we may plot the ratio of $Y_{\rm EQ}/Y$,

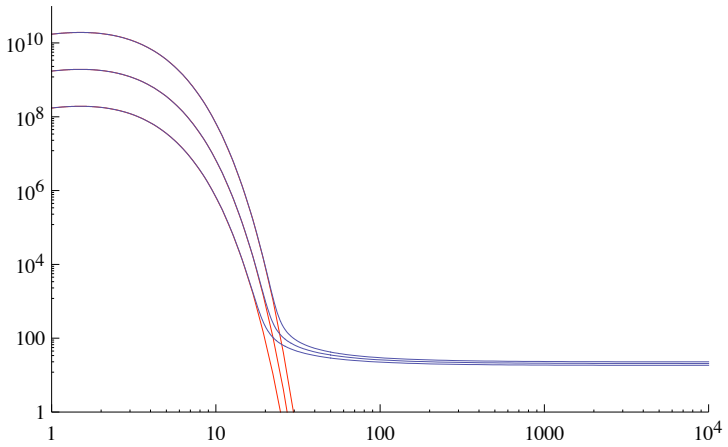

Figure 3: Varying $\langle\sigma v\rangle_0$: 10^{-10} GeV^{-2}, 10^{-11} GeV^{-2}, 10^{-12} GeV^{-2}.

```
LogLinearPlot[
 0.192 Subscript[M, Pl] m \[Sigma] x^(3/2)
   E^-x/Evaluate[y[x] /. solution1[[1]]] /. MyAssumptions, {x, 1, 50},
  PlotStyle -> RGBColor[1, 0, 0]]
```

which produces the plot in Fig. 4. You can check that the value of $y(\infty)$ is relatively insensitive to the dark matter mass m by varying the latter by an order of magnitude. As noted in our analytic work above, the deviation is logarithmic at leading order. This is shown in Fig. 5.

You can go ahead and modify the expressions above to generate the relevant plots for p-wave annihilation.

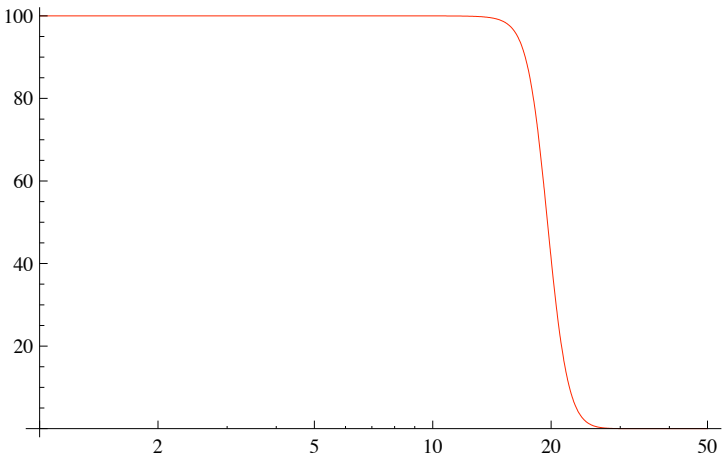

Figure 4: A plot of $Y/Y_{\rm EQ}$ as a function of x showing that we are free to use $Y = Y_{\rm EQ}$ as a boundary condition for any value of $x \lesssim 10$.

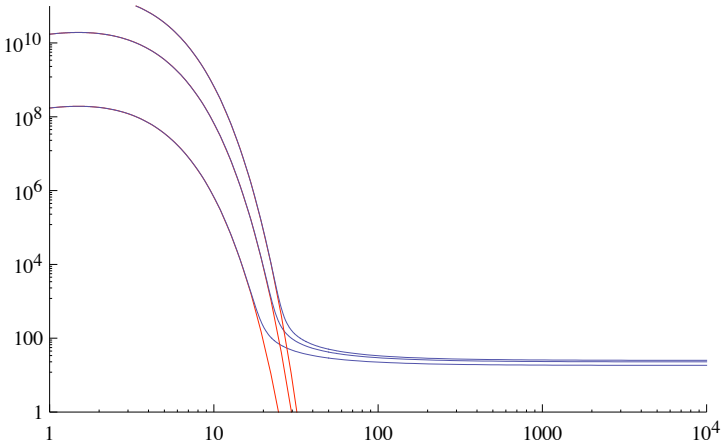

Figure 5: A plot of Y as a function of x for $m = 10,\ 10,000,\ 1,000,000$.

3.5 Abundance

Once a particle has frozen out, its number density falls off according to the scale factor, a^{-3}. Thus the [mass] density today is $m(a_1/a_0)^3 n$, where a_1 is assumed to be at a sufficiently late time that $Y \approx Y_\infty$. Recall that the number density at this late time is $n = Y_\infty T_1^3$. Thus the mass density today is

$$\rho = m Y_\infty T_0^3 \left(\frac{a_1 T_1}{a_0 T_0}\right)^3 \approx \frac{m Y_\infty T_0^3}{30}. \tag{3.47}$$

This last equality is exercise 11 of Dodelson's text (the solution is in the back); the point is that aT is not constant due to the reheating of photons from the annihilation of particles between 1 MeV and 100 GeV. Note that we've gone back to our normalization $Y = n/T^3$.

The relevant number to match is the fraction of the present-day critical density coming from χ, using (3.8):

$$\Omega_\chi = \frac{x_f}{\lambda}\frac{m T_0^3}{30\rho_{\rm crit}} = \frac{H(m) x_f T_0^3}{30 m^2 \langle\sigma v\rangle \rho_{\rm crit}}. \tag{3.48}$$

Recall that $\rho_{\rm crit} = 3H_0^2/8\pi G$. Using (3.9) and (3.10), the Hubble rate at $T = m$, which we assume to be during the radiation era, is

$$H(T) = T^2\sqrt{\frac{4\pi^3 G g_*(T)}{45}}, \tag{3.49}$$

where $g_*(T)$ is the effective number of degrees of freedom at temperature T, see Fig. 6 or Fig. 10 in Appendix C. Plugging $H(m)$ into the expression for Ω_χ shows that the latter quantity does not depend on the dark matter mass m except through the implicit dependence in x_f and g_*. This provides an important lesson: the relic abundance is primarily controlled by the cross section, $\langle\sigma v\rangle$.

The final expression is

$$\Omega_\chi = \sqrt{\frac{4\pi G g_*(m)\pi^3}{45}}\frac{x_f T_0^3}{30\langle\sigma v\rangle\rho_{\rm cr}} \tag{3.50}$$

$$= \sqrt{\frac{4\pi^3 g_*(m)}{45}}\frac{8\pi}{90 H_0^2}\frac{x_f}{\langle\sigma v\rangle}\frac{T_0^3}{M_{\rm Pl}^3} \tag{3.51}$$

$$= 0.3 h^{-2}\left(\frac{x_f}{10}\right)\left(\frac{g_*(m)}{100}\right)^{1/2}\frac{10^{-39}{\rm cm}^2}{\langle\sigma v\rangle}. \tag{3.52}$$

Assuming that χ makes up all of the dark matter, the correct density requires $\Omega_\chi = 0.3$. The $10^{-39}{\rm cm}^2$ cross section, which is right around what one would expect from a weakly interacting 100-ish GeV particle, is the "WIMP miracle."

3.5.1 Sanity check: another derivation

Just became I don't trust myself, let's re-do this derivation for $Y = n/s$. The dark matter density is

$$\rho = m Y_\infty s_0 = m\frac{s_0}{s(m)}\frac{H(m)}{\langle\sigma v\rangle_0} y_\infty, \tag{3.53}$$

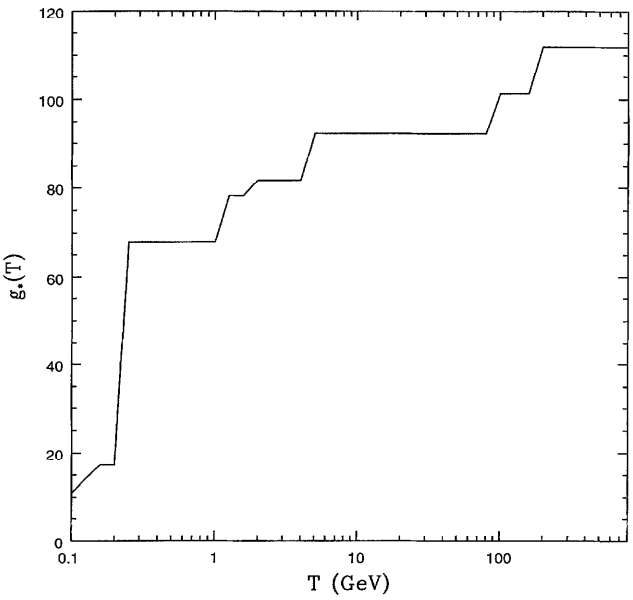

Figure 6: A plot of the number of relativistic degrees of freedom g_* as a function of temperature. Image from in Fig. 3 of JKG [95].

where y is given by (3.41). Further, we know from (3.25) that

$$Y_\infty = \frac{(n+1)}{\lambda} x_f^{n+1} \tag{3.54}$$

$$y_\infty = (n+1) x_f^{n+1}. \tag{3.55}$$

Now invoke the usual formulae (see... well, above all over the place)

$$\rho_{\rm crit} = \frac{3H_0^2}{8\pi G} \qquad H(T)^2 = \frac{8\pi G}{3} g_* \frac{\pi^2}{30} T^4 \qquad s(T) = \frac{2\pi^2}{45} g_* T^3. \tag{3.56}$$

We thus have

$$\Omega = \frac{\rho}{\rho_{\rm crit}} = m s_0 \left(\frac{2\pi^2}{45} g_* m^3 \right)^{-1} \sqrt{\frac{8\pi G}{3} g_* \frac{\pi^2}{30} m^4} \frac{(n+1) x_f^{n+1}}{\langle \sigma v \rangle_0} \times \frac{8\pi G}{3H_0^2} \tag{3.57}$$

$$= \underbrace{\left(\frac{45}{2\pi^2} \frac{1}{3} \sqrt{\frac{\pi^2}{90}} \right)}_{\approx 0.252} \frac{(n+1) x_f^{n+1} s_0}{g_* H_0^2 \langle \sigma v \rangle_0} (8\pi G)^{3/2} \tag{3.58}$$

Note that explicit factors of m have cancelled. We can now plug in $x_f \approx 20$, or whatever refinement thereof. The entropy of the universe today is given by the sum of the photon and neutrino entropies,

$$s_0 = s_{\gamma,0} + s_{\nu,0} = \left(1 + \frac{21}{22} \right) s_\gamma = \frac{43}{22} 2 \frac{2\pi^2}{45} T_0^3 = 2890 \text{ cm}^{-3}. \tag{3.59}$$

(Check this.) We have used $\hbar c = 0.1973 \times 10^{-4}$ MeV cm and $T_0 = 2.725$ K with K $= 8.617 \times 10^{-5}$ MeV. The Hubble constant is

$$H_0 = 100\,h \text{ km sec}^{-1} \text{ Mpc}^{-1} = 2.131 \times 10^{-42} \text{ GeV}h. \tag{3.60}$$

We end up with (recalling $\langle\sigma v\rangle = \langle\sigma v\rangle_0 x^n$)

$$\Omega h^2 = 0.0845 \times (n+1) x_f^{n+1} \times \sqrt{\frac{100}{g_*}} \left(\frac{10^{-10} \text{ GeV}^{-2}}{\langle\sigma v\rangle_0} \right). \tag{3.61}$$

For an s-wave process ($n = 1$) we obtain

$$\Omega h^2 = 1.69 \times \frac{x_f}{20} \sqrt{\frac{100}{g_*}} \left(\frac{10^{-10} \text{ GeV}^{-2}}{\langle\sigma v\rangle_0} \right). \tag{3.62}$$

Since we want $\Omega h^2 = 0.12$, this is too large. We need to enhance the annihilation cross section by about an order of magnitude to reduce the relic abundance.

3.6 Mini-summary: the Boltzmann Equation

A few quick formulae in one place. We use the definition $Y = n/T^3$, which differs from $Y = n/s$ by the factor in (3.6). This modifies the definitions of λ according to (3.39).

$$\frac{dY}{dx} = \frac{-\lambda}{x^2} \left(Y_{\text{Eq}}^2 - Y^2 \right) \tag{3.63}$$

$$\lambda = \frac{m^3 \langle\sigma v\rangle}{H(m)} \tag{3.64}$$

$$H^2(T) = \frac{\rho(T)}{\rho_{\text{crit}}} H_0^2 = \frac{8\pi}{3} G\rho(T) \tag{3.65}$$

$$\rho_R(T) = \frac{\pi^2}{30} g_* T^4 \tag{3.66}$$

$$\rho_{\text{crit}} = \frac{3H_0^2}{8\pi G} = \frac{3}{8\pi} H_0^2 M_{\text{Pl}}^2 \tag{3.67}$$

$$Y_{\text{EQ}} = \frac{g}{(2\pi)^{3/2}} x^{3/2} e^{-x}. \tag{3.68}$$

In the radiation era $H(T)$ is given by (3.49). Long after freeze-out, we may use $Y \gg Y_{\text{Eq}} \sim e^{-m/T}$ to solve the Boltzmann equation up to a boundary condition at freezeout, x_f:

$$Y_\infty = \frac{n+1}{\lambda_0} x_f^{n+1} = \frac{n+1}{\lambda} x_f \tag{3.69}$$

$$\langle\sigma v\rangle = \langle\sigma v\rangle_0 x^n \tag{3.70}$$

$$\lambda_0 = \frac{m}{\sqrt{8\pi G}} \sqrt{\frac{90}{\pi^2 g_*}} \langle\sigma v\rangle_0 = \lambda x^{-n} \tag{3.71}$$

$$x_f \approx 20, \tag{3.72}$$

or, more precisely,

$$x_f \approx \ln\left[\sqrt{\frac{45}{4\pi^5}}\frac{g}{\sqrt{g_*}}\frac{m}{\sqrt{8\pi G}}\langle\sigma v\rangle_0\right] - \left(n+\frac{1}{2}\right)\ln^2[\cdots] \tag{3.73}$$

Finally, we have a useful numerical value:

$$\Omega h^2 = 0.0845 \times (n+1)x_f^{n+1}\sqrt{\frac{100}{g_*}}\left(\frac{10^{-10}\text{ GeV}^{-2}}{\langle\sigma v\rangle_0}\right) \tag{3.74}$$

Note that in the above formulae we write $M_{\rm Pl}$ to mean the *reduced* Planck mass, $8\pi G = M_{\rm Pl}^{-2}$. If you're concerned about any ambiguities, stick with equations written in terms of G.

3.7 Polemics: WIMP agnosticism

[**Flip:** need to include citations from GFDM paper]

The WIMP miracle is often presented as strong evidence for new terascale physics connected to electroweak symmetry breaking. However, this should be taken with a grain of salt. First the statement of the WIMP miracle is valid only at the "within a few orders of magnitude" level. Note that a typical weak cross section is $\langle\sigma v\rangle \sim \text{pb} = 10^{-36}\text{ cm}^2$, so that some amount of tuning is required in the WIMP coupling.

A more sobering restriction comes from a tension between the correct relic abundance and recent direct detection bounds. As of the writing of this paragraph, XENON100 has set an upper limit on the spin-independent elastic WIMP-nucleon cross section on the order of $\sigma_{\rm SI} = 7.0\times10^{-45}\text{ cm}^2 = 7.0\times10^{-9}$ pb for a 50 GeV WIMP at 90% confidence. A very naive assumption is that the annihilation cross section should be roughly of the same order as the direct detection cross section, and so there appears to be significant tuning required to generate a difference on the order of several orders of magnitude between the two processes.

As a case study, consider the plight of the MSSM. The prototypical MSSM WIMP is a neutralino (the LSP) whose abundance is protected by R-parity. A standard approach is to consider parameters in which the direct detection bounds are satisfied and then attempt to boost the relic density using handy tricks (i.e. tuning). For example, for a pure bino LSP one could set up coannihilations due to an accidental slepton degeneracy or resonant annihilations (e.g. a Higgs resonance). Alternately, one may note that Higgsinos and winos have annihilation cross sections that are typically too *large* allows one to tune the LSP to be a specific combination of bino, Higgsino, and wino to generate the correct abundance. The parameter space for the latter 'well-tempered neutralino' scenario, however, is now strongly constrained by XENON100.

There remain ways to generate honest-to-goodness WIMPs in models of new physics, but these appear to be rather special cases in extended models rather than generic phenomena.

Counterpoint: even though there appears to be a 10^{few} tuning required, one may argue that there is still a 'miracle' because of the orders of magnitude that have to cancel. People point out the $(T_0/M_{\rm Pl})^3$ factor in the explicit formulae above. Of course, the point is that the smallness of $(T_0/M_{\rm Pl})^3$ is balanced by the smallness (weak scale cross section) of $\langle\sigma v\rangle$. In this sense it's a coincidence between the Weak scale, the Planck scale, and the CMB scale. (And note, very importantly, that it is *independent* of the WIMP mass up to logarithmic corrections.) Is this a miracle?

3.8 Thermally averaged cross section & identical particles

Note that v is the *relative* velocity, so that each of the initial state χ particles in the annihilation process has velocity $v/2$. The definition of $\langle\sigma v\rangle$ is given below in (B.21). Compared to the usual definition of σ in Peskin & Schröeder, (B.15), the thermal average includes an integral over the *initial* state momenta weighted by the Maxwell-Boltzmann contribution.

Practically, we don't need to do the thermal average over and over again for each cross section. Instead, we expand in powers of v^2 and insert the moments of the Maxwell-Bolztman velocity distribution. Typically one only needs the first or second term to get the relevant behavior. Thus we would like to find

$$\sigma v = a + bv^2 + \cdots . \tag{3.75}$$

The thermal average gives $\langle v^2\rangle = 6/x_f$, for example. Note that the overall prefactor $1/|v_a - v_b| = 1/v$ in the expression for $d\sigma$ cancels in σv.

The annihilation cross section is given by

$$d\sigma = \frac{1}{2E_a 2E_b |v_a - v_b|}\left(\prod_f \frac{d^3p_f}{(2\pi)^3}\frac{1}{2E_f}\right)(2\pi)^4\delta^{(4)}\left(p_a^\mu + p_b^\mu - \sum_f p_f^\mu\right)|\mathcal{M}|^2_{\text{s.a.}}, \tag{3.76}$$

where $|\mathcal{M}|^2$ should be understood to mean the spin averaged squared amplitude. The two-body phase space is,

$$d\text{PS}_2(p_1,p_2) = \left(\prod_f \frac{d^3p_f}{(2\pi)^3}\frac{1}{2E_f}\right)(2\pi)^4\delta^{(4)}\left(p_a^\mu + p_b^\mu - \sum_f p_f^\mu\right) = \frac{d\Omega_{\text{CM}}}{4\pi}\frac{1}{8\pi}\left(\frac{2|\mathbf{p_1}|}{E_{\text{CM}}}\right). \tag{3.77}$$

Here 1 and 2 label *final* state particles.

At this stage there are model-dependent factors of two which become important. Focusing on the case of $2 \to 2$ annihilations, we are concerned about symmetry factors which pop up for identical initial states (e.g. Majorana fermion dark matter) and identical final states.

First consider the *initial* states. Suppose the two initial state dark matter particles are identical. There is *no* additional factor of two coming from identical initial states. Here's a paragraph from Dreiner, Haber, and Martin [96]:

> Recall the standard procedure for the calculation of decay rates and cross-sections in field theory—*average over unobserved degrees of freedom of the initial state and sum over the unobserved degrees of freedom of the final state.* This mantra is well-known for dealing with spin and color degrees of freedom, but it is also applicable to degrees of freedom associated with global internal symmetries. Thus, the cross-section for the annihilation of a Dirac fermion pair into a neutral scalar boson can be obtained by computing the *average* of the cross-sections for $\xi_1(\mathbf{p_1}, s_1)\xi_2(\mathbf{p_2}, s_2) \to \phi$ and $\xi_2(\mathbf{p_1}, s_1)\xi_2(\mathbf{p_2}, s_2) \to \phi$. [Here ξ is an uncharged, massive, $(1/2, 0)$ fermion.] Since the annihilation cross-sections for $\xi_1\xi_1$ and $\xi_2\xi_2$ are equal, we confirm the resulting annihilation cross-section for the Dirac fermion pair obtained above in the χ–η basis. [Here $\Psi_{\text{D}} = (\chi, \eta^\dagger)^T$].

Thus there are *no additional factors* in the thermally averaged annihilation cross section $\langle \sigma v \rangle$ coming from having identical Majorana dark matter particles. (It is trivial that the above argument carries over to the case of where the particles have arbitrary spin.)

This should not be confused with the factor of 1/2 which appears when calculating **indirect detection** rates, which comes from the number densities in the flux,

$$\frac{d^2N}{dAdT} \sim \int d\ell \; n_1 n_2 \langle \sigma v \rangle. \tag{3.78}$$

This is explained by Dreiner et al. as follows,

> We assume that the number density of Dirac fermions and antifermions and the corresponding number density of Majorana fermions are all the same (and denoted by n). Above, we showed that σ is the same for the annihilation of a single species of Majorana and Dirac fermions. For the Dirac case, $n_1 n_2 = n^2$. For the Majorana case, because the Majorana fermions are identical particles, given N initial state fermions in a volume V, there are $N(N-1)/2$ possible scatterings. In the thermodynamic limit where $N, V \to \infty$ at fixed $n \equiv N/V$, we conclude that $n_1 n_2 = n^2/2$ for a single species of annihilating Majorana fermions. Hence the event rate of a Dirac fermion-antifermion pair is double that of a single species of Majorana fermions.

The factor of 1/2 is explained in [97] and is consistent with the interpretation of a Dirac fermion as a pair of mass-degenerate Majorana fermions. Alternately,

> The extra factor of 1/2 can also be understood by noting that in the case of annihilating dark matter particles, all possible scattering axes occur and are implicitly integrated over. But, integrating over 4π steradians double counts the annihilation of identical particles, hence one must include a factor of 1/2 by replacing $n_1 n_2 = n^2$ by $n^2/2$.

This interpretation for the factor of 1/2 in indirect detection (which is *not* relevant for the relic abundance calculation with which we are presently concerned) carries over to the degeneracy of the final states in the annihilation cross section.

Now consider the *final* state particles. If there are k identical final state particles, then we expect an additional factor of $1/k!$, which can be understood precisely as above: the phase space integral over-counts final state configurations. For $2 \to 2$ processes this is a factor of 1/2! which we will write out as $1/k!$ in the remainder of this section as a reminder.

Putting this all together, we have:

$$d\sigma = \frac{1}{k!}\frac{1}{4E^2 v}\left(\prod_f \frac{d^3p_f}{(2\pi)^3}\frac{1}{2E_f}\right)(2\pi)^4\delta^{(4)}\left(p_a^\mu + p_b^\mu - \sum_f p_f^\mu\right)\frac{1}{4}\sum_{\text{spins}}|\mathcal{M}|^2 \tag{3.79}$$

$$= \frac{1}{k!}\frac{1}{4E^2 v}\frac{d\Omega_{\text{CM}}}{4\pi}\frac{1}{8\pi}\left(\frac{2|\mathbf{p_1}|}{E_{\text{CM}}}\right)\frac{1}{4}\sum_{\text{spins}}|\mathcal{M}|^2. \tag{3.80}$$

We have written $2E_a 2E_b|v_a - v_b| = 4E^2 v$. Now note that

$$\frac{2|\mathbf{p_1}|}{E_{\text{CM}}} = \frac{|\mathbf{p_1}|}{E} = v_1 \tag{3.81}$$

where v_1 is the velocity of one of the final state axions. This is *not* integrated over (we've already done the final state phase space integrals) and must be converted into the initial state relative velocity v using conservation of $E_i^2 = m_i^2 + p_i^2$ and $v_i = p_i/E$,

$$\frac{m_\chi^2}{E^2} + \frac{v_\chi^2}{E^2} = \frac{m_a^2}{E^2} + \frac{v_1^2}{E^2}, \tag{3.82}$$

Recalling that $v = 2v_\chi$, we find

$$v_1^2 = \frac{v^2}{4} + \frac{m_\chi^2 - m_a^2}{E^2}. \tag{3.83}$$

Plugging this back in to $d\sigma$,

$$d\sigma = \frac{1}{k!}\frac{1}{4E^2 v}\frac{d\Omega_{\text{CM}}}{4\pi}\frac{1}{8\pi}\sqrt{\frac{v^2}{4} + \frac{m_\chi^2 - m_a^2}{E^2}}\,\frac{1}{4}\sum_{\text{spins}}|\mathcal{M}|^2 \tag{3.84}$$

$$v\,d\sigma = \frac{1}{k!}\frac{d\cos\theta}{(2E)^2}\frac{1}{16\pi}\frac{1}{4}\sum_{\text{spins}}|\mathcal{M}|^2\,(1 + \cdots), \tag{3.85}$$

where the expansion of the square root drops terms of order $\mathcal{O}(v)$ and $\mathcal{O}(m_a/m_\chi)$ since $E \approx m_\chi$. To be precise, $E = \gamma m_\chi$ where γ is the Lorentz factor $\left(1 - v_\chi^2\right)^{-1/2}$.

Comment/question: The expansion of the square root seems to give a higher order correction proportional to v. Shouldn't this mean that there's a term in σv that goes like v^3, i.e. the expansion in relative velocity includes odd powers of v in addition to even powers?

Simplifying a bit more, we have a leading order contribution of

$$v\,d\sigma = \frac{1}{k!}\frac{d\cos\theta}{64\pi}\frac{1}{s}\sum_{\text{spins}}|\mathcal{M}|^2. \tag{3.86}$$

Recall that $k!$ encodes the symmetry of the final states: $k = 1$ for non-identical final states, and $k = 2$ for two identical final state particles. One can perform the $d\cos\theta$ integral and expand in powers of v to obtain the coefficients in (3.75). From taking the first moment of the Boltzmann distribution, we can plug in those coefficients to obtain

$$\langle\sigma_{\text{ann.}} v\rangle = a + 6\frac{b}{x_f} + \cdots. \tag{3.87}$$

3.9 Co-annihilations

See Griest and Seckel [93], and a paper by the DarkSUSY[9] collaboration [99].

4 Sample calculation: Goldstone fermion annihilation

As a sample calculation we highlight some features of non-standard interactions. We consider the decays of Goldstone fermion dark matter to Goldstone bosons via s and t channel processes..

4.1 Feynman rules

The relevant part of the interaction Lagrangian is

$$\mathcal{L} = \frac{b_1}{\sqrt{2}}\frac{q}{f}\chi\sigma^\mu\bar{\chi}\partial_\mu a + i\frac{m_a}{f\sqrt{2}}(\alpha+\beta)a\left(\chi\chi - \bar{\chi}\bar{\chi}\right). \tag{4.1}$$

Note that each of these terms are already self-adjoint so no additional "+h.c." is necessary. The b_1 term is self-adjoint since the Hermitian conjugate just gives. This gives the following two-component Feynman rules (where p is the incoming scalar momentum):

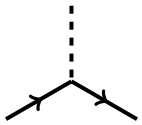
$$= \frac{b_1}{\sqrt{2}}\frac{q}{f}\sigma^\mu p_\mu = -\frac{b_1}{\sqrt{2}}\frac{q}{f}\bar{\sigma}^\mu p_\mu$$

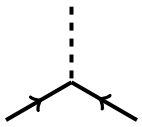
$$= \frac{-\sqrt{2}m_a(\alpha+\beta)}{f}$$

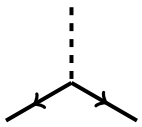
$$= \frac{\sqrt{2}m_a(\alpha+\beta)}{f}$$

To check: there seems to be a sign error for at least the last two rules. However, changing the sign of both rules should not affect the overall amplitude.

4.2 Amplitude

We assign momenta in the following way:

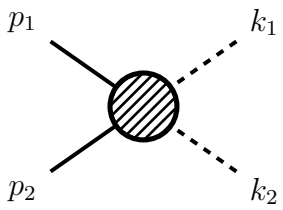

[9]DarkSUSY [98] is a tool for the numerical calculation of dark matter relic densities in SUSY while accounting for coannihilations. A similar tool is micrOMEGAS[43].

In the absence of any explicit U(1) breaking terms, we have the following diagrams:

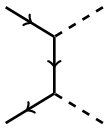

$$= \left(\frac{b_1 q}{\sqrt{2} f}\right)^2 \frac{i}{(p_1 - k_1)^2 - m_\chi^2}\, x_1 \not{k}_1 (\not{\bar{k}}_1 - \not{\bar{p}}_1) \not{k}_2 y_2^\dagger \tag{4.2}$$

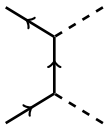

$$= \left(\frac{b_1 q}{\sqrt{2} f}\right)^2 \frac{i}{(p_1 - k_1)^2 - m_\chi^2}\, y_1^\dagger \not{\bar{k}}_1 (\not{k}_1 - \not{p}_1) \not{\bar{k}}_2 x_2 \tag{4.3}$$

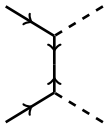

$$= \left(\frac{b_1 q}{\sqrt{2} f}\right)^2 \frac{-i m_\chi}{(p_1 - k_1)^2 - m_\chi^2}\, x_1 \not{k}_1 \not{\bar{k}}_2 x_2 \tag{4.4}$$

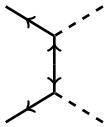

$$= \left(\frac{b_1 q}{\sqrt{2} f}\right)^2 \frac{-i m_\chi}{(p_1 - k_1)^2 - m_\chi^2}\, y_1^\dagger \not{\bar{k}}_1 \not{k}_2 y_2^\dagger \tag{4.5}$$

Note that the u-channel diagrams are given by the same expressions with $k_1 \leftrightarrow k_2$.
If we only consider explicit U(1)-breaking vertices, then we have the following diagrams:

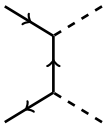

$$= \left(\frac{\sqrt{2} m_a (\alpha + \beta)}{f}\right)^2 \frac{-i}{(p_1 - k_1)^2 - m_\chi^2}\, x_1 (\not{k}_1 - \not{p}_1) y_2^\dagger \tag{4.6}$$

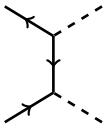

$$= \left(\frac{\sqrt{2} m_a (\alpha + \beta)}{f}\right)^2 \frac{-i}{(p_1 - k_1)^2 - m_\chi^2}\, y_1^\dagger (\not{\bar{k}}_1 - \not{\bar{p}}_1) x_2 \tag{4.7}$$

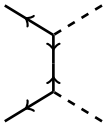

$$= \left(\frac{\sqrt{2} m_a (\alpha + \beta)}{f}\right)^2 \frac{i m_\chi}{(p_1 - k_1)^2 - m_\chi^2}\, y_1^\dagger y_2^\dagger \tag{4.8}$$

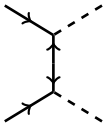

$$= \left(\frac{\sqrt{2} m_a (\alpha + \beta)}{f}\right)^2 \frac{i m_\chi}{(p_1 - k_1)^2 - m_\chi^2}\, x_1 x_2 \tag{4.9}$$

Note that the u-channel diagrams are given by the same expressions with $k_1 \leftrightarrow k_2$.

Finally, we can consider diagrams with one explicit breaking vertex and one U(1)-preserving vertex. There are three sources of signs: (1) the direction of the scalar momentum going *into* a b_1 vertex, (2) the ~~U(1)~~ vertex with *incoming* fermion arrows, and (3) picking the $\bar{\sigma}$ Feynman rule in the b_1 vertex rather than the σ rule.

The following diagrams pick up a factor of the momentum in the internal propagator:

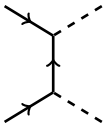

$$= \left(\frac{b_1 q}{\sqrt{2} f}\right)\left(\frac{\sqrt{2} m_a(\alpha+\beta)}{f}\right)\frac{-i}{(p_1-k_1)^2-m_\chi^2}\; x_1(\not{k}_1-\not{p}_1)\bar{\not{k}}_2 x_2 \tag{4.10}$$

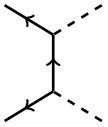

$$= \left(\frac{b_1 q}{\sqrt{2} f}\right)\left(\frac{\sqrt{2} m_a(\alpha+\beta)}{f}\right)\frac{i}{(p_1-k_1)^2-m_\chi^2}\; y_1^\dagger \bar{\not{k}}_1(\not{k}_1-\not{p}_1) y_2^\dagger \tag{4.11}$$

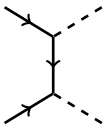

$$= \left(\frac{b_1 q}{\sqrt{2} f}\right)\left(\frac{\sqrt{2} m_a(\alpha+\beta)}{f}\right)\frac{i}{(p_1-k_1)^2-m_\chi^2}\; x_1 \not{k}_1(\bar{\not{k}}_1-\bar{\not{p}}_1) x_2 \tag{4.12}$$

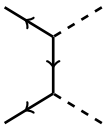

$$= \left(\frac{b_1 q}{\sqrt{2} f}\right)\left(\frac{\sqrt{2} m_a(\alpha+\beta)}{f}\right)\frac{-i}{(p_1-k_1)^2-m_\chi^2}\; y_1^\dagger(\bar{\not{k}}_1-\bar{\not{p}}_1)\not{k}_2 y_2^\dagger \tag{4.13}$$

Note that the u-channel diagrams are given by the same expressions with $k_1 \leftrightarrow k_2$.
The following diagrams pick up a mass insertion from the internal propagator:

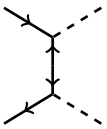

$$= \left(\frac{b_1 q}{\sqrt{2} f}\right)\left(\frac{\sqrt{2} m_a(\alpha+\beta)}{f}\right)\frac{i m_\chi}{(p_1-k_1)^2-m_\chi^2}\; x_1 \not{k}_2 y_2^\dagger \tag{4.14}$$

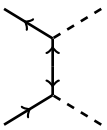

$$= \left(\frac{b_1 q}{\sqrt{2} f}\right)\left(\frac{\sqrt{2} m_a(\alpha+\beta)}{f}\right)\frac{-i m_\chi}{(p_1-k_1)^2-m_\chi^2}\; y_1^\dagger \bar{\not{k}}_1 x_2 \tag{4.15}$$

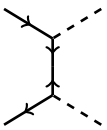

$$= \left(\frac{b_1 q}{\sqrt{2} f}\right)\left(\frac{\sqrt{2} m_a(\alpha+\beta)}{f}\right)\frac{-i m_\chi}{(p_1-k_1)^2-m_\chi^2}\; x_1 \not{k}_1 y_2^\dagger \tag{4.16}$$

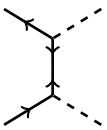

$$= \left(\frac{b_1 q}{\sqrt{2} f}\right)\left(\frac{\sqrt{2} m_a(\alpha+\beta)}{f}\right)\frac{i m_\chi}{(p_1-k_1)^2-m_\chi^2}\; y_1^\dagger \bar{\not{k}}_2 x_2 \tag{4.17}$$

Note that the u-channel diagrams are given by the same expressions with $k_1 \leftrightarrow k_2$.

4.3 Squared amplitude

One can then feed this into *Mathematica*. See Appendix E for an explicit realization of this; it's quite elegant (you'll never want to do an amplitude by hand again). Squaring the matrix element, averaging over initial state spins, and summing over final state spins, one finds a big ugly mess. See my notebook. Since our primary concern is just the overall prefactor, let me only list one term in the expression:

$$\frac{1}{4}\sum_{\text{spins}}|\mathcal{M}|^2 = -\frac{1}{4}\frac{32B^2 m_\chi^2(m_\chi^2-E^2)(m_a^2-E^2)}{\left[(m_a^2-2E^2)^2+4(m_a^2-E^2)(E^2-m_\chi^2)\cos^2\theta\right]^2}+\cdots, \tag{4.18}$$

where

$$B = \frac{\sqrt{2} m_a (\alpha + \beta)}{f}. \tag{4.19}$$

Fortunately the expression simplifies as we go on. Let us focus on picking up the right factors of 2 all over the place. Note that $E = p^0$ is the energy of one of the initial state particles so that $E_{\rm CM} = 2E$.

4.4 Cross section and phase space

We've taken care of the average over initial spins and sum over final spins in the squared matrix element. What remains to be done is to dress this with the appropriate prefactors and phase space integrals to get a thermally averaged cross section, $\langle \sigma v \rangle$.

Let's go back to the two-body phase space integral (3.77). Before attacking the integrals, we should account for factors of two that may pop out from identical particles. We have identical Majorana axinos, but recall from Sec. 3.8 that having identical *initial* states does *not* introduce any symmetry factor. There is an additional factor of 1/2! coming from the identical *final* state particles.

We can then go ahead and plug our amplitude into (3.86) to obtain an expression for $v d\sigma$. The expression for $\sum_{\rm spins} |\mathcal{M}|^2$ can be performed in *Mathematica*, see Appendix E for an explicit example. One can then perform the $d\cos\theta$ integral and expand in powers of v to get the coefficients in the expansion $\sigma v = a + bv^2 + \cdots$. The leading term is v^2.

As a reference expression to check your work, the value for σv in the limit where there are no explicit symmetry-breaking terms is

$$\sigma v = \frac{b_1^4 m_\chi^2 v^2}{96\pi f^4 \left(m_a^2 - 2m_\chi^2\right)^4} \left(3m_a^8 - 16 m_a^6 m_\chi^2 + 48 m_a^4 m_\chi^4 - 64 m_a^2 m_\chi^6 + 32 m_\chi^8\right). \tag{4.20}$$

5 Direct detection

This section follows the author's A-exam.

After the above long-winded historical introduction, we now discuss general features of direct dark matter detection. Direct detection first demonstrated by Goodman and Witten (yes, *that* Witten) at around the time when the author was born [100]. As explained in the introduction, we study the scattering of halo dark matter particles off of highly-shielded targets to determine information about their interactions (cross sections) and kinematics (mass). Because dark matter is so weakly interacting with the Standard Model such experiments require large detector volumes, as is the case with neutrino experiments. Unlike neutrino experiments, however, dark matter is heavy and the detection methods are rather different. While neutrinos may zip through a liquid detector relativistically and leave easy-to-detect Čerenkov radiation, WIMPs lumber along like giant elephants that will absent-mindedly bump into target nuclei[10]. One can intuitively appreciate that the two scenarios very different kinematics that require separate detection techniques.

[10]This behavior is very reminiscent of certain graduate students who shouldn't be trusted with delicate things.

The canonical review of the calculation of dark matter direct detection constraints is reviewed exceptionally well by Lewin and Smith [101]. We shall review these results following the pedagogical discussion in [61]. Additional comments and applications to the CDMS detector are presented in chapter 2 of [59]. The key result will be to understand the structure of dark matter exclusion plots. We will also briefly survey and classify the experimental techniques used in the range of direct detection experiments to help place our specific study of XENON100 into proper context.

5.1 General strategy

A garden-variety neutralino-like WIMP interacts with a target material primarily through elastic collisions with the target nuclei. Experiments can then use complementary detection techniques to detect and distinguish such interactions from background events to compare to theoretical predictions. These theoretical predictions can be parameterized by the dark matter mass and a single effective coupling for typical WIMPs or up to four effective couplings for more general dark matter models depending on, e.g., spin coupling. The primary quantity to connect experimental data to theoretical models is the elastic nuclear recoil spectrum, dR/dE_R, where R is the recoil event rate and E_R is the energy of the recoiling nucleus.

We will start by assembling some pieces required to construct the recoil spectrum: the astrophysical input data about the WIMP velocity distribution and the effective ('phenomenological') cross section. Since we will see that most events occur with low recoil energy, it will be advantageous to further parameterize the cross section in terms of a zero momentum transfer part and a **form factor** that encodes the momentum and target dependence. In doing so we will uncover important general features that feed into the design of direct detection experiments.

5.2 Astrophysical input

Our primary astrophysical assumption is that the dark matter in the halo has a 'sufficiently' Maxwellian velocity distribution. The **Maxwell-Boltzmann distribution** describes the velocities of particles which move freely up to short collisions and is derived in one's favorite statistical physics textbook. Here one assumes that the WIMPs are isothermal and isotropically distributed in phase space (i.e. gravitationally relaxed). It is important to remark that this is not actually fully accurate and thus that WIMPs cannot have an *exactly* Maxwellian distribution even though such an approximation should be sufficient (i.e. with uncertainties smaller than those coming from the WIMP-nucleus cross section) for garden-variety WIMP models. For a recent discussion of the implications of the expected departures from the Maxwell distribution at the large velocity tail and the kinds of models that would be affected by this, see [102].

The complete phase space distribution for such a halo for a dark matter species of mass m_χ, gravitational potential $\Phi(\vec{x})$, and velocity in the galaxy frame $\vec{v}_{\rm gal}$ is

$$f(\vec{x},\vec{v})\,d^3x\,d^3v \propto \exp\left(-\frac{m_\chi\left[v^2/2+\Phi(\vec{x})\right]}{k_BT}\right). \tag{5.1}$$

The Earth is effectively at a fixed point in the gravitational potential so that the position depen-

dence is is also fixed and can be absorbed into the overall normalization. We may thus write

$$f(v_{\rm gal}) = \frac{1}{k_0} e^{v_{\rm gal}^2/v_0^2} \tag{5.2}$$

where k is a factor to normalize the distribution

$$k_0 = \int d^3\vec{v}_{\rm gal}\, e^{v_{\rm gal}^2/v_0^2} = (\pi v_0^2)^{3/2} \tag{5.3}$$

and v_0 is the most probable WIMP speed and is given by the characteristic kinetic energy:

$$\frac{1}{2} m_\chi v_0^2 = k_B T \qquad\qquad v_0 \approx 220 \text{ km/s} \approx 0.75 \cdot 10^{-3}\, c. \tag{5.4}$$

Note that in (5.3) we have not defined the region of integration in velocity space, we will discuss this shortly. For now one can assume that we are integrating over the entire space. It is typically to write the $\vec{v}_{\rm gal}$ explicitly in terms of the velocity in the Earth (lab) frame, $\vec{v}$, and the velocity of this frame relative to the dark matter halo, $\vec{v}_E$,

$$\vec{v}_{\rm gal} = \vec{v} + \vec{v}_E. \tag{5.5}$$

The orbit of the Earth about the sun in the galactic halo frame provides the input for an annual modulation:

$$v_E = 232 + 15 \cos\left(2\pi \frac{t - 152.5 \text{ days}}{365.25 \text{ days}}\right) \text{ km s}^{-1}. \tag{5.6}$$

All astrophysical data in this section come from [59]. Further discussion this data can be found in, e.g., [103].

A key observation on the right-hand side of (5.4) is that the dark matter particle is very non-relativistic (we include an explicitly factor of $c = 1$). This will have important implications on our WIMP-nucleon cross section.

Let us remark once again that for the remainder of this document (except for isolated remarks), we will *assume* this astrophysical input. While we have mentioned in Section 2.7 that there are many new phenomenological dark matter models that can deviate from these assumptions, we will not consider them in our primary analysis[11].

5.3 Phenomenological cross section

Given a matrix element $\mathcal{M}(q)$ for the scattering of WIMPs of lab frame velocity $\vec{v}$ against target nuclei with characteristic momentum transfer q, we may use Fermi's Golden Rule to determine the differential WIMP-nucleus cross section,

$$\frac{d\sigma_N(q)}{dq^2} = \frac{1}{\pi v^2} |\mathcal{M}|^2 = \hat{\sigma}_N \cdot \frac{F^2(q)}{4 m_r^2 v^2}. \tag{5.7}$$

[11] This would be a novel topic for a future different A-exam, e.g. for Bibhushan Shakya.

The $(\pi v^2)^{-1}$ factor comes from the density of final states and the usual 2π in the Golden Rule formula. In the last equality we've written the cross section in terms of a q-independent factor $\hat{\sigma}_N = \sigma_N(q=0)$ and fit all of the momentum dependence into the remaining **form factor**, $F(q)$. We have written m_r for the reduced mass of the WIMP-nucleus system,

$$m_r = \frac{m_\chi m_N}{m_\chi + m_N}. \tag{5.8}$$

For a general interaction Lagrangian between WIMPs and nucleons, one can show that the $q=0$ cross section can be parameterized by four effective couplings $f_{p,n}$ and $a_{p,n}$ (subscripts refer to proton and neutron couplings) according to

$$\hat{\sigma}_N = \frac{4m_r^2}{\pi}\left[Zf_p + (A-Z)f_n\right]^2 + \frac{32G_F^2 m_r^2}{\pi}\frac{(J+1)}{J}\left[a_p\langle S_p\rangle + a_n\langle S_n\rangle\right] \tag{5.9}$$

where J is the nuclear spin, Z (A) is the atomic (mass) number, and $S_{p,n}$ are the spin content of the proton and neutron [104]. There is an implied sum over nucleons, p and n. We have separated the zero momentum transfer cross section into **spin independent** (SI) and **spin-dependent** (SD) pieces. We elucidate the derivation of this paramterization in Appendix **??**. The relevant point is that this is still a general formula for the effective, zero momentum transfer cross section.

Now one must consider the **coherence** effect coming from summing over nucleons. Nuclear physicists knew all about coherence effects in atomic interactions... but they're all old and wrinkly now. In this day and age, we have to invoke highfalutin ideas like decoupling: as good effective field theorists, we know that the nuclear scale is 'macroscopic' relative to the dark matter scale. We thus have to ask if it it is appropriate to sum the quantum mechanically over the amplitudes coming from each target nucleon. This is a question of energy dependence since higher energies probe smaller scales. We already know from our discussion of the WIMP velocity distribution that WIMPs are very non-relativistic in the lab frame so that they have a large de Broglie wavelength that indeed probes the *entire* target nucleus.

We harp upon this because this already provides a dramatic simplification. It is not surprising that an electrically neutral dark matter particle should couple in (roughly) the same way to the proton and neutron since these are related by isospin. Thus we may take $f_p = f_n \equiv f$ and note that the first term in (5.9) takes the form

$$\hat{\sigma}_N|_{\rm SI} \approx \frac{4m_r^2}{\pi} f^2 A^2, \tag{5.10}$$

i.e. the spin-independent cross section is enhanced by a factor of A^2 due to coherence. Further, since spins form anti-parallel pairs in ground state nuclei, most of the spin-dependent cross section cancels and only leaves a leftover coupling to an odd number of protons or neutrons in the nucleus. Thus for our garden-variety WIMP interacting with a garden-variety (e.g. Ge) target with low spin, we can completely neglect the spin-dependence,

$$\hat{\sigma}_N \approx \hat{\sigma}_N|_{\rm SI}\,. \tag{5.11}$$

We remark that this simplification (assumed in standard direct detection exclusion plots) provides a place for the DAMA results to hide since DAMA's NaI target is much more sensitive to spin-dependent coupling than other direct detection experiments of comparable volume[12].

[12] I know this is being read by LHC physicists, so I should say that detector volume $\sim$ [instantaneous] luminosity.

5.4 Differential recoil rate, a first pass

Let us now turn to the kinematics of the process. We assume elastic scattering since this dominates for point-like dark matter interacting with nuclei. This assumption provides another place to hide DAMA results, c.f. inelastic dark matter [78]. In the center of mass frame,

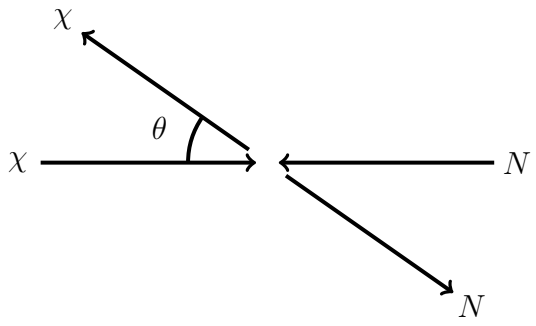

The kinematics of this scattering process are worked out thoroughly in first-year mechanics[13],

$$E_R = E_i r \frac{1-\cos\theta}{2}, \tag{5.12}$$

where r is a kinematic factor built out of the particle masses

$$r = \frac{4m_r}{m_\chi m_N} = \frac{4m_\chi m_N}{(m_\chi + m_N)^2}. \tag{5.13}$$

The key feature is that $0 < r \leq 1$ with the upper bound saturated for $m_\chi = m_N$. In other words, recoil energy is maximized when the masses of the WIMP and target nuclei are matched. The conventional cartoon to understand this is to consider the scattering of ping pong balls and bowling balls.

Now let us proceed to calculate the differential recoil rate for the case of zero momentum transfer $q = 0$ where we've already parameterized the relevant cross section. We will later correct for the q-dependence in the form factor. In the center of mass frame the scattering is isotropic so that E_R is uniform in $\cos\theta$ over the range

$$0 < E_R \leq E_i r = E_R^{\max}. \tag{5.14}$$

This gives us a relatively boring plot of differential recoil rate for an incident energy

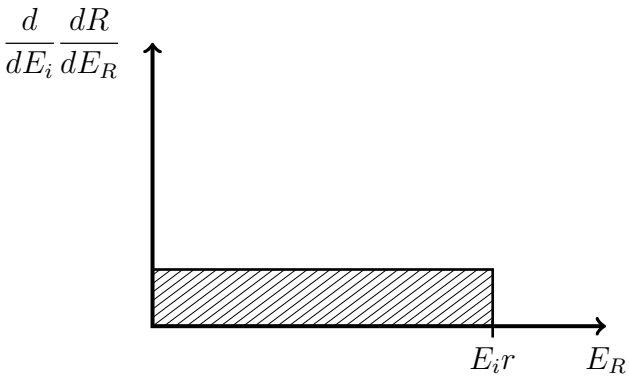

[13]This would be an excellent Q-exam question, but since this committee has already given me a thorough Q-exam, think it is not necessary to ask me to derive this—right?

Nondescriptness notwithstanding, it is important to understand what is being plotted here. The vertical axis gives the rate of nuclear recoils for a sliver of recoil energies between E_R and E_R+dE_R and a sliver of incident energies between E_i and $E_i + dE_i$. This is the differential of the recoil energy spectrum for the distribution of input WIMP velocities (i.e. E_i). The area of the shaded box represents the contribution to this differential rate coming from integrating over E_R for a given E_i. As promised this distribution is flat due to isotropy. The length of the box is given by $E_R^{\max}(E_i)$. The height of the box is a function of our zero momentum transfer cross section $\hat{\sigma}_N$ and E_i through the dependence of the rate on the WIMP velocity distribution. Thus we may write

$$\frac{d}{dE_i}\frac{dR}{dE_R} = \frac{\text{area}}{\text{length}} = \frac{dR}{E_i r}. \tag{5.15}$$

We would have a boring rectangular plot like this for *each* incident velocity (i.e. each E_i). The length of each rectangle is $E_i r$ and the height will be a more complicated function (given below) of the velocity distribution. In order to get the recoil spectrum, dR/dE_R, we can imagine stacking all of these boring rectangular plots on top of each other:

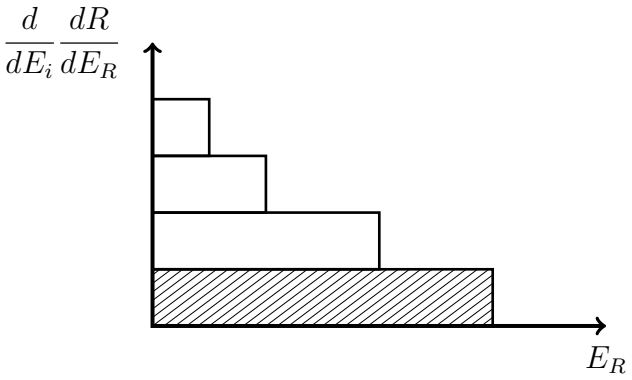

Now we can imagine summing together the contribution from each box to get the recoil spectrum, i.e. we can integrate (5.15)

$$\frac{dR}{dE_R} = \int_{E_i^{\min}}^{E_i^{\max}} \frac{dR(E_i)}{E_i r} \longrightarrow \int_{\vec{v}} \frac{dR(\vec{v}+\vec{v}_E)}{E_i r}, \tag{5.16}$$

where on the right we convert to an integral over WIMP velocity, i.e. $E_i = E_i(\vec{v}+\vec{v}_E)$. As we noted above when normalizing the Maxwellian velocity distribution, we have been glib about the limits of integration. To simplify our first pass, will take $E_i^{\max} \to \infty$ and $E_i^{\min} = E_R/r$ from the second inequality in (5.14). We will later address the effect of a finite $E_i^{\max}$ coming from the characteristic escape velocity v_{esc} of WIMPs in the dark matter halo.

To perform this integral we need an explicit form of the differential rate $dR(E_i)$ of scattering from an incident energy E_i to a recoil energy E_R. (We have only explicitly written the argument that is integrated over.) $dR(E_i)$ tells us how many such recoil events occur per kilogram-day of a target material of atomic mass A. Heuristically this is written as

$$dR = \frac{\#\text{ nuclei}}{\text{kg}} \cdot \frac{\text{rate}}{\text{nucleus}}, \tag{5.17}$$

i.e. the number of nuclei per unit mass multiplied by the rate per nuclei. To determine this latter quantity we can imagine each target nucleus traveling through space at velocity $\vec{v}_{\rm gal} = \vec{v} + \vec{v}_E$ in the WIMP rest frame with a cross section $\hat{\sigma}_N$.

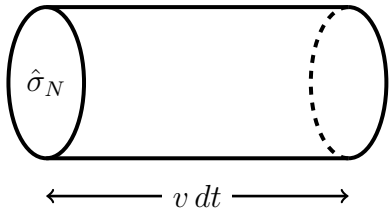

The nucleus effectively carves out an interaction volume $\hat{\sigma}_N v\,dt$ across a space with WIMP number density $n_0 f(\vec{v}+\vec{v}_E)\,d^3\vec{v}$. Thus the number of events is

$$\frac{\text{rate}}{\text{nucleus}} dt = \hat{\sigma}_N v_{\rm gal}\, n_0 f(\vec{v}+\vec{v}_E)\, d^3\vec{v}\, dt, \tag{5.18}$$

and the rate per nucleus is given by dropping the dt.

Plugging everything into (5.17), including the Maxwellian velocity distribution (5.2),

$$dR = \frac{N_0}{A} \cdot \hat{\sigma}_N v_{\rm gal}\, n_0 \frac{1}{k} e^{(\vec{v}+\vec{v}_E)^2/v_0^2}\, d^3\vec{v}, \tag{5.19}$$

where N_0 is Avogadro's number. Let us now perform the integral (5.16) in a very simplified 'toy' case which we will gradually make more sophisticated. In addition to setting $v_{\rm esc} \to \infty$, let us turn off the annual modulation from the Earth's motion in the galaxy, $\vec{v}_E = 0$ (this also sets $v_{\rm gal} = v$). The resulting integral is then

$$\frac{dR}{dE_R} = \int_{v_{\rm min}}^{\infty} \frac{1}{(\frac{1}{2}m_\chi v^2) r} \frac{R_0}{2\pi v_0^4} v\, e^{-v^2/v_0^2}\, 4\pi v^2\, dv. \tag{5.20}$$

The first term is just $(E_i r)^{-1}$, the second term defines R_0 to absorb constants in a way that will be convenient later, and the remainder contains the v dependence of dR. The minimum velocity is given by

$$E_i^{\rm min} = \frac{E_R}{r} = \frac{1}{2} m_\chi v_{\rm min}^2. \tag{5.21}$$

Proceeding to simplify and perform the integral,

$$\frac{dR}{dE_R} = \frac{R_0}{r\left(\frac{1}{2}m_\chi v_0^2\right)} \int_{v_{\rm min}}^{\infty} \frac{2}{v_0^2} e^{-v^2/v_0^2}\, v\, dv = \frac{R_0}{E_0 r} e^{-E_R/E_0 r}, \tag{5.22}$$

where we have defined $E_0 = \frac{1}{2}m_\chi v_0^2$ to be the most probable incident WIMP energy and R_0 can now be simply interpreted as the *total* rate for isotropic nuclear recoil from a non-relativistic

point-like particle moving through the galaxy. Explicitly writing in all of the factors that went into this constant, we find

$$R_0 = \frac{2}{\sqrt{\pi}} \frac{N_0}{A} n_0 \hat{\sigma}_N \, v_0 \approx \frac{500 \text{ GeV}}{A \, m_\chi} \cdot \frac{\hat{\sigma}_N}{1 \text{ pb}} \cdot \frac{\rho_{\text{DM}}}{0.4 \text{ GeV/cm}^3} \cdot \frac{\text{events}}{\text{kg day}}. \tag{5.23}$$

Sometimes people define silly units like tru ('**total rate unit**') = event kg^{-1} day^{-1} for this rate or the dru ('**differential rate unit**') for event kg^{-1} day^{-1} keV^{-1} [101]. However, the last thing particle physics needs is more units so we will not use these.

It is useful to pause for a moment to admire this toy result since it already gives a very rough estimate for what one might expect in the real world. Given a 100 kg detector made up of Xe ($A \approx 100$) and a 100 GeV WIMP with typical weak-scale nuclear cross section $\hat{\sigma}_N \sim 1$ pb, one ends up with about 5 events per day. This scales linearly with cross section, WIMP density (astrophysics), and inversely with the WIMP mass. Now suppose the target nucleus happens to have the same mass, $m_N = m_\chi = 100$ GeV (this is the right ballpark for Xe) so that $r = 1$, then we can calculate the mean recoil energy,

$$\langle E_R \rangle = E_0 r = \frac{1}{2} m_\chi v_0^2 = \frac{1}{2} 50 \text{ GeV } (.75 \cdot 10^{-3}) \approx 30 \text{ keV}. \tag{5.24}$$

This number is remarkably *small*, even though we're in the 'best case' scenario where the WIMP and target masses are matched. To compare to experiments that collider physicists (especially those at Fermilab) might appreciate a bit better, neutrino beam experiments typically detect events of MeV-scale energies. Dark matter experiments have to be significantly better than this.

5.5 Comparing apples to apples

Before moving on to make our toy model more realistic, let us pause to make an important point about meaningful ways to convey the information from a direct detection experiment. Assuming we have run such an experiment for some time and have detected no signal, we can make an exclusion plot to convey what our experiment has learned. We present such a plot in Fig. 7. The plot assumes that there are no events detected within the energy threshold; effectively one assumes that there was a maximal number of events of energy less than the threshold that would still be consistent with no observed events above threshold. Integrating (5.22) gives such a value for R for which one can plot $R_0/r \sim \hat{\sigma}_N$ over m_χ. One can qualitatively understand the features of this graph: at the minimum the kinetic factor r is maximized for $m_\chi \approx m_N$. Below this value there's not enough kinetic energy transferred (ping pong balls don't transfer much energy to bowling balls) and above this value the density of dark matter decreases ($n \sim \rho/m_\chi$) so that the bounds away from $m_\chi \approx m_N$ become weaker.

Such a plot can be generated for each direct detection experiment with null results. The key question is how one ought to combine the results of different experiments. Since we know that different experiments use different target material (and this is good since this provides sensitivity for a broad range of WIMP masses), we are particularly concerned about the dependence of the exclusion plot on the target. This can be summarized by fact that we are setting bounds on the [zero momentum transfer] WIMP-*nucleus* cross section $\hat{\sigma}_N$ for various WIMP masses. This clearly is not a useful quantity when comparing experiments with different target nuclei. Fortunately,

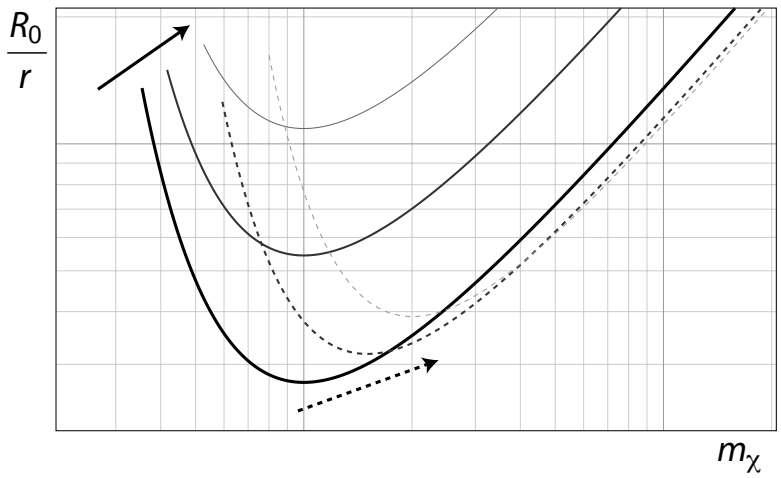

Figure 7: Model log-log exclusion plots from (5.22) in arbitrary units. Each line excludes points above it. Solid lines indicate increasing energy threshold (worse sensitivity) following the solid arrow while the dashed lines indicate increasing target atomic mass A. These plots were generated by the author, which should be taken as evidence that he knows what he's talking about.

there is a trivial fix: rescale everything so that we provide bounds on the WIMP-nucle*on* cross section $\hat{\sigma}_n$ which is thus independent of the particular nucleus. Note that we use the convention that lowercase n refers to nucleon (or 'neutron') while capital N refers to the entire nucleus. The conversion is straightforward,

$$\hat{\sigma}_N = \frac{m_r^2}{m_{rn}^2} A^2 \hat{\sigma}_n, \tag{5.25}$$

where m_{rn} is the reduced mass for the WIMP-nucleon system. Note that we pick up an additional factor of A^2 which, combined with (5.10), gives us a total coherence enhancement of A^4 in the WIMP-nucleon rate (the rate which is sensible to compare between experiments). Let us remind ourselves that we are restricting ourselves to the case of dominant spin-independent interactions, the case where spin-dependent scattering is appreciable requires more caution.

Plugging this back into our very rough (back of a very small envelope) estimate (5.23) and using $m_r^2/m_{rn}^2 \sim A^2$, we find that for our 100 kg Xe detector and 100 GeV WIMP, we get five events per day for a zero momentum transfer WIMP-nucle*on* cross section of $\hat{\sigma}_n \sim 10^{-8}$ pb.

5.6 More realistic velocities

The differential recoil rate in Section 5.4 is a handy estimate for what one would expect for an experiment, but it is a dramatic simplification. Let us make our toy expression slightly more sophisticated by taking into account the effect of a finite escape velocity and replace the effect of the Earth's annually modulated velocity relative to the dark matter halo. To make it clear which spectrum we are referring to, let us write

$$\frac{dR}{dE_R} \longrightarrow \frac{dR(v_E, v_{\rm esc})}{dE_R}, \tag{5.26}$$

where we explicitly write the dependence on the Earth's velocity and the escape velocity. The toy-model spectrum we derived above then $dR(0,\infty)/dE_R$.

Because the dark matter halo is gravitationally bound, there is a characteristic escape velocity at which the Maxwell distribution necessarily breaks down since any particles with such energies would escape the halo. Thus our integration over WIMP velocity (or, equivalently, incident energy) should have some upper limit. Technically, the gravitational potential modifies the Maxwell distribution at its tail, but it is typically sufficient to impose a hard cutoff. Typically $v_{\rm esc} \approx 600$ km s^{-1} should be used as the upper limit for the integration in (5.22). Note that this also requires a modification of the overall normalization of the Maxwell distribution. We define the finite $v_{\rm esc}$ normalization by

$$k_{\rm esc} = k_0 \left[\text{erf}\left(\frac{v_{\rm esc}}{v_0}\right) - \frac{2}{\sqrt{\pi}} \frac{v_{\rm esc}}{v_0} e^{-v_{\rm esc}^2/v_0^2} \right], \tag{5.27}$$

where the error function is a convenient shorthand for the integral over the finite velocity domain. The modified recoil spectrum can be written in terms of the $v_{\rm esc} \to \infty$ spectrum as

$$\frac{dR(0,v_{\rm esc})}{dE_R} = \frac{k_0}{k_{\rm esc}} \left[\frac{dR(0,\infty)}{dE_R} - \frac{R_0}{E_0 r} e^{-v_{\rm esc}^2/v_0^2} \right], \tag{5.28}$$

where we see the effect of the rescaled normalization and an additional term which vanishes in the $v_{\rm esc} \to \infty$ limit. Let us remark that typically these large velocity effects are negligible relative to our toy model since our garden-variety WIMPs tend to be rather heavy and don't carry much kinetic energy. This allowed us, for example, to simply truncate the distribution above the escape velocity. However, the light WIMP candidates introduced in Section 2.7 can populate more of the tail of the velocity distribution and proper treatment of this region is important [102].

Now let us account for the modulated velocity of the Earth relative to the dark matter halo, which we wrote above as:

$$v_E = 232 + 15 \cos\left(2\pi \frac{t - 152.5 \text{ days}}{365.25 \text{ days}}\right) \text{ km s}^{-1}. \tag{5.29}$$

Due to the unfortunate placement of our solar system in the Milky Way galaxy, the average velocity (232 km/s) is not very well known, though the amplitude of the modulation (15 km/s) is well measured. We should further remark that there are small errors since the modulation isn't exactly sinusoidal. This modulation clearly does not affect the finite $v_{\rm esc}$ term in (5.28) since the large $v_{\rm esc}$ dominates over v_E. However, this *does* affect the $dR(0,\infty)/dE_R$ term. Going through the same analysis as Section 5.4 with $v^2 \to (\vec{v} + \vec{v}_E)^2$, we find

$$\frac{dR(v_E,\infty)}{dE_R} = \frac{R_0}{E_0 r} \frac{\sqrt{\pi}}{4} \frac{v_0}{v_E} \left[\text{erf}\left(\frac{v_{\rm min} + v_E}{v_0}\right) - \text{erf}\left(\frac{v_{\rm min} - v_E}{v_0}\right) \right]. \tag{5.30}$$

Combining this with (5.28) finally gives us

$$\frac{dR(v_E,v_{\rm esc})}{dE_R} = \frac{k_0}{k_{\rm esc}} \left[\frac{dR(v_E,\infty)}{dE_R} - \frac{R_0}{E_0 r} e^{-v_{\rm esc}^2/v_0^2} \right]. \tag{5.31}$$

This certainly brings us closer to a realistic expression (though we still have not included q-dependence), but (5.30) and (5.31) leaves much to be desired in terms of having something tractable to interpret. Fortunately, it turns out that (5.30) can be approximated very well by a simpler form,

$$\frac{dR(v_E,\infty)}{dE_R} = c_1 \frac{R_0}{E_0 r} e^{-c_2 E_R/E_0 r}, \tag{5.32}$$

for some fitting 'constants' c_1 and c_2 which vary slightly with the time of year

$$.73 \leq c_1 \leq .77 \qquad\qquad .53 \leq c_2 \leq .59. \tag{5.33}$$

A detailed time-dependence can be found in Appendix C of [101], but for most cases it is sufficient to set them to their average values $\langle c_1 \rangle = 0.75$ and $\langle c_2 \rangle = 0.56$. Note that these are not independent, since integration of the above equation forces $c_1/c_2 = R(v_E,\infty)/R_0$. In this simplified form we can see that the that the effects of the Earth's motion can increase rate and make the spectrum slightly harder (from c_2).

Finally, let's remark that integrating the spectrum (5.30) to get a total rate and differentiating with respect to the Earth's velocity gives

$$\frac{d}{dv_E}\left(\frac{R}{R_0}\right) = \frac{1}{v_E}\left[\frac{R}{R_0} - \frac{\sqrt{\pi} v_0}{2v_E}\text{erf}\left(\frac{v_E}{v_0}\right)\right] \approx \frac{1}{2v_E}\frac{R}{R_0}, \tag{5.34}$$

where our final approximation assumes $v_E \approx v_0$. From this we can see that the 6% modulation in v_E causes a 3% modulation in the rate. A nice plot of this effect is show in Fig. 8.

5.7 Form factor suppression: coherence lost

Perhaps the most obvious omission in our toy model thus far has been the approximation of zero momentum transfer, $q = 0$. This came from our ansatz all the way back in (5.7) that we could reliably treat the q-dependence as a correction to the $q = 0$ cross section which we parameterized as a form factor, $F(q)$. Now we should justify this parameterization and determine the form of $F(q)$. See [105] for a discussion.

Momentum transfer from the WIMP-nucleus collision is

$$q = \sqrt{2 m_N E_R}. \tag{5.35}$$

For large enough values of q we expect coherence to break down as the de Broglie wavelength becomes smaller than the scale of the nucleus. A simple way to develop an intuition for the form factor is to work in the first Born approximation (i.e. plane wave approximation):

$$\mathcal{M}(q) = f_n A \int d^3\vec{x}\, \rho(\vec{x}) e^{i\vec{q}\cdot\vec{x}}, \tag{5.36}$$

where ρ is the density distribution of scattering sites. The form factor is precisely the this Fourier transform over the scattering lattice,

$$F(q) = \int d^3\vec{x}\, \rho(x) e^{i\vec{q}\cdot\vec{x}} = \frac{4\pi}{q}\int_0^\infty r\, \sin(qr)\, \rho(r)\, dr. \tag{5.37}$$

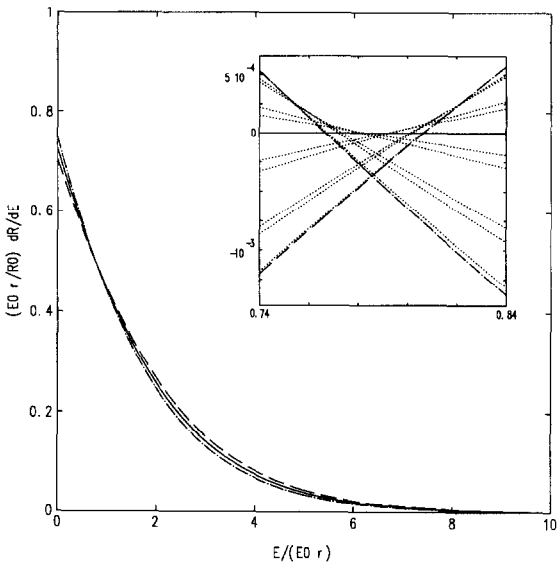

Figure 8: Plot of $dR(E_R)/dE$ showing the seasonal variation of the rate spectrum. The solid line is the annual average, dashed line is June, dotted-dashed line is December. The inset shows an enlargement of the crossover region with the annual average subtracted. Dotted lines in the inset are monthly averages. Image from [101].

For spin independent interactions, a simple model of the nucleus as a solid sphere turns out to be a very good approximation. In this case the form factor takes the form

$$F(qr_N) = \frac{j_1(qr_N)}{qr_N} = 3\frac{\sin(qr_N) - qr_N\cos(qr_N)}{(qr_N)^3}, \tag{5.38}$$

where we've written the momentum dependence in terms of a dimensionless quantity qr_N where $r_N \sim A^{1/3}$ is a characteristic nuclear radius. Recall that $q \sim \sqrt{AE_R}$ where the A-dependence comes from $m_N \sim A$. Thus the leading A and E_R dependence of qr_N goes like

$$qr_N \sim A^{5/2}E_R^{1/2}. \tag{5.39}$$

A more accurate parameterization from [101] is

$$qr_N = 6.92 \cdot 10^{-3}A^{1/2}\left(\frac{E_R}{\text{keV}}\right)^{1/2}\left(a_N A^{1/3} + b_N\right), \tag{5.40}$$

where a_N and b_N are 'fudge factors' to give the correct nuclear radius r_N from its A dependence. We will simply take $a_N = 1$ and $b_N = 0$ (to this precision $6.92 \to 7$) so that a reasonable-to-detect 100 keV recoil of a Xe ($A \approx 100$) nucleus gives $qr_N \approx 3.2$. From our argument about length scales one might worry that this is the regime where coherence breaks down. Indeed, plugging into our solid sphere nuclear model, we get an $F^2(qr_N)$ suppression as plotted in Fig. 9.

We see that for light target nuclei, the form factor doesn't make much difference. For heavy nuclei, on the other hand, we can resolve the structure of the Bessel function (the Fourier transform

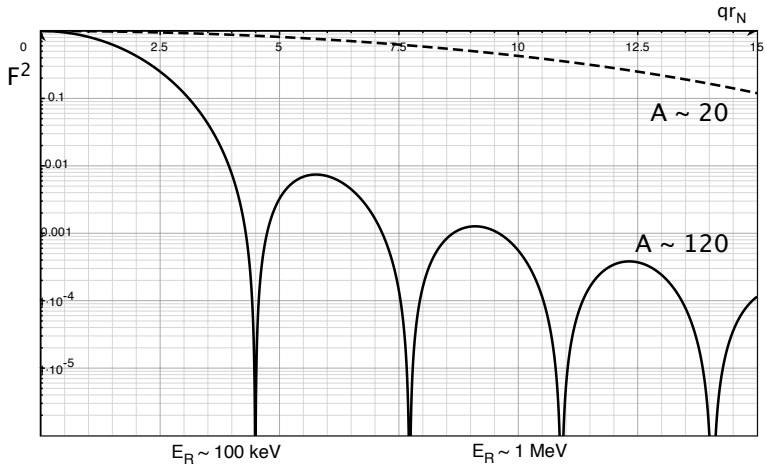

Figure 9: Form factor suppression $F^2(qr_N)$ on a log plot. Solid line: F^2 suppression for fixed $A \sim$ 120 over different recoil energies and corresponding qr_N values on the top axis. Dashed line: F^2 suppression for fixed $A \sim 20$ for the same recoil energies. (Note: the qr_N values for the dashed lines are related to the top axis by an additional factor of ~ 0.2.)

of our solid sphere nuclear model) and we find ourselves hitting the zeroes of j_1 and brushing up against its exponential suppression.

This is a very important plot to take into account when designing a direct detection experiment. We saw in (5.10) that the spin-independent nuclear cross section scales as A^2. This is enhanced to A^4 when considering the more useful nucleon cross section. While we know that having too large an A (so that $m_N \gg m_\chi$) leads to penalty in the kinetic factor r, we know from (5.13) that this is only A^{-1}. Thus it would still seem advantageous to build detectors with the heaviest target materials available to maximize the interaction cross section. As we've now seen (and could have expected), this breaks down when the WIMP is no longer able to scatter coherently off the entire nucleus. One must then balance the coherence from having heavy nuclei with the form factor suppressing coming from decoherence.

As we consider larger nuclei (large A), the region around $q = 0$ where $F^2(qr_N)$ is not prohibitive becomes smaller. The trade off when designing an experiment then depends crucially on how low one can push the energy threshold: what is the smallest nuclear recoil that one can measure? If you can efficiently detect arbitrarily low threshold recoils, then you can go ahead and use the heaviest nuclei you can find for your detector. However, real experiments only have a finite energy threshold (partially a function of the target material). For this minimum recoil energy, one must consider to what extent the form factor suppression from one's target material will suppress one's signal.

Thus in Fig. 9, the $A \sim 20$ detector takes a big hit in the interaction cross section because of its low A value. However, we see that one is free to use a detector technology with a less prohibitive energy threshold since F^2 doesn't decrease very quickly. The $A \sim 120$ detector, on the other hand, gives a nice enhancement from coherence, but *only* for sufficiently low energy recoils so that one must be very sensitive to low energy signals. As a rule of thumb, targets lighter than Ge start start to lose a lot from A^2 suppression; i.e. current detector technology does not require

A any lower than this to ensure reasonable efficiency.

This is an important lesson to put the CDMS and XENON experiments in context. While Xe is appreciably heavier than Ge, form factor suppression (decoherence) in Xe leads to the two being roughly the same in their ability to detect WIMPs.

Failure for spin-dependent case: see [11] of LS [105, 106]

5.8 Further refinement

If you are doing everything well, you are not doing enough.
– Howard Georgi, personal motto [107]

In addition to proper inclusion of spin-dependence and refinements of the models used above (e.g. the halo, Born approximation with a hard sphere), a good and honest experimentalist ought to properly consider the effects of detector resolution and statistics. (Un-)Fortunately, as a theory grad student I am neither particularly good nor honest when it comes to such matters and I will leave their detailed discussion to pedagogical expositions in [101] and [59]. Let us briefly address some salient effects.

Detection efficiency. First on the list of experimental considerations is the efficiency at which the nuclear recoil energy is detected. As we already know, nuclear recoils and electron recoils are very different interactions. Given an electron and a nuclear interaction with the *same* recoil energy, a given detector technology will measure different values for such events due to the nature of the detection technique (we will mention canonical examples below). This means that instead of the spectrum with respect to the recoil energy dR/dE_R, one should calculate the spectrum with respect to the *visible* energy dR/dE_v where $E_v = f_n E_R$ so that

$$\frac{dR}{dE_R} \approx f_n \left(1 + \frac{E_R}{f_n}\frac{df_n}{dE_R}\right)\frac{dR}{dE_v}. \tag{5.41}$$

A related issue that is important to discuss is **quenching**[14]; see [108] for a nice discussion. Because detectors respond differently to nuclear recoils than to electron recoils, we need useful units to measure our visible energy. The difference between the visible energy coming from electron and nuclear events of the same recoil energy is parameterized by a **quenching factor**, Q. This leads to some silly notation: $\mathrm{keV_{ee}}$ for the "electron equivalent" energy (i.e. observed energy had the event come from an electron) and $\mathrm{keV_r}$ for the energy signature from a "nuclear recoil."

$$E_e(\mathrm{keV_{ee}}) = Q \times E_r(\mathrm{keV_r}) \tag{5.42}$$

Energy resolution. The next effect to consider is the finite resolution for any real detector. This means that if there were *exactly* N signal recoils each of a single energy $E_v = E'_v$, then our real detector would observe a spread of energies smeared out in an approximately Gaussian manner with some energy-dependent width ΔE,

$$\frac{dN}{dE_v} = \frac{N}{\sqrt{2\pi}\Delta E} e^{(E_v - E'_v)^2} 2\Delta E^2. \tag{5.43}$$

[14] Is it just me, or do experimentalists use this word to refer to *way* too many different phenomena?

Thus the actual spectrum that we measure should be transformed to

$$\frac{dR}{dE_v} = \frac{1}{\sqrt{2\pi}} \int dE'_v \, \frac{1}{\Delta E} \frac{dR}{dE'_v} e^{(E_v - E_v)^2/2\Delta E^2}, \tag{5.44}$$

where $\Delta E(E'_v) \sim \sqrt{E'_v}$. Real experimentalists should also 'fold in' the other terms in ΔE relevant to a given detector technology. For low energy events one should also worry that the Gaussian statistics above might lead to erroneous loss of counts due to negative energies. This can be solved by using a Poisson distribution, but leads to issues regarding the energy threshold.

Energy threshold. As discussed above, the most favorable rates come from low energy events where the de Broglie wavelength of the WIMP is large enough to permit coherent scattering against an entire target nucleus. However, detectors (e.g. photomultiplier tubes) can only resolve events above a given threshold energy. Noise reduction also sets a threshold dependent on nearby radioactive sources (e.g. impurities in the target material) and shielding. These cutoffs must be taken into account for each experiment when constructing exclusion plots.

Target mass fractions. Let us comment in passing that in detectors with compound targets (e.g. NaI for DAMA) one must calculate the rate limit separately for each target.

To summarize, let use write out the recoil spectrum with respect to *measured* energy as a handy mnemonic:

$$\frac{dR}{dE_v} = R_0 \sum_A f_A S_A F_A^2 I_A, \tag{5.45}$$

where R_0 is the total rate, A runs over the relevant atomic mass numbers, f_A gives the detection efficiency for nuclear recoil, S_A is the spectral function, F^2 is the form factor suppression, and I_A is a reminder about which sort of interaction (spin-independent or spin-dependent) we are considering. S_A is essentially the spectrum in (5.22) modified by all of the above velocity and detector effects. It gives the same qualitative behavior as in Fig. 7.

6 Indirect detection

7 Cosmological bounds

7.1 BBN

7.2 Structure formation

Acknowledgements

This work is supported in part by the NSF grant number PHY-0355005, an NSF graduate research fellowship, and a Paul & Daisy Soros Fellowship For New Americans. Part of this work was completed at the Kavli Institute for Theoretical Physics which is supported in part by the National Science Foundation under Grant No. NSF PHY05-51164. The contents of this article do not necessarily represent the views of any of the above institutions.

A Notation and Conventions

Here we present a set of self-consistent notation and conventions that we (try to) use in this document. One should be mindful that the 'useful formulae' in Appendix B do *not* necessarily conform to these conventions.

A.1 Field labels

Chiral superfields are typically written with capital Roman letters, e.g., S, N, X. Complex conjugation is denoted by a star, $(a+ib)^* = (a-ib)$. A bar, on the other hand, is used to distinguish pairs of vector-like chiral superfields, e.g, N and $\bar{N}$ have opposite charges under a particular symmetry. Do not confuse this bar with complex conjugate. To avoid confusion, it is typical to use a tilde to denote the vector-like pair, e.g., N and $\widetilde{N}$. We denote the axino by χ rather than the usual $\widetilde{a}$ to avoid cumbersome notation and to reinforce its identity as dark matter. The dual gauge field strength $*F$ is defined in component notation relative to the field strength via

$$\widetilde{F}_{\mu\nu} = \frac{1}{2} F^{\alpha\beta} \epsilon_{\alpha\beta\mu\nu}. \tag{A.1}$$

A.2 Spacetime and spinors

There is no completely standard set of spacetime and spinor conventions in the SUSY literature, but the choices that make the most sense to us are those by Dreiner et al. [96]; see their appendix for a thorough discussion of how to passing between metric conventions[15]. See also Problem 1 of Appendix C in Binetruy's supersymmetry textbook [109] which identifies all possible sources of sign ambiguities and writes relevant formulae with all choices made explicit. Pedagogical introductions to Weyl and Majorana spinors can be found in Aitchison [110] and the article by Pal [111].

4D Minkowski indices are written with lower-case Greek letters from the middle of the alphabet, $\mu, \nu, \cdots$. We use the particle physics ('West Coast,' mostly-minus) metric for Minkowski space, $(+,-,-,-)$. Our convention for σ^0 and the three Pauli matrices $\vec{\sigma}$ is

$$\sigma^0 = \begin{pmatrix} 1 & 0 \\ 0 & 1 \end{pmatrix} \quad \sigma^1 = \begin{pmatrix} 0 & 1 \\ 1 & 0 \end{pmatrix} \quad \sigma^2 = \begin{pmatrix} 0 & -i \\ i & 0 \end{pmatrix} \quad \sigma^3 = \begin{pmatrix} 1 & 0 \\ 0 & -1 \end{pmatrix}. \tag{A.2}$$

The un-barred Pauli matrices have indices $\sigma^\mu_{\alpha\dot{\beta}}$ while the barred Pauli matrices, $\bar{\sigma}^\mu = (\sigma^0, -\vec{\sigma})$, have indices $\bar{\sigma}^{\mu\dot{\alpha}\beta}$. The two types of Pauli matrices are related by

$$\bar{\sigma}^{\mu\dot{\alpha}\alpha} = \epsilon^{\dot{\alpha}\dot{\beta}} \epsilon^{\alpha\beta} \sigma^\mu{}_{\beta\dot{\beta}}, \tag{A.3}$$

[15] To see this in action, see their source file at `http://zippy.physics.niu.edu/spinors.html`, which includes a macro to allow one to change metric conventions. The implementation is an excellent example of where the metric choice is (and isn't) relevant.

where our convention for the sign of ϵ is given below. The Weyl representation for the Dirac γ matrices is

$$\gamma^\mu = \begin{pmatrix} & \sigma^\mu \\ \bar{\sigma}^\mu & \end{pmatrix} \qquad \gamma^5 = i\gamma^0\gamma^1\gamma^2\gamma^3 = \begin{pmatrix} -\mathbb{1} & \\ & \mathbb{1} \end{pmatrix}. \tag{A.4}$$

Note that the definition of γ^5 is the usual 4D Weyl basis convention, whereas the sensible 5D convention is $\Gamma^5 = \mathrm{diag}(i, -i)$ so that the 5D Clifford algebra is satisfied. The antisymmetric products of Pauli matrices are

$$\sigma^{\mu\nu} = \frac{i}{4}\sigma^{[\mu}\bar{\sigma}^{\nu]} \qquad \bar{\sigma}^{\mu\nu} = \frac{i}{4}\bar{\sigma}^{[\mu}\sigma^{\nu]}. \tag{A.5}$$

I don't like the factor of i, but this is the price of sticking with the conventions in [96].

The totally antisymmetric tensor [densities] are chosen to have

$$\epsilon^{12} = \epsilon_{21} = 1 \qquad \epsilon^{0123} = -\epsilon_{0123} = 1. \tag{A.6}$$

This convention agrees with Wess & Bagger [112], Terning [113], and Dreiner et al. [96] but has a relative sign from Bailin and Love [114]. The significance of this choice is described in footnotes 4–6 of Dreiner et al. [96], but the point is that Weyl spinor indices are raised and lowered via matrix multiplication from the left,

$$\psi_\alpha = \epsilon_{\alpha\beta}\psi^\beta \qquad \psi^\alpha = \epsilon^{\alpha\beta}\psi_\beta \qquad \bar{\psi}_{\dot{\alpha}} = \epsilon_{\dot{\alpha}\dot{\beta}}\bar{\psi}^{\dot{\beta}} \qquad \bar{\psi}^{\dot{\alpha}} = \epsilon^{\dot{\alpha}\dot{\beta}}\bar{\psi}_{\dot{\beta}}, \tag{A.7}$$

where we've introduced the notation $\bar{\psi}_{\dot{\alpha}} = (\psi_\alpha)^*$ and $\chi^\alpha = (\bar{\chi}^{\dot{\alpha}})^*$. Note the use of $*$ here rather than $\dagger$, though the distinction is mostly poetic. If one is perturbed by this, an excellent reference is the relevant chapter in Aitchison's elementary text [110]. The relative sign between ϵ^{12} and ϵ_{12} sets $\epsilon_{\alpha\rho}\epsilon^{\rho\beta} = \delta_\alpha^\beta$ so that no signs appear when an index is raised and then lowered again. Alternately, this relative sign appears when relating the ϵ tensor to charge conjugation as we will see below. With this convention, special care is required to keep track of minus signs when raising and lowering indices of ϵ tensors (see [96]), but this is usually a silly thing to do to begin with. Using Lorentz invariance, one can write relations like $\theta^\alpha\theta^\beta \propto \epsilon^{\alpha\beta}\theta\theta$. The overall constant of proportionality can be found by contracting the indices of both sides. One finds

$$\theta^\alpha\theta^\beta = -\frac{1}{2}\epsilon^{\alpha\beta}\theta\theta \qquad \theta_\alpha\theta_\beta = +\frac{1}{2}\epsilon_{\alpha\beta}\theta\theta \tag{A.8}$$

$$\bar{\theta}^{\dot{\alpha}}\bar{\theta}^{\dot{\beta}} = +\frac{1}{2}\epsilon^{\dot{\alpha}\dot{\beta}}\bar{\theta}\bar{\theta} \qquad \bar{\theta}_{\dot{\alpha}}\bar{\theta}_{\dot{\beta}} = -\frac{1}{2}\epsilon_{\dot{\alpha}\dot{\beta}}\bar{\theta}\bar{\theta}. \tag{A.9}$$

Similarly,

$$\theta\sigma^\mu\bar{\theta}\,\theta\sigma^\nu\bar{\theta} = +\frac{1}{2}\theta^2\bar{\theta}^2\eta^{\mu\nu} \tag{A.10}$$

$$(\theta\psi)(\theta\chi) = -\frac{1}{2}(\psi\chi)(\theta\theta) \tag{A.11}$$

$$(\bar{\theta}\bar{\psi})(\bar{\theta}\bar{\chi}) = -\frac{1}{2}(\bar{\psi}\bar{\chi})(\bar{\theta}\bar{\theta}). \tag{A.12}$$

The placement of Weyl spinors (with their natural index placement) within a Dirac spinor is

$$\Psi_{\rm D} = \begin{pmatrix} \psi_\alpha \\ \bar{\chi}^{\dot{\alpha}} \end{pmatrix}. \tag{A.13}$$

Spinor contractions are descending for undotted indices and ascending for dotted indices:

$$\psi\chi \equiv \psi^\alpha \chi_\alpha \qquad\qquad \bar{\psi}\bar{\chi} \equiv \bar{\psi}_{\dot{\alpha}} \bar{\chi}^{\dot{\alpha}}. \tag{A.14}$$

With this convention, contractions are independent of the order of the spinors: $\psi\chi = \chi\psi$ and similarly for the barred spinors $\bar{\psi}\bar{\chi} = \bar{\chi}\bar{\psi}$. The Dirac conjugate spinor is given by

$$\bar{\Psi}_D = \Psi^\dagger \gamma^0 = \begin{pmatrix} \psi^{\dagger\alpha} & \bar{\chi}^\dagger_{\dot{\alpha}} \end{pmatrix} \begin{pmatrix} & {\sigma^0}_{\alpha\dot{\beta}} \\ \bar{\sigma}^{0\dot{\alpha}\beta} & \end{pmatrix} = \begin{pmatrix} \psi^{\dagger\alpha} & \bar{\chi}^\dagger_{\dot{\alpha}} \end{pmatrix} \begin{pmatrix} & \mathbb{1}_{\alpha\dot{\beta}} \\ \mathbb{1}^{\dot{\alpha}\beta} & \end{pmatrix} \equiv \begin{pmatrix} \chi^\alpha & \bar{\psi}_{\dot{\beta}} \end{pmatrix}. \tag{A.15}$$

One may take this as a definition of χ and $\bar{\psi}$ in terms of ψ and $\bar{\chi}$ in Ψ_D. It shows how γ^0 is used to convert the dotted index of $\bar{\chi}^\dagger$ into the undotted index of χ (and vice versa for $\psi^\dagger$ and $\bar{\psi}$).

The charge conjugate of a Dirac fermion Ψ^c is given by

$$\Psi^c = C\bar{\Psi}^T \qquad\qquad C = \begin{pmatrix} i\bar{\sigma}^2 & \\ & i\sigma^2 \end{pmatrix} = \begin{pmatrix} \epsilon_{\alpha\beta} & \\ & \epsilon^{\dot{\alpha}\dot{\beta}} \end{pmatrix}, \tag{A.16}$$

This comes from taking the Hermitian conjugate of the Dirac equation

$$i(\partial\!\!\!/ - ieA\!\!\!/)\Psi = 0 \quad \Rightarrow \quad -i\bar{\Psi}\gamma^0\gamma^{\mu\dagger}(\overleftarrow{\partial}_\mu + ieA_\mu) = 0 \quad \Rightarrow \quad -i\gamma^{\mu\mathrm{T}}(\partial_\mu + ieA)\bar{\Psi}^{\mathrm{T}} = 0, \tag{A.17}$$

where we've made use of the identities $\gamma^0\gamma^{\mu\dagger}\gamma^0 = \gamma^\mu$ and $(\gamma^0)^2 = \mathbb{1}$. Because $-\gamma^{\mu\mathrm{T}}$ satisfies the 4D Clifford algebra, there exists a charge conjugation matrix C such that $C^{-1}\gamma^\mu C = -\gamma^{\mu\mathrm{T}}$. In particular, $C\bar{\Psi}^{\mathrm{T}}$ is a solution to the Dirac equation with opposite charge,

$$i\gamma^\mu(\partial_\mu + ieA_\mu)C\bar{\Psi}^{\mathrm{T}} = 0. \tag{A.18}$$

The above property of C implies that $C \sim \gamma^0\gamma^2$. The constant of proportionality must be a pure phase so that $(\Psi^c)^c = \Psi$. We choose this proportionality so that

$$C = i\gamma^0\gamma^2, \tag{A.19}$$

which matches (A.16). This can be understood as the reason why the ϵ tensor density appears with a different overall sign when written with upper versus lower indices; the sign comes from σ^2 versus $\bar{\sigma}^2$. Writing out indices slightly more carefully,

$$\Psi^c = C\bar{\Psi}^T = \begin{pmatrix} i\bar{\sigma}^2 & \\ & i\sigma^2 \end{pmatrix} \begin{pmatrix} \chi^\alpha \\ \bar{\psi}_{\dot{\alpha}} \end{pmatrix} = \begin{pmatrix} \epsilon_{\alpha\beta} & \\ & \epsilon^{\dot{\alpha}\dot{\beta}} \end{pmatrix} \begin{pmatrix} \chi^\alpha \\ \bar{\psi}_{\dot{\alpha}} \end{pmatrix} = \begin{pmatrix} \chi_\alpha \\ \bar{\psi}^{\dot{\alpha}} \end{pmatrix}. \tag{A.20}$$

A Majorana fermion obeys $\Psi_{\rm M} = \Psi^c_{\rm M}$ so that

$$\begin{pmatrix} \psi_\alpha \\ \bar{\chi}^{\dot{\alpha}} \end{pmatrix} = \begin{pmatrix} \chi_\alpha \\ \bar{\psi}^{\dot{\alpha}} \end{pmatrix}, \tag{A.21}$$

that is $\psi_\alpha = \chi_\alpha$ and $\bar{\chi}^{\dot{\alpha}} = \bar{\psi}^{\dot{\alpha}}$. In other words,

$$\Psi_{\rm M} = \begin{pmatrix} \psi_\alpha \\ \bar{\psi}^{\dot{\alpha}} \end{pmatrix}. \tag{A.22}$$

Sometimes the right-hand side is written somewhat impressionistically as $(\psi, i\bar{\sigma}^2\psi^*)^{\mathrm{T}}$; the intended meaning is identical to the above expression.

A.3 Superfields and superspace

The superspace measure is

$$d^2\theta = -\frac{1}{4}d\theta^\alpha d\theta^\beta \epsilon_{\alpha\beta} = -\frac{1}{4}d\theta^\alpha d\theta_\alpha \qquad\qquad d^2\bar{\theta} = -\frac{1}{4}d\bar{\theta}_{\dot{\alpha}} d\theta_{\dot{\beta}} \epsilon^{\dot{\alpha}\dot{\beta}} = -\frac{1}{4}d\bar{\theta}_{\dot{\alpha}} d\bar{\theta}^{\dot{\alpha}}. \tag{A.23}$$

The field strength superfield is

$$\mathcal{W} = -i\lambda + [D - \sigma^{\mu\nu}F_{\mu\nu}]\,\theta - \theta\theta\sigma\partial\bar{\lambda}, \tag{A.24}$$

so that the SYM Lagrangian is $\mathcal{L} = \int d^2\theta \frac{1}{4}\mathcal{W}\mathcal{W} + \text{h.c.}$; occasionally I may write $\mathbb{W}$ instead of $\mathcal{W}$. I've chosen the definition $\sigma^{\mu\nu} = \frac{i}{4}\sigma^{[\mu}\bar{\sigma}^{\nu]}$, c.f. (A.1).

A.4 2-component plane waves

See [96] for details.

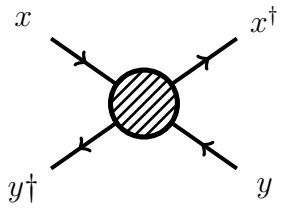

B Useful formulae

B.1 Units and conversions

Most of these are from the PDG [115].

$$c = 3.0 \times 10^8 \text{ m/s} \tag{B.1}$$
$$h = 6.626 \times 10^{-34} \text{ J s} \tag{B.2}$$
$$\hbar = 6.582 \times 10^{-25} \text{ GeV s} \tag{B.3}$$
$$\hbar c = 197 \text{ MeV fm} \approx 2 \times 10^7 \text{ GeV nm} \tag{B.4}$$
$$(\hbar c)^2 = 0.389 \text{ GeV mb} \approx 0.4 \times 10^{-9} \text{ GeV pb} \tag{B.5}$$
$$G_\text{F} = 1.166 \times 10^{-5} \text{ GeV}^{-2} \tag{B.6}$$
$$G_\text{N} = 6.709 \times 10^{-39} \text{ GeV}^{-2} \tag{B.7}$$
$$M_\text{Pl} = \sqrt{\hbar c/G_N} = 1.22 \times 10^{19} \text{ GeV}/c^2 \tag{B.8}$$
$$M_\text{Pl,r} = \sqrt{\hbar c/8\pi G_N} = 2.43 \times 10^{18} \text{ GeV}/c^2. \tag{B.9}$$

Throughout this document we will implicitly be writing M_Pl to mean the *reduced* Planck mass. I think this is the usual convention.

B.2 Pauli matrices

These formulae follow our convention for $\sigma^0 = \mathrm{diag}(1,1)$.

$$\mathrm{Tr}(\sigma^\mu \bar{\sigma}^\nu) = 2\eta^{\mu\nu} \tag{B.10}$$

$$\mathrm{Tr}(\sigma^\mu \bar{\sigma}^\nu \sigma^\rho \bar{\sigma}^\delta) = 2\eta^{\mu\nu}\eta^{\rho\delta} - 2\eta^{\mu\rho}\eta^{\nu\delta} + 2\eta^{\mu\delta}\eta^{\nu\rho}. \tag{B.11}$$

B.3 Wess & Bagger

Sign subtlety. Please note that Wess & Bagger use the opposite (mostly plus) metric.

Expanding a chiral superfield in the chiral coordinates $y = x + i\theta\sigma\bar{\theta}$,

$$\Psi = A(y) + \sqrt{2}\theta\psi(y) + \theta\theta F(y) \tag{B.12}$$

$$= A(x) + i\theta\sigma\bar{\theta}\partial A(x) + \frac{1}{4}\theta^4\partial^2 A(x) + \sqrt{2}\theta\psi(x) - \frac{i}{\sqrt{2}}\theta^2\partial\psi(x)\sigma\bar{\theta} + \theta^2 F(x). \tag{B.13}$$

The θ^4 component of the product of two superfields is

$$\Phi_i^\dagger \Phi_j\Big|_{\theta^4} = F_i^* F_j + \frac{1}{4}A_i^*\Box A_j + \frac{1}{4}\Box A_i^* A_j - \frac{1}{2}\partial A_i^*\partial A_j + \frac{i}{2}\partial\bar{\psi}_i\bar{\sigma}\psi_j - \frac{i}{2}\bar{\psi}_i\bar{\sigma}\partial\psi_j \tag{B.14}$$

B.4 Peskin & Schroeder

The differential cross section for a process is given by

$$d\sigma = \frac{1}{2E_a 2E_b |v_a - v_b|}\left(\prod_f \frac{d^3p_f}{(2\pi)^3}\frac{1}{2E_f}\right)|\mathcal{M}|^2(2\pi)^4\delta^{(4)}\left(p_a^\mu + p_b^\mu - \sum_f p_f^\mu\right), \tag{B.15}$$

where E_a and E_b are the energies of the two initial state particles. The squared amplitude is assumed to already be spin averaged. The differential decay rate of a particle of mass M is

$$d\Gamma = \frac{1}{2M}\left(\prod_f \frac{d^3p_f}{(2\pi)^3}\frac{1}{2E_f}\right)|\mathcal{M}|^2(2\pi)^4\delta^{(4)}\left(p_a^\mu + p_b^\mu - \sum_f p_f^\mu\right), \tag{B.16}$$

where for the specific case of a two-body final state the phase space integral is

$$d\mathrm{PS}_2(p_1,p_2) = \left(\prod_f \frac{d^3p_f}{(2\pi)^3}\frac{1}{2E_f}\right)(2\pi)^4\delta^{(4)}\left(p_a^\mu + p_b^\mu - \sum_f p_f^\mu\right) = \frac{d\Omega_{\mathrm{CM}}}{4\pi}\frac{1}{8\pi}\left(\frac{2|\mathbf{p_1}|}{E_{\mathrm{CM}}}\right). \tag{B.17}$$

B.5 Murayama

The expression for the two-body phase space can be simplified by evaluating the δ function. In fact, multi-body phase space can be decomposed into two-body phase space integrals. This is done explicitly in Murayama's QFT notes[16]. We simply cite relevant results here.

$$d\mathrm{PS}_2(p_1, p_2) = \frac{\bar{\beta}}{8\pi} \frac{d\cos\theta}{2} \frac{d\phi}{2\pi}, \tag{B.18}$$

where

$$\bar{\beta} = \sqrt{1 - \frac{2(m_1^2 + m_2^2)}{s} + \frac{(m_1^2 - m_2^2)^2}{s^2}} \tag{B.19}$$

is a kinematic factor which reduces to the usual velocity $\beta = v/c$ in the case where $m_1 = m_2 = m$,

$$\bar{\beta}_{m_{1,2}=m} = \sqrt{1 - \frac{4m^2}{s}} = \sqrt{1 - \frac{m^2}{E_1^2}}. \tag{B.20}$$

B.6 Dodelson, Kolb & Turner

These are from Dodelson's *Modern Cosmology* [1] and Kolb & Turner's *The Early Universe* [2]. The thermally averaged cross section for a $1, 2 \to 3, 4$ process is

$$\langle \sigma v \rangle = \frac{1}{\bar{n_1} \bar{n_2}^0} \left(\prod_{i=1}^{4} \int \frac{đ^3 p_i}{2E_i} \right) e^{-(E_1+E_2)/T} (2\pi)^4 \delta^{(4)}(p_1 + p_2 - p_3 - p_4) |\mathcal{M}|^2, \tag{B.21}$$

where $\bar{n}$ refers to the equilibrium number density,

$$n_{\mathrm{EQ},i} = g_i \int đ^3 p e^{-E_i/T} \begin{cases} g_i \left(\frac{m_i T}{2\pi}\right)^{3/2} & \text{if } m_i \gg T \\ g_i \frac{T^3}{\pi^2} & \text{if } m_i \ll T. \end{cases} \tag{B.22}$$

Here g_i is the degeneracy (number of degrees of freedom) of the species, e.g. $g_\gamma = 2$ since the photon has two spin states.

B.7 Jungman, Kamionkowski, Griest

These are from the supersymmetric dark matter review [95]. From Section 3.3,

$$\sigma_{\mathrm{ann.}} v = a + b v^2 + \cdots, \tag{B.23}$$

so that

$$\langle \sigma_{\mathrm{ann.}} v \rangle = a + 6\frac{b}{x_f} + \cdots, \tag{B.24}$$

[16] http://hitoshi.berkeley.edu/233B/phasespace.pdf

where (noting that a and b have dimensions of cross section)

$$x_f = \ln\left[0.0764\, M_{\rm Pl}\left(a + 6\frac{b}{x_f}\right) c(2+c)\frac{m_\chi}{\sqrt{g_* x_f}}.\right] \tag{B.25}$$

The relation for x_f must be solved iteratively (note the x_f on the right-hand side), where c is a numerical coefficient which can be taken by matching to numerical solutions of the Boltzmann equation. Typically $c = 1/2$ may be used to within 10% accuracy.

B.8 CORE

These are relations from the Compendium of Relations [116] that are useful. Note CORE's definition $\sigma^{\mu\nu} = \frac{1}{4}\sigma^{[\mu}\bar{\sigma}^{\nu]}$ with $\sigma^\mu = (\mathbb{1}, -\vec{\sigma})$. Apparently every reference has to have at least one stubbornly contrarian minus sign floating around.

$$\begin{aligned}\sigma^{\alpha\beta}\sigma^{\mu\nu} = \;& g^{\alpha\nu}g^{\beta\mu} - g^{\alpha\mu}g^{\beta\nu} - i\epsilon^{\alpha\beta\mu\nu}\gamma^5 \\ &+ \left(g^{\alpha\nu}g^{\beta\lambda}g^{\mu\sigma} - g^{\alpha\mu}g^{\beta\lambda}g^{\nu\sigma} - g^{\beta\nu}g^{\alpha\lambda}g^{\mu\sigma} + g^{\beta\mu}g^{\alpha\lambda}g^{\nu\sigma}\right)\sigma_{\lambda\sigma} \qquad \text{(B.26)}\\ \left\{\sigma^{\alpha\beta}, \sigma^{\mu\nu}\right\} = \;& 2\left(g^{\alpha\nu}g^{\beta\mu} - g^{\alpha\mu}g^{\beta\nu} - i\epsilon^{\alpha\beta\mu\nu}\gamma^5\right) \qquad \text{(B.27)}\end{aligned}$$

C Cosmology basics

Here we give a very quick review of relevant background topics in cosmology at a very low level. These are based primarily on Ryden's undergraduate-level textbook [23] with additional remarks from Kolb & Turner [2] and Dodelson [1]. For more advanced treatments, see any of the other literature on the topic. See also brief review in the PDG [115].

C.1 Friedmann equation

For a spatially homogeneous and isotropic (Friedmann-Robertson-Walker or FRW) universe the non-trivial part of the metric reduces to an overall scale factor $a(t)$ such that

$$ds^2 = dt^2 - a^2(t)d\mathbf{x}^2. \tag{C.1}$$

One may now turn the crank of general relativity to derive the Friedmann equation, but for our purposes a Newtonian example is more physically intuitive and almost gives the exact correct answer. Following Ryden, instead of using the Einstein equations, a Newtonian argument for the gravitational force of an FRW universe on itself. Consider a comoving sphere of radius $R(t)$ containing total mass M. In such a comoving volume the number density 'static' objects do not change with the expansion of the universe. A test mass m on the surface of the sphere experiences a Newtonian gravitational force

$$F = -\frac{GMm}{R(t)^2}. \tag{C.2}$$

This means that the gravitational acceleration on the test mass is

$$\ddot{R}(t) = -\frac{GM}{R(t)^2}. \tag{C.3}$$

We can convert this into familiar energies by multiplying by $\dot{R}$ and integrating to give

$$\frac{1}{2}\dot{R}^2 = \frac{GM}{R} + U, \tag{C.4}$$

for a constant of integration U. We can identify the left-hand side as the kinetic energy per unit mass and the right-hand side as (minus) a potential energy per unit mass. We see that kinetic plus potential energy is constant.

Now let's massage things into more common quantities. The radius of the sphere can be written in terms of a reference radius times the scale factor,

$$R(t) = a(t)r. \tag{C.5}$$

Next, we can write the total mass within the sphere in terms of the density,

$$M = \frac{4\pi}{3}\rho(t)R(t)^3, \tag{C.6}$$

from which (C.4) takes the form

$$\frac{1}{2}r^2\dot{a}^2 = \frac{4\pi}{3}Gr^2\rho(t)a(t)^2 + U. \tag{C.7}$$

Finally, we can divide by $r^2a^2/2$ to finally obtain the **Newtonian Friedmann equation**,

$$\left(\frac{\dot{a}}{a}\right)^2 = \frac{8\pi G}{3}\rho(t) + \frac{2U}{r^2}\frac{1}{a^2}. \tag{C.8}$$

One can see that if you assume an expanding universe, $\dot{a} > 0$, the fate of the universe is controlled by the value of U.

While the above argument gives a correct heuristic picture of what's going on, one must honestly solve Einstein's equations to obtain the honest-to-goodness **Friedmann equation**,

$$\left(\frac{\dot{a}}{a}\right)^2 = \frac{8\pi G}{3}\rho(t) - \frac{\kappa}{R_0^2}\frac{1}{a^2}. \tag{C.9}$$

This is derived from the $0-0$ component of the Einstein equation. We implicitly promoted the Newtonian mass density ρ a the relativistic energy density. If we wanted to be pedantic we could have given this a different variable, say ε. Further, we have associated the potential U to the curvature κ via

$$\frac{2U}{r^2} = -\frac{\kappa}{R_0^2}, \tag{C.10}$$

where R_0 is related to the radius of curvature of the universe, $R(t) = a(t)R_0$. The different fates of the universe thus correspond to different values of the curvature. Note that it is typical to write the Friedmann equation in terms of the Hubble parameter, $H(t) \equiv \dot{a}/a$.

C.2 Density of the universe

Define the **critical density**, $\rho_c(t)$, to be the energy density for which the universe is flat, $\kappa = 0$:

$$\rho_c(t) \equiv \frac{3}{8\pi G} H(t)^2. \tag{C.11}$$

This gives a natural way to define dimensionless density parameters,

$$\Omega \equiv \frac{\rho}{\rho_c}, \tag{C.12}$$

so that the Friedmann equation may be written

$$1 - \Omega(t) = \frac{-\kappa}{R^2 H^2}. \tag{C.13}$$

Note that the right-hand side does not change sign so that the universe cannot change the sign of its curvature. For $\Omega > 1$ we have $\kappa = +1$ and a closed universe. Conversely, for $\Omega < 1$ we have $\kappa = -1$ and an open universe. The intermediate case $\Omega = 1$ and $\kappa = 0$ yields a flat universe.

C.3 The fluid and acceleration equations

We saw that the Friedmann equation was essentially a statement about comoving conservation of energy. This has another manifestation in physics, the First Law of Thermodynamics,

$$dQ = dE + PdV. \tag{C.14}$$

For a perfectly homogeneous universe we can have no bulk heat flow so that the expansion of the universe is adiabatic, $dQ = 0$. Writing $V = 4\pi R^3/3$ and $E = V\rho$ and plugging into the First Law we thus find

$$\dot{\rho} + 3\frac{\dot{a}}{a}(\rho + P) = 0. \tag{C.15}$$

This is known as the **fluid equation**.

We mentioned above that the Friedmann equation corresponds to the $0 - 0$ component of the Einstein equation given the FRW ansatz. We could also solve for the $i - i$ component, but it turns out that this is related to the Friedmann and fluid equations through the Bianchi identity. Indeed, combining the two equations gives the **acceleration equation**,

$$\frac{\ddot{a}}{a} = -\frac{4\pi G}{3}(\rho + 3P). \tag{C.16}$$

Ordinary stuff has a positive pressure, whereas dark energy has negative pressure $P = -\rho$.

C.4 Equations of state

An equation of state relates pressure and energy density, $P = w\rho$ for some constant w. The assumption that the equation of state is linear and time-independent is good for dilute gases. Requiring that the speed of sound waves $c_{\rm s} = dP/d\rho$ is non-tachyonic, $c_{\rm s} < 1$, imposes $w \leq 1$. One way of recasting the First Law of Thermodynamics is

$$d\left[R^3(\rho + P)\right] = R^3 dP, \tag{C.17}$$

from which we note that the evolution of a given species of energy densities goes like

$$\rho \propto R^{-3(1+w)}. \tag{C.18}$$

The most important examples are

- $w = 0$ for non-relativistic matter. (Non-relativistic matter has zero pressure.)
- $w = 1/3$ for a relativistic gas (e.g. of photons).
- $w = -1$ for vacuum energy.

Equation of state for a relativistic gas. See Carroll chapter 8.3 [117]. The trace of the energy momentum tensor for an FRW metric is $T^{\mu}{}_{\mu} = -\rho + 3P$. Relativistic matter can be treated as photons, for which we know that

$$T^{\mu}{}_{\mu} = F^{\mu\lambda}F_{\mu}\lambda - \frac{1}{4}4F^{\lambda\sigma}F_{\lambda\sigma} = 0. \tag{C.19}$$

In order for these to be consistent, $w = 1/3$. Physically, matter has an energy density which goes like $\rho \sim a^{-3}$ reflecting dilution due to the expansion of the universe. Radiation has an energy density which goes like $\rho \sim a^{-4}$ since, in addition to the expansion of the universe, the photons are also redshifted.

C.5 Equilibrium thermodynamics

This is based primarily on Kolb & Turner [2] chapter 3.3–3.4. For dark matter we are primarily interested in thermodynamics out of equilibrium since this is the regime in which thermal freeze out occurs. As background, however, let us review salient aspects of equilibrium thermodynamics. First: we should point out that that 'temperature' is something which is species dependent. When we mention '*the* temperature' T we mean the photon temperature, $T = T_\gamma$. Next recall the usual Fermi-Dirac (+) and Bose-Einstein (−) phase space distributions,

$$f(\mathbf{p}) = \frac{1}{\exp((E-\mu)/T) \pm 1}, \tag{C.20}$$

where the chemical potential (the free energy cost of adding an additional particle, e.g. due to a conserved charge) may be related to the chemical potentials of other species which are in chemical

equilibrium with the particle. From this we can write the number density, energy density, and pressure of a dilute, weakly interacting as as

$$n = g \int đ^3 p f(\mathbf{p}) \tag{C.21}$$

$$\rho = g \int đ^3 p E(\mathbf{p}) f(\mathbf{p}) \tag{C.22}$$

$$P = g \int đ^3 p \frac{|\mathbf{p}|^2}{3E} f(\mathbf{p}), \tag{C.23}$$

where g is the number of internal degrees of freedom (e.g. spin). The last expression is explained in chapter 7.13 of Reif [118]. The main idea is to consider the momentum transfer to an imaginary wall perpendicular to the $+\hat{z}$-direction in a unit amount of time. The force on a unit area A is

$$\mathbf{F} = A \int đ^3 p f(\mathbf{p}) v_z \mathbf{p}, \tag{C.24}$$

where the explicit factor of $v_z = p_z/m$ is there to account for the total number of particles striking the wall; if you want this is $v_z\, dt$ with $dt = 1$. The integral over all directions accounts for particles striking the wall in the $-\hat{z}$-direction. The pressure is given by $P = F/A$ so that $P = \int đ^3 p f(\mathbf{p}) p_z^2/m$, since the $p_z p_{x,y}$ components vanish. One may then use $\langle p \rangle = 3\langle p_z \rangle$. This gives the usual ideal gas law. To obtain the above expression for P, one should remember to promote the mass m to energy E.

The integrals for n, ρ, and P may be computed to yield analytic results. See Kolb & Turner for more cases. In the relativistic limit $T \gg m$ with $T \gg \mu$,

$$n = \begin{cases} \frac{\zeta(3)}{\pi^2} g T^3 & \text{(Bose)} \\ \frac{3}{4}\frac{\zeta(3)}{\pi^2} g T^3 & \text{(Fermi)} \end{cases} \tag{C.25}$$

$$\rho = \begin{cases} \frac{\pi^2}{30} g T^4 & \text{(Bose)} \\ \frac{7}{8}\frac{\pi^2}{30} g T^3 & \text{(Fermi)} \end{cases} \tag{C.26}$$

$$P = \frac{\rho}{3}. \tag{C.27}$$

Note the famous factor of 7/8 in the relativistic Fermi-Dirac energy density. In the non-relativistic limit $m \gg T$,

$$n = g \left(\frac{mT}{2\pi}\right)^{3/2} e^{-(m-\mu)/T} \tag{C.28}$$

$$\rho = mn \tag{C.29}$$

$$P = nT \ll \rho. \tag{C.30}$$

A useful quantity for CP violation is the number excess of a fermion species over its antiparticle. Assuming that reactions like $f + \bar{f} \leftrightarrow \gamma + \gamma$ occur rapidly, then $\mu = -\bar{\mu}$ and the net fermion number

density is

$$n - \bar{n} = \frac{g}{2\pi^2}\int_m^\infty dE\, E\sqrt{E^2-m^2}\left(\frac{1}{1+\exp[(E-\mu)/T]} - \frac{1}{1+\exp[(E+\mu)/T]}\right) \tag{C.31}$$

$$= \begin{cases} \frac{gT^3}{6\pi^2}\left[\pi^2\left(\frac{\mu}{T}\right) + \left(\frac{\mu}{T}\right)^3\right] & (T \gg m) \\ 2g\left(\frac{mT}{2\pi}\right)^{3/2}\sinh(\mu/T)\exp(-m/T) & (T \ll m) \end{cases}. \tag{C.32}$$

In the early universe, interactions between different species kept them in equilibrium with a common temperature. As the universe cooled, species decoupled from thermal equilibrium. It turns out to be handy to measure the total energy density and pressure of all species in equilibrium in terms of the photon temperature T:

$$\rho_R = T^4 \sum_i \left(\frac{T_i}{T}\right)^4 \frac{g_i}{2\pi^2}\int_{x_i}^\infty \frac{\sqrt{u^2-x_i^2}\,u^2 du}{\exp(u-y_i)\pm 1} \tag{C.33}$$

$$P_R = T^4 \sum_i \left(\frac{T_i}{T}\right)^4 \frac{g_i}{6\pi^2}\int_{x_i}^\infty \frac{(u^2-x_i^2)^{3/2}\,u^2 du}{\exp(u-y_i)\pm 1}, \tag{C.34}$$

where i runs over all species and we have defined the dimensionless variables $x_i \equiv m_i/T$ and $y_i \equiv \mu_i/T$. Further, since the energy density and pressure of non-relativistic species ($m \gg T$) are exponentially suppressed, we may restrict the sum to only relativistic species so that the above expressions simplify,

$$\rho_R = \frac{\pi^2}{30} g_* T^4 \tag{C.35}$$

$$P_R = \frac{\pi^2}{90} g_* T^4, \tag{C.36}$$

where g_* counts the number of effectively massless degrees of freedom,

$$g_* = \sum_{i=\text{bosons}} g_i \left(\frac{T_i}{T}\right)^4 + \frac{7}{8}\sum_{i=\text{fermions}} g_i \left(\frac{T_i}{T}\right)^4. \tag{C.37}$$

The famous factor of 7/8 accounts for the difference in Bose and Fermi statistics in the equilibrium distribution function. The value of g_* is monotonically decreasing.

C.6 Entropy

In the early universe, the interaction rate of particles in the thermal bath was much greater than the expansion rate so that local thermal equilibrium is maintained. In this case, the entropy per comoving volume is preserved and this becomes a useful fiducial quantity. Further, for most of the early universe, the chemical potential is much smaller than the temperature and the distribution functions depend only on E/T. This means that

$$\frac{\partial P}{\partial T} = g\int đ^3p \frac{\partial f(\mathbf{p})}{\partial T}\frac{|\mathbf{p}|^2}{3E} = g\int đ^3p \left(\frac{-E}{T}\right)\frac{\partial f(\mathbf{p})}{\partial E}\frac{|\mathbf{p}|^2}{3E}. \tag{C.38}$$

Integrating this by parts (dropping the surface term) yields

$$\frac{\partial P}{\partial T} = \frac{\rho + P}{T}. \tag{C.39}$$

This can also be derived from integrability, $\partial^2 S/\partial T \partial V = \partial^2 S/\partial V \partial T$. We'll get back to this shortly.

The right-hand side is identified with entropy density. To remember this, recall that the Second Law tells us that

$$TdS = d(\rho V) + PdV = d\left[(\rho + P) + V\right] - VdP. \tag{C.40}$$

Making use of (C.39), we may write

$$dS = \frac{d\left[(\rho + P)V\right]}{T} - \frac{(\rho + P)VdT}{T^2} = d\left[\frac{(\rho + P)V}{T} + \text{const.}\right]. \tag{C.41}$$

Ignoring the overall constant, the entropy per comoving volume is

$$S = R^3 \frac{\rho + P}{T}, \tag{C.42}$$

so that we may identify (C.39) with the entropy density,

$$s \equiv \frac{S}{V} = \frac{\rho + P}{T}. \tag{C.43}$$

Now invoke the First Law (C.14) with $dQ = 0$ and $E = \rho V$, which we may write as

$$d\left[(\rho + P)V\right] = VdP. \tag{C.44}$$

combining this with (C.39) gives

$$s = d\left[\frac{(\rho + P)V}{T}\right] = 0, \tag{C.45}$$

so that entropy is indeed conserved.

Entropy is dominated by the contribution of relativistic particles, (C.35) and (C.36), so that

$$s = \frac{2\pi^2}{45} g_{*s} T^3, \tag{C.46}$$

where

$$g_{*s} = \sum_{i=\text{bosons}} g_i \left(\frac{T_i}{T}\right)^3 + \frac{7}{8} \sum_{i=\text{fermions}} g_i \left(\frac{T_i}{T}\right)^3, \tag{C.47}$$

which differs from (C.37) only in the exponent of the (T_i/T) factors. However, since most particles had the same temperature in the early (equilibrium) universe, $g_{*s} = g_*$. This is depicted in Fig. 10. Note that by virtue of its dependence on T, s is proportional to the number density of relativistic

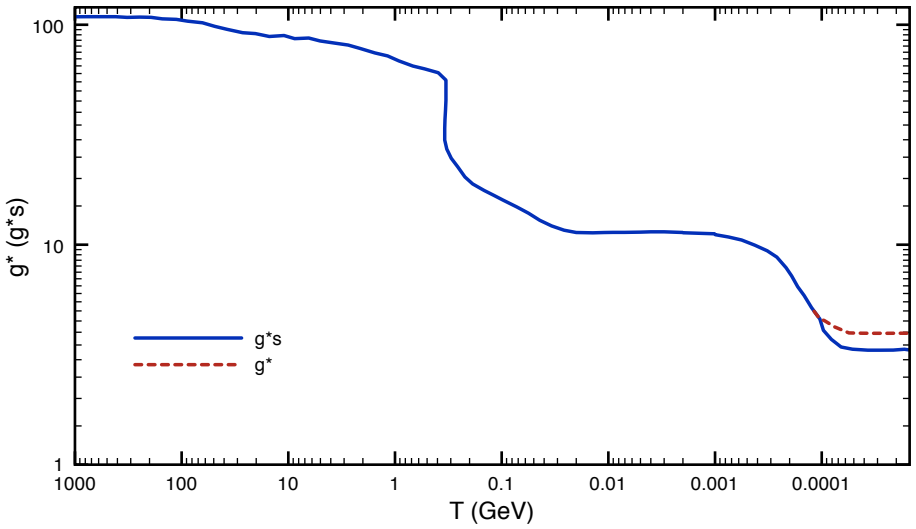

Figure 10: Solid (dashed) line: A plot of the number of relativistic degrees of freedom g_* (g_{*s}) as a function of temperature. Note that g_{*s} tracks g_* until late times (low temperatures) when species fall out of thermal equilibrium and $(T_i/T)^3 \neq (T_i/T)^4$. Image from Kolb & Turner [2] using GraphClick [119]. There's another nice plot in Fig. 3 of JKG [95]; I used that in Fig. 6 above.

particles, (C.25). We also remark that (C.46) is a useful equation when converting between the definitions $Y = n/T^3$ versus $Y = n/s$.

It is convenient to normalize s relative to the photon density,

$$s = 1.80\, g_{*s} n_\gamma. \tag{C.48}$$

Since $s \sim a^{-3}$, the total number of particles in a comoving volume, $N = R^3 n$, is equal to the number density divided by the entropy, $N = n/s$.

Why two g_* values? Even though $g_* = g_{*s}$ when all relativistic particles share the same temperature, these quantities differ when one species decouples and has a lower temperature. Such a species would contribute less to the effective number of relativistic degrees of freedom by a factor that depends on whether we're looking at g_* or g_{*s}. The reason why we need two counts of the number of degrees of freedom is that g_* relates the temperature to energy density via (C.35), while g_{*s} relates the temperature to the scale factor via $T \sim g_{*s}^{-1/3} a^{-1}$, c.f. (C.48).

C.7 Example: Neutrinos

As a handy example, let us consider the cosmological thermodynamics of neutrinos. Neutrinos have a Fermi-Dirac distribution with zero chemical potential. Because of their weak (at energies on the order of their mass) interaction strength, they decouple from the thermal plasma at late times. However, the Fermi-Dirac distribution is maintained with their temperature falling as a^{-1}.

Note that unlike thermal WIMPs, neutrinos are relativistic. We would like to relate the neutrino temperature to the present day photon temperature. The subtlety is that neutrinos decouple just before e^+e^- annihilations and so do not inherit any of the this energy; i.e. photons have a higher temperature than neutrinos.

We can now calculate the entropy using the formulae in the previous subsection. Prior to e^+e^- annihilations, there were electrons (2 spins), positrons (2 spins), neutrinos (3 generations $\times$ 1 spin), and anti-neutrinos (3 generations $\times$ 1 spin). [This is morally the same as saying that there are three generations of light Majorana neutrinos with 2 spin states.] This gives an entropy s_1 before annihilation that is

$$s_1 = \frac{2\pi^2}{45} T_1^3 \left[2 + \frac{7}{8} (2 + 2 + 3 + 3) \right] = \frac{43\pi^2}{90} T_1^3. \tag{C.49}$$

After annihilation, the electrons and positrons are removed and the photon and neutrino temperatures no longer match. The entropy is then

$$s_2 = \frac{2\pi^2}{45} \left[2T_\gamma^3 + \frac{7}{8} \cdot 6T_\nu^3 \right]. \tag{C.50}$$

Requiring entropy conservation in a comoving volume, $s_1 a_1^3 = s_2 a_2^3$ sets

$$\frac{43}{2} (a_1 T_1)^3 = 4 \left[\left(\frac{T_\gamma}{T_\nu} \right)^3 + \frac{21}{8} \right] (T_\nu a_2)^3 . \tag{C.51}$$

The neutrino temperature scales like a^{-1} throughout the entire process, so $a_1 T_1 = a_2 T_\nu$ so that we find

$$\frac{T_\nu}{T_\gamma} = \left(\frac{4}{11} \right)^{1/3}. \tag{C.52}$$

Armed with this information, we can now determine the cosmological neutrino abundance. We can start with the photon energy density (C.33). Since the chemical potential is zero, we can just write ρ_γ as

$$\rho_\gamma = 2 \int đ^3 p \frac{p}{e^{p/T} - 1}. \tag{C.53}$$

To get the neutrino density we swap the sign in the denominator and then multiply by 7/8 to account for the Fermi-Dirac statistics (c.f. (C.26)). Since the energy density of a massless particle scales like T^4, then we have to include a fourth power of the right-hand side of (C.52). Lastly, we tack on an extra factor of three to account for the three neutrino generations. (The two photon spin states match the degeneracy in neutrinos and anti-neutrinos.) We thus find

$$\rho_\nu = 3 \cdot \frac{7}{8} \left(\frac{4}{11} \right)^{4/3} \rho_\gamma. \tag{C.54}$$

In the limit where there are three massless neutrinos today, the contribution to the energy density is

$$\Omega_\nu h^2 \equiv \frac{\rho}{\rho_{\rm cr}} = 1.68 \times 10^{-5}. \tag{C.55}$$

Of course, neutrinos are not actually massless and this formalism should be modified by including the neutrino mass in the expression for ρ_ν. One finds that at late times, $n_\nu = 2n_\gamma/11$ with $\rho_\nu = m_\nu n_\nu$. Finally,

$$\Omega_\nu h^2 = \frac{m_\nu}{94h^2 \text{ eV}}. \tag{C.56}$$

Thus the critical density leads to strong bounds on the neutrino mass.

D Kinetic Theory and the Boltzmann Equation

> *In the 1960s a national magazine ran a cartoon showing dozens of businessmen and -women walking the streets of Manhattan looking very serious. Though bubbles over each head revealed their true focus: each was imagining a raucus sex scene. In at least some ways, the Boltzmann equation plays a similar role for physicists and astronomers: no one ever talks about it, but everyone is always thinking about it.* – Dodelson, chapter 4 [1]

We present a thorough derivation of the Boltzmann equation. This treatment is based on statistical physics lectures by Eun-Ah Kim[17]. Alternately, one may peruse the usual statistical mechanics texts or chapter 4 of Dodelson [1].

D.1 Kinetic theory

Define the unconditional s-particle probability in an N-particle system,

$$\rho_s(\mathbf{p}_1, \mathbf{q}_1, \cdots, \mathbf{p}_s, \mathbf{q}_s; t) = \int \prod_{i=s+1}^{N} d\vec{\mu}_i \, \rho(\mathbb{p}, \mathbb{q}, t). \tag{D.1}$$

Here $\rho(\mathbb{p}, \mathbb{q}, t)$ is the one-particle probability in phase space. The product on the right-hand side runs over the $(N - s)$ particles which are not specified by the arguments of the left-hand side. From this we can define particle densities. We begin with the **single particle density** which is the expectation for finding *any* of the N particles in the state $(\mathbf{p}, \mathbf{q})$,

$$f_1(\mathbf{p}, \mathbf{q}; t) = \left\langle \sum_{j=1}^{N} \delta^{(3)}(\mathbf{p} - \mathbf{p}_j)\delta^{(3)}(\mathbf{q} - \mathbf{q}_j) \right\rangle \tag{D.2}$$

$$= N \int \prod_{j=2}^{N} d\vec{\mu} \, \rho(\mathbf{p_1} = \mathbf{p}, \mathbf{q_1} = \mathbf{q}, \mathbf{p}_2, \mathbf{q}_2, \cdots, \mathbf{p_N}, \mathbf{q}_N; t) \tag{D.3}$$

$$= N\rho_1(\mathbf{p}, \mathbf{q}; t). \tag{D.4}$$

[17] `http://eunahkim.ccmr.cornell.edu/teaching/6562_S11/Welcome.html`

We've written the phase space measure as $d\vec{\mu}$. From here we can generalize to an s-**particle density**,

$$f_s(\mathbf{p}, \cdots, \mathbf{q}_s; t) = N(N-1)\cdots(N-S+1)\rho_s(\mathbf{p}_1, \cdots, \mathbf{q}_s; t) = \frac{N!}{(N-S)!}\rho_s(\mathbf{p}_1, \cdots, \mathbf{q}_s; t). \quad \text{(D.5)}$$

A good question is to ask how these densities evolve with time. Fortunately, we only have to look at ρ_1:

$$\frac{\partial \rho_1}{\partial t} = \int \prod_{i=2}^{N} d\vec{\mu}_i \, \frac{\partial \rho}{\partial t} = -\int \prod_{i=2}^{N} d\vec{\mu}_i \, \{\rho, H\}, \quad \text{(D.6)}$$

where ρ is the full phase space density ($6N$ variables) and we've use Liouville's theorem. Let us organize the Hamiltonian into three pieces, $H = H_1 + H_{N-1} + H'$, where,

$$H_1 = \frac{\mathbf{p}_1^2}{2m} + U(\mathbf{q}_1) \quad \text{(D.7)}$$

$$H_{N-1} = \sum_{i=2}^{N} \left[\frac{\mathbf{p}_1^2}{2m} + U(\mathbf{q}_1) \right] + \frac{1}{2} \sum_{i,j=2}^{N} V(\mathbf{q}_i - \mathbf{q}_j) \quad \text{(D.8)}$$

$$H' = \sum_{i=2}^{N} V(\mathbf{q} - \mathbf{q}_i). \quad \text{(D.9)}$$

Here $U(\mathbf{q})$ is an external potential, while $V(\mathbf{q}_i - \mathbf{q}_j)$ is an interaction potential between different particles. We can thus write

$$\frac{\partial \rho_1}{\partial t} = -\int \prod_{i=2}^{N} d\vec{\mu}_i \, \{\rho, (H_1 + H_{N-1} + H')\}. \quad \text{(D.10)}$$

Let us consider each term one at a time.

$$\int \prod_{i=2}^{N} d\vec{\mu}_i \, \{\rho, H_1\} = \int \prod_{i=2}^{N} d\vec{\mu}_i \, \{\rho, H_1\} = \{\rho_1, H_1\}. \quad \text{(D.11)}$$

Here we've used the fact that H_1 is independent of $\vec{\mu}_i$ for $i \neq 1$.

$$\int \prod_{i=2}^{N} \{\rho, H_{N-1}\} = \int \prod_{i=2}^{N} d\vec{\mu}_i \sum_{j=1}^{N} \left(\frac{\partial \rho}{\partial \mathbf{p}_j} \frac{\partial H_{N-1}}{\partial \mathbf{q}_j} - \frac{\partial \rho}{\partial \mathbf{q}_j} \frac{\partial H_{N-1}}{\partial \mathbf{p}_j} \right) \quad \text{(D.12)}$$

$$= \int \prod_{i=2}^{N} d\vec{\mu}_i \sum_{j=1}^{N} \left[\frac{\partial \rho}{\partial \mathbf{p}_j} \left(\frac{\partial U}{\partial \mathbf{q}_j} + \frac{1}{2} \sum_{k=2}^{N} \frac{\partial V(\mathbf{q}_j - \mathbf{q}_k)}{\partial q_j} \right) - \frac{\partial \rho}{\partial \mathbf{q}_j} \frac{\mathbf{p}_j}{m} \right] \quad \text{(D.13)}$$

$$= 0. \quad \text{(D.14)}$$

Here we've noted that the term in the parentheses is independent of $\mathbf{p}_j$ while the remaining term is independent of $\mathbf{q}_j$; thus the entire line vanishes upon the appropriate integration by parts.

$$\int \prod_{i=2}^{N} d\vec{\mu}_i \sum_{j=1}^{N} \left[\frac{\partial \rho}{\partial \mathbf{p}_j} \frac{\partial H'}{\partial \mathbf{q}_j} - \cancel{\frac{\partial \rho}{\partial \mathbf{q}_j} \frac{\partial H'}{\partial \mathbf{p}_j}} \right] = \int \prod_{i=2}^{N} d\vec{\mu}_i \sum_{j=1}^{N} \left[\frac{\partial \rho}{\partial \mathbf{p}_1} \sum_{j=2}^{N} \frac{\partial V(\mathbf{q}_i - \mathbf{q}_j)}{\partial \mathbf{q}_1} + \sum_{j=2}^{N} \cancel{\frac{\partial \rho}{\partial \mathbf{p}_j} \frac{\partial V(\mathbf{q}_i - \mathbf{q}_j)}{\partial \mathbf{q}_j}} \right]$$

$$= (N-1) \int \prod_{i=2}^{N} d\vec{\mu}_i \, \frac{\partial \rho}{\partial \mathbf{p}_1} \cdot \frac{\partial V(\mathbf{q}_i - \mathbf{q}_j)}{\partial \mathbf{q}_1} \tag{D.15}$$

$$= (N-1) \int d\vec{\mu}_2 \, \frac{\partial V(\mathbf{q}_i - \mathbf{q}_j)}{\partial \mathbf{q}_1} \cdot \frac{\partial}{\partial \mathbf{p}_1} \left(\prod_{i=3}^{N} d\vec{\mu}_i \, \rho \right) \tag{D.16}$$

$$= (N-1) \int d\vec{\mu}_2 \, \frac{\partial V(\mathbf{q}_i - \mathbf{q}_j)}{\partial \mathbf{q}_1} \cdot \frac{\partial \rho_2}{\partial \mathbf{p}_1}. \tag{D.17}$$

On the first line we used the independence of H' on $\mathbf{p}$ and, on the right-hand side, integration by parts. What a mess. Fortunately we can clearn this all up and then generalize. Plugging this into (D.10) yields

$$\frac{\partial \rho_1}{\partial t} - \{H_1, \rho_1\} = (N-1) \int d\vec{\mu}_2 \, \frac{\partial V(\mathbf{q}_1 - \mathbf{q}_2)}{\partial \mathbf{q}_1} \cdot \frac{\partial \rho_2}{\partial \mathbf{p}_1}. \tag{D.18}$$

Multiplying by N allows us to convert this into an expression for the time evolution of f_1,

$$\frac{\partial f_1}{\partial t} - \{H_1, f_1\} = \int d\vec{\mu}_2 \, \frac{\partial V(\mathbf{q}_1 - \mathbf{q}_2)}{\partial \mathbf{q}_1} \cdot \frac{\partial f_2}{\partial \mathbf{p}_1}. \tag{D.19}$$

The right-hand side of this equation is a collision integral that tells us about the pair-wise interactions of particles in this system. It is now straightforward to see how this generalizes for the time evolution of a general multi-particle density,

$$\frac{\partial f_s}{\partial t} - \{H_s, f_s\} = \sum_{n=1}^{s} \int d\vec{\mu}_2 \, \frac{\partial V(\mathbf{q}_n - \mathbf{q}_{s+1})}{\partial \mathbf{q}_n} \cdot \frac{\partial f_{s+1}}{\partial \mathbf{p}_n}. \tag{D.20}$$

The general point that one should glean from this is that the expression for $\partial f_s / \partial t$ requires knowledge of f_{s+1}. In order to find out f_1, one needs to know f_2, but to know f_2 one needs f_3, an so forth. This is sometimes referred to as the BGGKY hierarchy.

D.2 The Boltzmann equation

The physical approximation that allows us to bypass the BGGKY hierarchy is the Boltzmann equation. The key assumption is that interactions are short range. Even with this assumption, one should take pause: mechanics was already boring and tedious for two-particle scattering. Now we will be going to $N \sim 10^{23}$-particle scattering! We will give a loose, 'plausible' presentation. You may fill in the details as you feel necessary.

Let us explictly write out the first two equations of the hierarchy:

$$\left[\frac{\partial}{\partial t} - \frac{\partial U}{\partial \mathbf{q}_1} \frac{\partial}{\partial \mathbf{p}_1} + \frac{\mathbf{p}_1}{m} \frac{\partial}{\partial \mathbf{q}_1} \right] f_1 = \int d\vec{\mu}_2 \, \frac{\partial V(\mathbf{q}_1 - \mathbf{q}_2)}{\partial \mathbf{q}_1} \frac{\partial f_2}{\partial \mathbf{p}_1} \tag{D.21}$$

$$\left[\frac{\partial}{\partial t} - \frac{\partial U}{\partial \mathbf{q}_1}\frac{\partial}{\partial \mathbf{p}_1} - \frac{\partial U}{\partial \mathbf{q}_2}\frac{\partial}{\partial \mathbf{p}_2} + \frac{\mathbf{p}_1}{m}\frac{\partial}{\partial \mathbf{q}_1} + \frac{\mathbf{p}_2}{m}\frac{\partial}{\partial \mathbf{q}_2} - \frac{\partial V(\mathbf{q}_1\mathbf{q}_2)}{\partial \mathbf{q}_1}\left(\frac{\partial}{\partial \mathbf{p}_1} - \frac{\partial}{\partial \mathbf{p}_2}\right)\right] f_2$$
$$= \int d\vec{\mu}_3 \left[\frac{\partial V(\mathbf{q}_1 - \mathbf{q}_3)}{\partial \mathbf{q}_1}\frac{\partial}{\partial \mathbf{p}_1}\frac{\partial V(\mathbf{q}_2 - \mathbf{q}_3)}{\partial \mathbf{q}_2}\frac{\partial}{\partial \mathbf{p}_2}\right] f_3 \tag{D.22}$$

D.2.1 Time scales

Now we get to do some physics. Let us identify the (inverse) time scales that appear in the expressions above (this is just dimensional analysis). In fact, before we identify any of the terms, you should already have some intuition for the relevant scales in the problem.

- The length scale of the external potential
- The length scale of particle-particle interactions
- The length scale for free particle propagation.

These can be converted into time scales though the average particle velocity of the system. First we have the **time scale of the external potential**,

$$\frac{1}{\tau_U} = \frac{\partial U}{\partial \mathbf{q}}\frac{\partial}{\partial \mathbf{p}} \sim \frac{v}{L}. \tag{D.23}$$

Recall that $\partial U/\partial \mathbf{q}$ is a force and that momentum divided by force indeed gives the time scale for momentum change. We've written v for the average velocity of the particles and L to be the characteristic length scale for changes in U. Similarly, note that $(\mathbf{p}/m)\partial/\partial \mathbf{q}$ is a velocity times gradient, or $v \cdot \nabla f$.

Next there is a time scale associated with the **mean free time** between particle interactions. Consider the right-hand side of (D.21), which we may write heuristically as

$$\left[\int d\vec{\mu}_2 \frac{\partial V}{\partial \mathbf{q}_1}\frac{\partial f_2}{\partial \mathbf{p}_1}\frac{1}{f_1}\right] f_1. \tag{D.24}$$

We've written it this way to obtain a quantity that may sensibly be compared to the left-hand side of the same equation. Indeed, this allows us to define the mean free time more generally as

$$\frac{1}{\tau_X} \sim \int d\vec{\mu}\, \frac{\partial V}{\partial \mathbf{q}}\frac{\partial}{\partial \mathbf{p}}\frac{f_{s+1}}{f_s} \sim \frac{v}{d} \cdot nd^3, \tag{D.25}$$

where d is a length scale characterizing the range of the interaction. τ_X is the timescale between particle interactions: given an interaction, when is the next interaction? The factor f_2/f_1 in the $s = 2$ case is the conditional probability of finding a second particle given the first. This should be associated with the factor of nd^3 on the right-hand side, where n is the number density (so that this is just the probability of finding another particle per unit volume). The right-hand sides of both (D.21) and (D.22) are thus terms which represent free particle propagation within the system.

Finally, we can consider the **collision duration**, which appears as term containing a gradient of V on the left-hand side of (D.22).

$$\frac{1}{\tau_{\mathrm{c}}} \sim \frac{\partial V}{\partial \mathbf{q}} \frac{\partial}{\partial \mathbf{p}} \sim \frac{v}{d}. \tag{D.26}$$

We see that (D.21) is an equation that compares τ_U with τ_X, while (D.22) also introduces τ_{c}. Our goal is to try to truncate the BGGKY hierarchy by taking the correct (physically motivated) limits. First we take the **dilute limit**, where

$$nd^3 \ll 1 \qquad \Longleftrightarrow \qquad \frac{1}{\tau_{\mathrm{c}}} \gg \frac{1}{\tau_X}. \tag{D.27}$$

Next, we can augment this with the assumption that the external potential is not vary much on short time scales,

$$\frac{1}{\tau_U} \ll \frac{1}{\tau_X} \ll \frac{1}{\tau_{\mathrm{c}}}. \tag{D.28}$$

In fact, typically the last relation is $\tau_X^{-1} \lll \tau_{\mathrm{c}}^{-1}$. Lastly, we will need to assume **molecular chaos**, which is the statement that the two-particle density is well approximated by the product of one-particle densities. We will quantify this shortly.

D.2.2 Deriving the Boltzmann equation

First not that the limits that we have chosen do not allow us to truncate (D.21). In the regime $\tau_U^{-1} \ll \tau_X^{-1}$, we cannot drop the right-hand side of the one-particle kinetic equation and we're stuck with the full expression. We can do more with (D.22). Here the dilute limit allows us to note that

$$\frac{\tau_{\mathrm{c}}}{\tau_X} \approx nd^3 \ll 1. \tag{D.29}$$

In other words, as long as we have a τ_{c}^{-1} floating around (and only when we have such a term), we are free to drop terms that go like τ_X^{-1}. Needless to say we can also drop the τ_U term on the left-hand side. Further, as we are interested in long time scales, i.e. 'steady state' situations. We can thus drop the $\partial/\partial t$ on the left-hand side. Typically $\tau_U^{-1} \ll 1/t \ll \tau_{\mathrm{c}}^{-1}$. Thus means that we can simplify (D.22) quite a bit:

$$\left[\frac{\mathbf{p}_1}{m} \cdot \frac{\partial}{\partial \mathbf{q}_1} + \frac{\mathbf{p}_2}{m} \cdot \frac{\partial}{\partial \mathbf{q}_2} - \frac{\partial V(\mathbf{q}_1 - \mathbf{q}_2)}{\partial \mathbf{q}_1} \cdot \left(\frac{\partial}{\partial \mathbf{p}} - \frac{\partial}{\partial \mathbf{p}_2}\right)\right] f_2 = 0. \tag{D.30}$$

Our assumption regarding the slow variation of the external potential motivates us to use relative spacetime coordinates,

$$\mathbf{Q} \equiv \frac{1}{2}(\mathbf{q}_1 + \mathbf{q}_2) \qquad\qquad \mathbf{q} \equiv \mathbf{q}_2 - \mathbf{q}_1, \tag{D.31}$$

where the factor of $1/2$ is intentionally only on $\mathbf{Q}$. We note that in these coordinates,

$$\frac{\partial f_2}{\partial \mathbf{q}_1} \approx -\frac{\partial f_2}{\partial \mathbf{q}} \approx -\frac{\partial f_2}{\partial \mathbf{q}_2}. \tag{D.32}$$

Using (D.30), we may thus write

$$\frac{\partial V(\mathbf{q}_1 - \mathbf{q}_2)}{\partial \mathbf{q}_1} \cdot \left(\frac{\partial}{\partial \mathbf{p}} - \frac{\partial}{\partial \mathbf{p}_2} \right) f_2 = \left(\frac{\mathbf{p}_1 - \mathbf{p}_2}{m} \right) \cdot \frac{\partial f_2}{\partial \mathbf{q}}. \tag{D.33}$$

We can now use this to rewrite the right-hand side of (D.21). We start by adding a term proportional to $0 = \partial f_2 / \partial \mathbf{p}_2$ (this vanishes upon integration by parts),

$$\int d\vec{\mu}_2 \, \frac{\partial V(\mathbf{q}_1 - \mathbf{q}_2)}{\partial \mathbf{q}_1} \frac{\partial f_2}{\partial \mathbf{p}_1} = \int d\vec{\mu}_2 \, \frac{\partial V(\mathbf{q}_1 - \mathbf{q}_2)}{\partial \mathbf{q}_1} \left(\frac{\partial}{\partial \mathbf{p}_1} - \frac{\partial}{\partial \mathbf{p}_2} \right) f_2 = \int d\vec{\mu}_2 \, \left(\frac{\mathbf{p}_1 - \mathbf{p}_2}{m} \right) \cdot \frac{\partial f_2}{\partial \mathbf{q}}.$$

Now we express the collision integral in terms of the collision kinematics. We need to recall some of our favorite quantities from two-particle scattering. In particular, we introduce the **impact vector**, $\mathbf{b}$, which lives in the plane perpendicular to the scattering axis and quantifies how off-axis the initial particle trajectories are. We choose angular coordinates so that θ measures the particle deflection from scattering axis and ϕ is the azimuthal angle. We may thus write

$$\begin{aligned} &\int d^3\mathbf{p}_2 d^3\mathbf{q}_2 \, \left(\frac{\mathbf{p}_2 - \mathbf{p}_1}{m} \right) \frac{\partial}{\partial \mathbf{q}} f_2(\mathbf{p}_1, \mathbf{q}_1, \mathbf{p}_2, \mathbf{q}_2; t) \\ &= \int d^3\mathbf{p}_2 d^2\mathbf{b} \, |\mathbf{v}_1 - \mathbf{v}_2| \left[f_2(\mathbf{p}_1, \mathbf{q}_1, \mathbf{p}_2, \mathbf{b}, +; t) - f_2(\mathbf{p}_1, \mathbf{q}_1, \mathbf{p}_2, \mathbf{b}, -; t) \right], \end{aligned} \tag{D.34}$$

where we've introduced different arguments in f_2: $\pm$ denotes the state before $(-)$ or after $(+)$ the collision. We would like to work exclusively in terms of the 'before collision' variables (we are taking the limit of an instantaneous collision). We thus write

$$f_2(\mathbf{p}_1, \mathbf{q}_1, \mathbf{p}_2, \mathbf{b}, +; t) = f_2(\mathbf{p}_1', \mathbf{q}_1', \mathbf{p}_2', \mathbf{b}, -; t), \tag{D.35}$$

where we've defined the primed phase space coordinates to denote the momenta which trace into the unprimed coordinates upon collision. In some sense this is just a slick use of time reversal; but really it's just a definition of the primed coordinates.

Finally, the most drastic approximation we shall make is that of **molecular chaos**. Here we assume that particles 1 and 2 are independent before collision so that the two-particle phase space density is well-approximated by the product of single-particle densities,

$$f_2(\cdots, \mathbf{b}, -; t) = f_1(\mathbf{p}_1, \mathbf{q}_1; t) f_1(\mathbf{p}_2, \mathbf{q}_2; t). \tag{D.36}$$

Taking all of this into account in (D.21), we finally obtain

$$\left. \frac{df_1}{dt} \right|_{\text{coll}} = \int d^3\mathbf{p}_2 d^2\mathbf{b} \, |\mathbf{v}_1 - \mathbf{v}_2| \left[f_1(\mathbf{p}_1, \mathbf{q}_1; t) f_1(\mathbf{p}_2, \mathbf{q}_2; t) - f_1(\mathbf{p}_1', \mathbf{q}_1; t) f_1(\mathbf{p}_2', \mathbf{q}_2; t) \right]. \tag{D.37}$$

E Sample Annihilation Calculation

Below is a sample calculation for $\chi\chi \to aa$ in Goldstone Fermion Dark Matter [120]. It demonstrates how to use *Mathematica* to calculate amplitudes and cross sections with Weyl spinors.

First we define our metric and Pauli matrices.

```
Clear["Global`*"]
\[Eta] = ( {
    {1, 0, 0, 0},
    {0, -1, 0, 0},
    {0, 0, -1, 0},
    {0, 0, 0, -1}
   } );
\[Eta]diag = {1, -1, -1, -1};

\[Sigma] = {( {
     {1, 0},
     {0, 1}
    } ), ( {
     {0, 1},
     {1, 0}
    } ), ( {
     {0, -I},
     {I, 0}
    } ), ( {
     {1, 0},
     {0, -1}
    } )};
\[Sigma]bar = {( {
     {1, 0},
     {0, 1}
    } ), -( {
      {0, 1},
      {1, 0}
     } ), -( {
      {0, -I},
      {I, 0}
     } ), -( {
      {1, 0},
      {0, -1}
     } )};
\[Eta]dot[p_, q_] := p.\[Eta].q;
\[Eta]sq[p_] := \[Eta]dot[p, p];
slash[p_] := Sum[p[[i]] \[Eta]diag[[i]] \[Sigma][[i]], {i, 1, 4}]
slashbar[p_] :=
 Sum[p[[i]] \[Eta]diag[[i]] \[Sigma]bar[[i]], {i, 1, 4}]
```

Note that we've also defined the four-vector dot product and the contraction with the Pauli four-vector. Next we define the plane-wave spinors following Appendix C of [96]. We label helicity by `λ[[1]]` and `λ[[2]]`, corresponding to $\lambda = \pm 1/2$. This makes it easier to do the spin sum in

the squared matrix element. For now we'll just write spinors for the incoming states along the $\pm z$ direction. Note that this section is not fully general. In particular, we do not include all of the Euler angles in $\chi \cdot \omega$.

```
\[Lambda] = {1/2, -1/2};
\[Omega][p_, \[Lambda]_] := Sqrt[
 p[[1]] + 2 \[Lambda] Sqrt[Sum[p[[i]]^2, {i, 2, 4}]]]
Angle[p_] := ArcTan[p[[4]], p[[3]]]

(* Assuming \[Phi] = \[Gamma] = 0 *)
\[Chi][p_, 1/
  2] := {Cos[Angle[p]/2], Sin[Angle[p]/2]}
\[Chi][p_, -(1/2)] := {-Sin[Angle[p]/2], Cos[Angle[p]/2]}

(* Plane wave external state spinors *)
(* d = dagger, u/l = \
upper/lower index i.e. ydu = y^(\[Dagger]
\!\(\*OverscriptBox["\[Alpha]", "."]\)) *)

xl[p_, s_] := \[Omega][p, -\[Lambda][[s]]] \[Chi][p, \[Lambda][[s]]]
xu[p_, s_] := -2 \[Lambda][[s]] \[Omega][
   p, -\[Lambda][[s]]] Conjugate[\[Chi][p, -\[Lambda][[s]]]]
ydu[p_, s_] := \[Omega][p, \[Lambda][[s]]] \[Chi][p, \[Lambda][[s]]]
ydl[p_, s_] :=
 2 \[Lambda][[s]] \[Omega][p, \[Lambda][[s]]]
  Conjugate[\[Chi][p, -\[Lambda][[s]]]]
```

Now we make a few definitions to make life easier later. We define the external momenta, the assumptions, and a few replacements. From here on the details are not important (they're model-specific), but the general method is instructive.

```
p1 = {p0, 0, 0, pz};
p2 = {p0, 0, 0, -pz};
k1 = {p0, 0, kz Sin[\[Theta]], kz Cos[\[Theta]]};
k2 = {p0, 0, -kz Sin[\[Theta]], -kz Cos[\[Theta]]};

(*assumptions, help make things run quickly*)

assume = {p0 \[Element] Reals, pz \[Element] Reals,
   kz \[Element] Reals, \[Theta] \[Element] Reals, p0 > 0, pz > 0,
   kz > 0, p0 > m\[Chi], p0 > pz, p0 > kz, b1 \[Element] Reals,
   f \[Element] Reals, p0 > ma, p0 > m\[Chi], m\[Chi] > ma, ma > 0,
   m\[Chi] > 0, A \[Element] Reals, B \[Element] Reals};

(* Replacements *)

kz2mass = {pz -> Sqrt[p0^2 - m\[Chi]^2], kz -> Sqrt[p0^2 - ma^2]};
co2long = {A -> (b1 q)/(Sqrt[2] f),
   B -> (ma (\[Alpha] + \[Beta]) Sqrt[2])/f};
(* A=(b1 q)/(Sqrt[2]f);  U(1)-preserving coupling coefficient *)
(* \
B=(ma (\[Alpha]+\[Beta]) Sqrt[2])/f;  U(1)-breaking coupling \
```

```
coefficient *)

(* normalize charge *)
q = 1;
```

Now we write out each diagram. Compare this to Section 4.2.

```
(* Only U(1) symmetric interactions *)

Mt1[s1_, s2_, k1_, k2_] :=
 A^2 I/(\[Eta]sq[k1 - p1] - m\[Chi]^2)
  ydl[p1, s1].slashbar[k1].slash[k1 - p1].slashbar[k2].xl[p2, s2]
Mt2[s1_, s2_, k1_, k2_] :=
 A^2 I/(\[Eta]sq[k1 - p1] - m\[Chi]^2)
  xu[p1, s1].slash[k1].slashbar[k1 - p1].slash[k2].ydu[p2, s2]
Mt3[s1_, s2_, k1_, k2_] :=
 A^2 (-I m\[Chi])/(\[Eta]sq[k1 - p1] - m\[Chi]^2)
  xu[p1, s1].slash[k1].slashbar[k2].xl[p2, s2]
Mt4[s1_, s2_, k1_, k2_] :=
 A^2 (-I m\[Chi])/(\[Eta]sq[k1 - p1] - m\[Chi]^2)
  ydl[p1, s1].slashbar[k1].slash[k2].ydu[p2, s2]

Msym[s1_, s2_] :=
 Mt1[s1, s2, k1, k2] + Mt2[s1, s2, k1, k2] + Mt3[s1, s2, k1, k2] +
  Mt4[s1, s2, k1, k2] +
  Mt1[s1, s2, k2, k1] + Mt2[s1, s2, k2, k1] + Mt3[s1, s2, k2, k1] +
  Mt4[s1, s2, k2, k1]


(* U(1) breaking interactions only *)

Mx1[s1_, s2_, k1_, k2_] :=
 B^2 (I m\[Chi])/(\[Eta]sq[k1 - p1] - m\[Chi]^2)
   xu[p1, s1].xl[p2, s2]
Mx2[s1_, s2_, k1_, k2_] :=
 B^2 (I m\[Chi])/(\[Eta]sq[k1 - p1] - m\[Chi]^2)
   ydl[p1, s1].ydu[p2, s2]
Mx3[s1_, s2_, k1_, k2_] :=
 B^2 -I /(\[Eta]sq[k1 - p1] - m\[Chi]^2)
   xu[p1, s1].slash[k1 - p1]. ydu[p2, s2]
Mx4[s1_, s2_, k1_, k2_] :=
 B^2 -I /(\[Eta]sq[k1 - p1] - m\[Chi]^2)
   ydl[p1, s1].slashbar[k1 - p1].xl[p2, s2]

Mbr[s1_, s2_] :=
 Mx1[s1, s2, k1, k2] + Mx2[s1, s2, k1, k2] + Mx3[s1, s2, k1, k2] +
  Mx4[s1, s2, k1, k2] +
  Mx1[s1, s2, k2, k1] + Mx2[s1, s2, k2, k1] + Mx3[s1, s2, k2, k1] +
  Mx4[s1, s2, k2, k1]

(* Cross terms: U(1) sym and U(1)-breaking vertex in each diagram *)
```

```
Mc1[s1_, s2_, k1_, k2_] :=
 A B (I m\[Chi])/(\[Eta]sq[k1 - p1] - m\[Chi]^2)
   xu[p1, s1].slash[k2]. ydu[p2, s2]
Mc2[s1_, s2_, k1_, k2_] :=
 A B (-I m\[Chi])/(\[Eta]sq[k1 - p1] - m\[Chi]^2)
   ydl[p1, s1].slashbar[k1].xl[p2, s2]
Mc3[s1_, s2_, k1_, k2_] :=
 A B (-I m\[Chi])/(\[Eta]sq[k1 - p1] - m\[Chi]^2)
   xu[p1, s1].slash[k1].ydu[p2, s2]
Mc4[s1_, s2_, k1_, k2_] :=
 A B (I m\[Chi])/(\[Eta]sq[k1 - p1] - m\[Chi]^2)
   ydl[p1, s1].slashbar[k2].xl[p2, s2]

Mc5[s1_, s2_, k1_, k2_] :=
 A B -I/(\[Eta]sq[k1 - p1] - m\[Chi]^2)
   xu[p1, s1].slash[k1 - p1].slashbar[k2]. xl[p2, s2]
Mc6[s1_, s2_, k1_, k2_] :=
 A B I/(\[Eta]sq[k1 - p1] - m\[Chi]^2)
   ydl[p1, s1].slashbar[k1].slash[k1 - p1] .ydu[p2, s2]
Mc7[s1_, s2_, k1_, k2_] :=
 A B I/(\[Eta]sq[k1 - p1] - m\[Chi]^2)
   xu[p1, s1].slash[k1].slashbar[k1 - p1] .xl[p2, s2]
Mc8[s1_, s2_, k1_, k2_] :=
 A B -I/(\[Eta]sq[k1 - p1] - m\[Chi]^2)
   ydl[p1, s1].slashbar[k1 - p1].slash[k2] .ydu[p2, s2]

Mcr[s1_, s2_] :=
 Mc1[s1, s2, k1, k2] + Mc2[s1, s2, k1, k2] + Mc3[s1, s2, k1, k2] +
  Mc4[s1, s2, k1, k2] +
  Mc5[s1, s2, k1, k2] + Mc6[s1, s2, k1, k2] + Mc7[s1, s2, k1, k2] +
  Mc8[s1, s2, k1, k2] +
  Mc1[s1, s2, k2, k1] + Mc2[s1, s2, k2, k1] + Mc3[s1, s2, k2, k1] +
  Mc4[s1, s2, k2, k1] +
  Mc5[s1, s2, k2, k1] + Mc6[s1, s2, k2, k1] + Mc7[s1, s2, k2, k1] +
  Mc8[s1, s2, k2, k1]

(* Sum over all *)

M[s1_, s2_] := Msym[s1, s2] + Mbr[s1, s2] + Mcr[s1, s2]

(* Only Mbr *)
(*M[s1_,s2_]:=Mbr[s1,s2]*)

(* Only U(1) symmetric *)
(*M[s1_,s2_]:=Msym[s1,s2]*)
```

Now we can write out the squared amplitude, ready to plug into a cross section formula:

```
SquaredAmp = FullSimplify[
  Sum[
   M[s1, s2] Conjugate[M[s1, s2]] /. kz2mass, {s1, 1, 2}, {s2, 1,
    2}],
```

```
  Assumptions -> assume]
```

We can make further simplifications massage things into a nicer form:

```
SquaredAmp = % /. {Cos[2 \[Theta]] -> (2 ct^2 - 1),
   Sin[2 \[Theta]]^2 -> 4 (1 - ct^2) ct^2, Cos[\[Theta]] -> ct}
```

Finally, we can plug into an expression for σv that is ready for thermal averaging. To do this we need to make factors of v explicit.

```
dsigv = 1/(4 p0^2) 1/(128 \[Pi]) SquaredAmp
Integrate[dsigv, {ct, -1, 1}, Assumptions -> assume]
% /. {p0 -> m\[Chi]/Sqrt[1 - (v/2)^2]};
FullSimplify[Normal[Series[%, {v, 0, 2}]]]
```

Some final remarks: parts of the code took a few minutes to run, but I was able to debug in real time with collaborators. In other words, if it's taking *ages* to compute, then you probably did something wrong.

References

[1] S. Dodelson, *Modern Cosmology*. Academic Press, 1 ed., 2003.

[2] E. Kolb and M. Turner, *The Early Universe*. Westview Press, 1994.

[3] G. Bertone, ed., *Particle dark matter: observations, models and searches*. Cambridge University Press, 2010.

[4] *XXXV SLAC Summer Institute (SSI 2007), Dark Matter: from the Cosmos to the Laboratory*. eConf C070730, SPIRES Conf Num: C07/07/30, 2007. http://www-conf.slac.stanford.edu/ssi/2007/.

[5] "Dark matter portal: Experiments, conferences, tools." http://lpsc.in2p3.fr/mayet/dm.php. "Infn dark matter page." http://www.nu.to.infn.it/Dark_Matter/. "Net advance of physics: Dark matter." http://web.mit.edu/redingtn/www/netadv/Xdarkmatte.html.

[6] G. Jungman, M. Kamionkowski, and K. Griest, "Supersymmetric dark matter," hep-ph/9506380v1. http://arxiv.org/abs/hep-ph/9506380v1.

[7] E. Aprile and S. Profumo, "Focus on dark matter and particle physics," *New J. Phys.* **11** (2009) 105002.

[8] J. Einasto, "Dark matter," 0901.0632v1. http://arxiv.org/abs/0901.0632v1.

[9] *XXXV SLAC Summer Institute (SSI 2007), Dark Matter: from the Cosmos to the Laboratory*. eConf C070730, SPIRES Conf Num: C07/07/30, 2007. http://www-conf.slac.stanford.edu/ssi/2007/. See lectures by Leo Blitz, recordings available online.

[10] S. van den Bergh, "The Early History of Dark Matter," **111** (June, 1999) 657–660, arXiv:astro-ph/9904251.

[11] F. Zwicky, "Spectral displacement of extra galactic nebulae," *Helv. Phys. Acta* **6** (1933) 110–127.

[12] F. Zwicky, "Republication of: The redshift of extragalactic nebulae," *General Relativity and Gravitation* **41** (Jan., 2009) 207–224.

[13] S. Smith, "The Mass of the Virgo Cluster," **83** (Jan., 1936) 23–+.

[14] F. D. Kahn and L. Woltjer, "Intergalactic Matter and the Galaxy.," **130** (Nov., 1959) 705–+.

[15] "Fritz zwicky, scientist." http://www.mentalfloss.com/blogs/archives/1843#comment-2160.

[16] H. W. Babcock, "The rotation of the Andromeda Nebula," *Lick Observatory Bulletin* **19** (1939) 41–51.

[17] V. C. Rubin, "One hundred years of rotating galaxies," *Publications of the Astronomical Society of the Pacific* **112** (2000) no. 772, 747–750. http://www.journals.uchicago.edu/doi/abs/10.1086/316573.

[18] P. Giromini, F. Happacher, M. J. Kim, M. Kruse, K. Pitts, F. Ptohos, and S. Torre, "Phenomenological interpretation of the multi-muon events reported by the cdf collaboration," 0810.5730v1. http://arxiv.org/abs/0810.5730v1.

[19] J. P. Ostriker and P. J. E. Peebles, "A Numerical Study of the Stability of Flattened Galaxies: or, can Cold Galaxies Survive?," **186** (Dec., 1973) 467–480.

[20] D. Lynden-Bell, "Statistical mechanics of violent relaxation in stellar systems," **136** (1967) 101–+.

[21] J. P. Ostriker, P. J. E. Peebles, and A. Yahil, "The size and mass of galaxies, and the mass of the universe," **193** (Oct., 1974) L1–L4.

[22] *32nd SLAC Summer Institute on Particle Physics 32nd SLAC Summer Institute on Particle Physics: Nature's Greatest Puzzles*. eConf C040802, SPIRES Conf Num: C04/08/02, 2007. http://www.slac.stanford.edu/econf/C040802/index.htm.

[23] B. Ryden, *Introduction to Cosmology*. Addison Wessley, 2003.

[24] C. Csaki, N. Kaloper, M. Peloso, and J. Terning, "Super-gzk photons from photon-axion mixing," hep-ph/0302030v2. http://arxiv.org/abs/hep-ph/0302030v2.

[25] K. M. Ashman, "Dark matter in galaxies," **104** (Dec., 1992) 1109–1138.

[26] M. Roos, "Dark matter: The evidence from astronomy, astrophysics and cosmology," 1001.0316v1. http://arxiv.org/abs/1001.0316v1. K. Freese, "Review of observational evidence for dark matter in the universe and in upcoming searches for dark stars," 0812.4005v1. http://arxiv.org/abs/0812.4005v1. G. D'Amico, M. Kamionkowski, and K. Sigurdson, "Dark matter astrophysics," 0907.1912v1. http://arxiv.org/abs/0907.1912v1.

[27] D. Fabricant, M. Lecar, and P. Gorenstein, "X-ray measurements of the mass of M87," **241** (Oct., 1980) 552–560.

[28] R. Massey, T. Kitching, and J. Richard, "The dark matter of gravitational lensing," 1001.1739v1. http://arxiv.org/abs/1001.1739v1.

[29] D. Clowe, M. Bradac, A. H. Gonzalez, M. Markevitch, S. W. Randall, C. Jones, and D. Zaritsky, "A direct empirical proof of the existence of dark matter," astro-ph/0608407v1. http://arxiv.org/abs/astro-ph/0608407v1.

[30] S. Kachru, "Physics 153A: String Theory, Stanford University." Comment during lecture, 2006.

[31] S. Weinberg, *Cosmology*. Oxford University Press, USA, 2008.

[32] S. Sarkar, "Primordial nucleosynthesis and dark matter," astro-ph/9611232v1. http://arxiv.org/abs/astro-ph/9611232v1. K. A. Olive, "Primordial nucleosynthesis and dark matter," astro-ph/9707212v1. http://arxiv.org/abs/astro-ph/9707212v1.

[33] J. E. Carlstrom, G. P. Holder, and E. D. Reese, "Cosmology with the sunyaev-zel'dovich effect," astro-ph/0208192v1. http://arxiv.org/abs/astro-ph/0208192v1.

[34] D. H. Weinberg, R. Dav'e, N. Katz, and J. A. Kollmeier, "The lyman-alpha forest as a cosmological tool," astro-ph/0301186v1. http://arxiv.org/abs/astro-ph/0301186v1.

[35] E. L. Wright *et al.*, "Preliminary spectral observations of the Galaxy with a 7 deg beam by the Cosmic Background Explorer (COBE)," *Astrophys. J.* **381** (1991) 200–209.

[36] N. Jarosik, C. L. Bennett, J. Dunkley, B. Gold, M. R. Greason, M. Halpern, R. S. Hill, G. Hinshaw, A. Kogut, E. Komatsu, D. Larson, M. Limon, S. S. Meyer, M. R. Nolta, N. Odegard, L. Page, K. M. Smith, D. N. Spergel, G. S. Tucker, J. L. Weiland, E. Wollack, and E. L. Wright, "Seven-year wilkinson microwave anisotropy probe (wmap) observations: Sky maps, systematic errors, and basic results," 1001.4744v1. http://arxiv.org/abs/1001.4744v1.

[37] W. Hu and S. Dodelson, "Cosmic microwave background anisotropies," astro-ph/0110414v1. http://arxiv.org/abs/astro-ph/0110414v1. W. Hu, N. Sugiyama, and J. Silk, "The physics of microwave background anisotropies," astro-ph/9604166v1. http://arxiv.org/abs/astro-ph/9604166v1.

[38] G. R. Blumenthal, S. M. Faber, J. R. Primack, and M. J. Rees, "Formation of galaxies and large-scale structure with cold dark matter," **311** (Oct., 1984) 517–525. J. R. Primack, "Dark matter and structure formation," arXiv:astro-ph/9707285.

[39] K. Jedamzik and M. Pospelov, "Big Bang Nucleosynthesis and Particle Dark Matter," *New J. Phys.* **11** (2009) 105028, arXiv:0906.2087 [hep-ph].

[40] P. Peebles, *Principles of Physical Cosmology*. Princeton University Press, 1993.

[41] P. Gondolo, J. Edsjo, P. Ullio, L. Bergstrom, M. Schelke, and E. Baltz, "Darksusy: Computing supersymmetric dark matter properties numerically," astro-ph/0406204v1. http://arxiv.org/abs/astro-ph/0406204v1.

[42] G. Belanger *et al.*, "Indirect search for dark matter with micrOMEGAs2.4," arXiv:1004.1092 [hep-ph].

[43] "micromegas." http://lappweb.in2p3.fr/lapth/micromegas/.

[44] J. Hisano, K. Kohri, and M. M. Nojiri, "Neutralino warm dark matter," *Phys. Lett.* **B505** (2001) 169–176, arXiv:hep-ph/0011216. X.-l. Chen, M. Kamionkowski, and X.-m. Zhang, "Kinetic decoupling of neutralino dark matter," *Phys. Rev.* **D64** (2001) 021302, arXiv:astro-ph/0103452.

[45] L. A. Popa and A. Vasile, "Constraints on non-thermal Dark Matter from Planck lensing extraction," *JCAP* **0710** (2007) 017, arXiv:0708.2030 [astro-ph].

[46] J. L. Feng, "Dark matter candidates from particle physics and methods of detection," 1003.0904v2. http://arxiv.org/abs/1003.0904v2. F. Steffen, "Dark matter candidates - axions, neutralinos, gravitinos, and axinos,".

[47] J. L. Feng, "Dark matter at the fermi scale," astro-ph/0511043v1. http://arxiv.org/abs/astro-ph/0511043v1.

[48] *Theoretical Advanced Study Institute In Elementary Particle Physics (TASI 2009, Physics Of The Large And The Small), Dark Matter Theory*. SPIRES Conf Num: C09/06/01.3, 2009. http://www.colorado.edu/physics/Web/tasi09_annc.html. See lectures by Neal Weiner, recordings available online.

[49] F. Sánchez-Salcedo, E. Martínez-Gómez, and J. Magaña, "On the fraction of dark matter in charged massive particles (champs)," *Journal of Cosmology and Astroparticle Physics* **2010** (2010) no. 02, 031. http://stacks.iop.org/1475-7516/2010/i=02/a=031.

[50] S. Davidson, S. Hannestad, and G. Raffelt, "Updated bounds on milli-charged particles," *JHEP* **05** (2000) 003, arXiv:hep-ph/0001179.

[51] D. N. Spergel and P. J. Steinhardt, "Observational evidence for self-interacting cold dark matter," *Phys. Rev. Lett.* **84** (2000) 3760–3763, arXiv:astro-ph/9909386.

[52] L. Ackerman, M. R. Buckley, S. M. Carroll, and M. Kamionkowski, "Dark Matter and Dark Radiation," *Phys. Rev.* **D79** (2009) 023519, arXiv:0810.5126 [hep-ph].

[53] M. Kesden and M. Kamionkowski, "Galilean Equivalence for Galactic Dark Matter," *Phys. Rev. Lett.* **97** (2006) 131303, arXiv:astro-ph/0606566.

[54] M. Taoso, G. Bertone, and A. Masiero, "Dark Matter Candidates: A Ten-Point Test," *JCAP* **0803** (2008) 022, arXiv:0711.4996 [astro-ph].

[55] Wikipedia, "Baroque — wikipedia, the free encyclopedia," 2010. http://en.wikipedia.org/w/index.php?title=Baroque&oldid=355347171.

[56] "The dama project." http://people.roma2.infn.it/dama/. Collaboration website. **DAMA** Collaboration, R. Bernabei *et al.*, "First results from DAMA/LIBRA and the combined results with DAMA/NaI," *Eur. Phys. J.* **C56** (2008) 333–355, arXiv:0804.2741 [astro-ph]. R. Bernabei *et al.*, "Results from the DAMA/LIBRA experiment," *J. Phys. Conf. Ser.* **203** (2010) 012003.

[57] "The cdms homepage." http://cdms.berkeley.edu/.

[58] **CDMS II** Collaboration, "Dark Matter Search Results from the CDMS II Experiment,".

[59] S. R. Golwala, "Exclusion limits on the WIMP nucleon elastic scattering cross section from the Cryogenic Dark Matter Search,". UMI-99-94586.

[60] "Resonaances: What's really behind dama." http://resonaances.blogspot.com/2009/10/whats-really-behind-dama.html.

[61] *Theoretical Advanced Study Institute In Elementary Particle Physics (TASI 2009, Physics Of The Large And The Small), Dark Matter Experiment.* SPIRES Conf Num: C09/06/01.3, 2009. http://www.colorado.edu/physics/Web/tasi09_annc.html. See lectures by Richard Schnee, recordings available online.

[62] J. Carr, G. Lamanna, and J. Lavalle, "Indirect detection of dark matter," *Rept. Prog. Phys.* **69** (2006) 2475–2512.

[63] M. Cirelli and A. Strumia, "Minimal Dark Matter predictions and the PAMELA positron excess," *PoS* **IDM2008** (2008) 089, arXiv:0808.3867 [astro-ph].

[64] "Pamela mission official website." http://pamela.roma2.infn.it.

[65] **HEAT** Collaboration, S. W. Barwick *et al.*, "Measurements of the cosmic-ray positron fraction from 1- GeV to 50-GeV," *Astrophys. J.* **482** (1997) L191–L194, arXiv:astro-ph/9703192.

[66] **PAMELA** Collaboration, O. Adriani *et al.*, "An anomalous positron abundance in cosmic rays with energies 1.5.100 GeV," *Nature* **458** (2009) 607–609, arXiv:0810.4995 [astro-ph].

[67] O. Adriani, G. C. Barbarino, G. A. Bazilevskaya, R. Bellotti, M. Boezio, E. A. Bogomolov, L. Bonechi, M. Bongi, V. Bonvicini, S. Bottai, A. Bruno, F. Cafagna, D. Campana, P. Carlson, M. Casolino, G. Castellini, M. P. D. Pascale, G. D. Rosa, D. Fedele, A. M. Galper, L. Grishantseva, P. Hofverberg, S. V. Koldashov, S. Y. Krutkov, A. N. Kvashnin, A. Leonov, V. Malvezzi, L. Marcelli, W. Menn, V. V. Mikhailov, M. Minori, E. Mocchiutti, M. Nagni, S. Orsi, G. Osteria, P. Papini, M. Pearce, P. Picozza, M. Ricci, S. B. Ricciarini, M. Simon, R. Sparvoli, P. Spillantini, Y. I. Stozhkov, E. Taddei, A. Vacchi, E. Vannuccini, G. Vasilyev, S. A. Voronov, Y. T. Yurkin, G. Zampa, N. Zampa, and V. G. Zverev, "A new measurement of the antiproton-to-proton flux ratio up to 100 gev in the cosmic radiation," 0810.4994v2. http://arxiv.org/abs/0810.4994v2.

[68] **LAT** Collaboration, W. B. Atwood *et al.*, "The Large Area Telescope on the Fermi Gamma-ray Space Telescope Mission," *Astrophys. J.* **697** (2009) 1071–1102, arXiv:0902.1089 [astro-ph.IM]. A. A. Abdo, M. Ackermann, M. Ajello, W. B. Atwood, M. Axelsson, L. Baldini, J. Ballet, G. Barbiellini, D. Bastieri, M. Battelino, B. M. Baughman, K. Bechtol, R. Bellazzini, B. Berenji, R. D. Blandford, E. D. Bloom, G. Bogaert, E. Bonamente, A. W. Borgland, J. Bregeon, A. Brez, M. Brigida, P. Bruel, T. H. Burnett, G. A. Caliandro, R. A. Cameron, and P. A. Caraveo, "Measurement of the cosmic ray $e++e-$ spectrum from 20 gev to 1 tev with the fermi large area telescope," *Phys. Rev. Lett.* **102** (May, 2009) 181101. K. M. Z. Bruce Winstein, "Cosmic light matter probes heavy dark matter," *Physics* **2** (May, 2009) 37.

[69] N. J. Shaviv, E. Nakar, and T. Piran, "Natural explanation for the anomalous positron to electron ratio with supernova remnants as the sole cosmic ray source," *Phys. Rev. Lett.* **103** (2009) 111302, arXiv:0902.0376 [astro-ph.HE]. S. Profumo, "Dissecting Pamela (and ATIC) with Occam's Razor: existing, well-known Pulsars naturally account for the 'anomalous' Cosmic-Ray Electron and Positron Data," arXiv:0812.4457 [astro-ph].

[70] D. Finkbeiner, "Indirect Detection and Theoretical Models," *APS Meeting Abstracts* (Feb., 2010) 1002–+.

[71] **H.E.S.S.** Collaboration, F. Aharonian *et al.*, "HESS observations of the galactic center region and their possible dark matter interpretation," *Phys. Rev. Lett.* **97** (2006) 221102, arXiv:astro-ph/0610509. **HESS** Collaboration, F. Aharonian *et al.*, "Search for Gamma-rays from Dark Matter annihilations around Intermediate Mass Black Holes with the H.E.S.S. experiment," *Phys. Rev.* **D78** (2008) 072008, arXiv:0806.2981 [astro-ph].

[72] C. Boehm, D. Hooper, J. Silk, M. Casse, and J. Paul, "MeV Dark Matter: Has It Been Detected?," *Phys. Rev. Lett.* **92** (2004) 101301, arXiv:astro-ph/0309686.

[73] W. de Boer, "Evidence for dark matter annihilation from galactic gamma rays?," *New Astron. Rev.* **49** (2005) 213–231, arXiv:hep-ph/0408166. W. de Boer, C. Sander,

V. Zhukov, A. V. Gladyshev, and D. I. Kazakov, "Egret excess of diffuse galactic gamma rays as tracer of dark matter," *A&A* **444** (dec, 2005) 51–67. http://dx.doi.org/10.1051/0004-6361:20053726. W. de Boer, C. Sander, V. Zhukov, A. V. Gladyshev, and D. I. Kazakov, "The supersymmetric interpretation of the EGRET excess of diffuse Galactic gamma rays," *Phys. Lett.* **B636** (2006) 13–19, arXiv:hep-ph/0511154.

[74] P. Mertsch and S. Sarkar, "Systematic effects in the extraction of the 'WMAP haze'," arXiv:1004.3056 [astro-ph.HE].

[75] G. Dobler, D. P. Finkbeiner, I. Cholis, T. R. Slatyer, and N. Weiner, "The Fermi Haze: A Gamma-Ray Counterpart to the Microwave Haze," arXiv:0910.4583 [astro-ph.HE].

[76] N. Weiner, "Beyond minimal dark matter." Talk at the ITS/CUNY Emerging Problems in Particle Phenomenology Workshop, 2010.

[77] A. Bottino, F. Donato, N. Fornengo, and S. Scopel, "Light neutralinos and WIMP direct searches," *Phys. Rev.* **D69** (2004) 037302, arXiv:hep-ph/0307303.

[78] D. Tucker-Smith and N. Weiner, "Inelastic dark matter," *Phys. Rev.* **D64** (2001) 043502, arXiv:hep-ph/0101138.

[79] D. Tucker-Smith and N. Weiner, "The status of inelastic dark matter," *Phys. Rev.* **D72** (2005) 063509, arXiv:hep-ph/0402065.

[80] I. Cholis, L. Goodenough, D. Hooper, M. Simet, and N. Weiner, "High Energy Positrons From Annihilating Dark Matter," *Phys. Rev.* **D80** (2009) 123511, arXiv:0809.1683 [hep-ph].

[81] P. W. Graham, R. Harnik, S. Rajendran, and P. Saraswat, "Exothermic Dark Matter," arXiv:1004.0937 [hep-ph].

[82] J. L. Feng, "Non-WIMP Candidates," arXiv:1002.3828 [hep-ph].

[83] J. L. Feng and J. Kumar, "The WIMPless Miracle: Dark-Matter Particles without Weak-Scale Masses or Weak Interactions," *Phys. Rev. Lett.* **101** (2008) 231301, arXiv:0803.4196 [hep-ph].

[84] L. D. Duffy and K. van Bibber, "Axions as Dark Matter Particles," *New J. Phys.* **11** (2009) 105008, arXiv:0904.3346 [hep-ph].

[85] N. Arkani-Hamed and N. Weiner, "LHC Signals for a SuperUnified Theory of Dark Matter," *JHEP* **12** (2008) 104, arXiv:0810.0714 [hep-ph].

[86] C. Savage, G. Gelmini, P. Gondolo, and K. Freese, "Compatibility of DAMA/LIBRA dark matter detection with other searches," *JCAP* **0904** (2009) 010, arXiv:0808.3607 [astro-ph].

[87] C. Savage, P. Gondolo, and K. Freese, "Can WIMP spin dependent couplings explain DAMA data, in light of null results from other experiments?," *Phys. Rev.* **D70** (2004) 123513, arXiv:astro-ph/0408346.

[88] D. S. Gemmell, "Channeling and related effects in the motion of charged particles through crystals," *Rev. Mod. Phys.* **46** (1974) 129–227.

[89] R. Bernabei *et al.*, "Possible implications of the channeling effect in NaI(Tl) crystals," *Eur. Phys. J.* **C53** (2008) 205–213, arXiv:0710.0288 [astro-ph].

[90] R. Foot, "A CoGeNT confirmation of the DAMA signal," arXiv:1004.1424 [hep-ph]. S. Chang, J. Liu, A. Pierce, N. Weiner, and I. Yavin, "CoGeNT Interpretations," arXiv:1004.0697 [hep-ph]. A. L. Fitzpatrick, D. Hooper, and K. M. Zurek, "Implications of CoGeNT and DAMA for Light WIMP Dark Matter," arXiv:1003.0014 [hep-ph].

[91] P. Gondolo and G. Gelmini, "Cosmic abundances of stable particles: Improved analysis," *Nucl. Phys.* **B360** (1991) 145–179.

[92] L. J. Hall, K. Jedamzik, J. March-Russell, and S. M. West, "Freeze-In Production of FIMP Dark Matter," *JHEP* **03** (2010) 080, arXiv:0911.1120 [hep-ph]. C. Cheung, G. Elor, L. J. Hall, and P. Kumar, "Origins of Hidden Sector Dark Matter I: Cosmology," arXiv:1010.0022 [hep-ph]. C. Cheung, G. Elor, L. J. Hall, and P. Kumar, "Origins of Hidden Sector Dark Matter II: Collider Physics," arXiv:1010.0024 [hep-ph].

[93] K. Griest and D. Seckel, "Three exceptions in the calculation of relic abundances," *Phys. Rev.* **D43** (1991) 3191–3203.

[94] R. J. Scherrer and M. S. Turner, "On the Relic, Cosmic Abundance of Stable Weakly Interacting Massive Particles," *Phys. Rev.* **D33** (1986) 1585.

[95] G. Jungman, M. Kamionkowski, and K. Griest, "Supersymmetric dark matter," *Phys. Rept.* **267** (1996) 195–373, arXiv:hep-ph/9506380.

[96] H. K. Dreiner, H. E. Haber, and S. P. Martin, "Two-component spinor techniques and Feynman rules for quantum field theory and supersymmetry," *Phys. Rept.* **494** (2010) 1–196, arXiv:0812.1594 [hep-ph].

[97] P. Ullio, L. Bergstrom, J. Edsjo, and C. G. Lacey, "Cosmological dark matter annihilations into gamma-rays: A closer look," *Phys. Rev.* **D66** (2002) 123502, arXiv:astro-ph/0207125.

[98] P. Gondolo, J. Edsjö, P. Ullio, L. Bergström, M. Schelke, E.A. Baltz, T. Bringmann and G. Duda, "DarkSUSY webpage." http://www.physto.se/~edsjo/darksusy.

[99] J. Edsjo, M. Schelke, P. Ullio, and P. Gondolo, "Accurate relic densities with neutralino, chargino and sfermion coannihilations in mSUGRA," *JCAP* **0304** (2003) 001, arXiv:hep-ph/0301106 [hep-ph].

[100] M. W. Goodman and E. Witten, "Detectability of certain dark-matter candidates," *Phys. Rev.* **D31** (1985) 3059.

[101] J. D. Lewin and P. F. Smith, "Review of mathematics, numerical factors, and corrections for dark matter experiments based on elastic nuclear recoil," *Astropart. Phys.* **6** (1996) 87–112.

[102] M. Kuhlen *et al.*, "Dark Matter Direct Detection with Non-Maxwellian Velocity Structure," *JCAP* **1002** (2010) 030, `arXiv:0912.2358 [astro-ph.GA]`.

[103] C. S. Kochanek, "The Mass of the Milky Way galaxy," *Astrophys. J.* **457** (1996) 228, `arXiv:astro-ph/9505068`. M. Weber and W. de Boer, "Determination of the Local Dark Matter Density in our Galaxy," `arXiv:0910.4272 [astro-ph.CO]`.

[104] A. Kurylov and M. Kamionkowski, "Generalized analysis of weakly-interacting massive particle searches," *Phys. Rev.* **D69** (2004) 063503, `arXiv:hep-ph/0307185`.

[105] J. Engel, "Nuclear form-factors for the scattering of weakly interacting massive particles," *Phys. Lett.* **B264** (1991) 114–119.

[106] J. Engel, S. Pittel, and P. Vogel, "Nuclear physics of dark matter detection," *Int. J. Mod. Phys.* **E1** (1992) 1–37. J. Engel and P. Vogel, "Spin dependent cross-sections of weakly interacting massive particles on nuclei," *Phys. Rev.* **D40** (1989) 3132–3135. M. A. Nikolaev and H. V. Klapdor-Kleingrothaus, "Quenching of the spin-dependent scattering of weakly interacting massive particles on heavy nuclei,". Given at 3rd International Symposium on Weak and Electromagnetic Interactions in Nuclei (WEIN 92), Dubna, USSR, 16-22 Jun 1992.

[107] "Howard georgi's home page." `http://www.people.fas.harvard.edu/~hgeorgi/`.

[108] R. J. Gaitskell, "Direct detection of dark matter," *Ann. Rev. Nucl. Part. Sci.* **54** (2004) 315–359.

[109] P. Binetruy, *Supersymmetry: Theory, Experiment, and Cosmology*. Oxford Graduate Texts. Oxfor University Press, 2007.

[110] I. Aitchison, *Supersymmetry in Particle Physics: An Elementary Introduction*. Cambridge University Press, 2007.

[111] P. B. Pal, "Dirac, Majorana and Weyl fermions," `arXiv:1006.1718 [hep-ph]`.

[112] J. Wess and J. Bagger, *Supersymmetry and Supergravity*. Princeton University Press, 2 revised ed., 1992.

[113] J. Terning, *Modern Supersymmetry: Dynamics and Duality*. Oxford University Press, USA, 2006.

[114] D. Bailin and A. Love, *Supersymmetric Gauge Field Theory and String Theory*. Taylor Francis, 1 ed., 1994.

[115] **Particle Data Group** Collaboration, K. Nakamura *et al.*, "Review of particle physics," *J. Phys.* **G37** (2010) 075021.

[116] V. I. Borodulin, R. N. Rogalev, and S. R. Slabospitsky, "CORE: COmpendium of RElations: Version 2.1," `arXiv:hep-ph/9507456`.

[117] S. Carroll, *Spacetime and geometry: an introduction to general relativity*. Addison Wesley, 2004.

[118] F. Reif, *Fundamentals of statistical and thermal physics*. McGraw-Hill series in fundamentals of physics. McGraw-Hill, 1985.

[119] Arizona Software, "Graphclick," 2011. `http://www.arizona-software.ch/graphclick/`.

[120] B. Bellazzini, C. Csaki, J. Hubisz, J. Shao, and P. Tanedo, "Goldstone Fermion Dark Matter," `arXiv:1106.2162 [hep-ph]`.